TRANSIENT HYDROGEOPHYSICAL INVESTIGATION OF A GASOLINE IMPACTED SITE, ENID, OKLAHOMA

By

SHANNON N. JEFFRIES

Bachelor of Science in Geology

Missouri State University

Springfield, Missouri

2008

Submitted to the Faculty of the
Graduate College of the
Oklahoma State University
in partial fulfillment of
the requirements for
the Degree of
MASTER OF SCIENCE
May 2012

TRANSIENT HYDROGEOPHYSICAL

INVESTIGATION OF A GASOLINE

IMPACTED SITE, ENID, OKLAHOMA

Thesis Approved:

Dr. Todd Halihan

Thesis Adviser

Dr. Estella Atekwana

Dr. Anna Cruse

Dr. Sheryl Tucker

Dean of the Graduate College

TABLE OF CONTENTS

Chapter Page

LIST OF TABLES

Table Page

LIST OF FIGURES

Figure Page

Figure Page

CHAPTER I

INTRODUCTION

In 2010 it was reported that there were over 696,000 active underground storage tanks (UST) in the United States that store petroleum and other hazardous substances (US EPA, 2010). The EPA UST/LUST (Leaky Underground Storage Tanks) reported that over 488,000 of those systems had confirmed releases. The same report listed over 10,700 UST systems in Oklahoma of which 4,700 had confirmed releases (US EPA, 2010).

The materials stored in LUSTs are a significant source of groundwater contamination. Due to this, it is important to monitor USTs for LUSTs and to remediate contamination from LUSTs. To do this, Congress passed the first of many laws that are now used to regulate USTs in 1984 (US EPA, 2010). Although laws have been passed to help regulate and prevent UST leakage into the subsurface, there are still many LUSTs nationwide. Site characterization, contamination remediation, and monitoring are the three primary procedures for correcting the problem of LUSTs.

For monitoring and remediation to occur, it is important to properly characterize the contamination in the subsurface. This can be done using monitoring wells, core samples, and geophysics. Different geophysical methods used for site characterization include ground penetrating radar, electromagnetic, seismology, and electrical resistivity.

While all of the methods listed would be applicable for this study, electrical resistivity and multichannel analysis of surface seismic waves (MASW) were chosen for site characterization and monitoring contamination remediation.

Electrical resistivity was chosen because it is dependent upon water saturation, solute concentration, and temperature (Wilkinson et al., 2010). This makes it a valuable geophysical tool for site characterization. Several authors (e.g., Che-Alota et al., 2009; Halihan et al., 2005a; Halihan et al., 2005b; Slater et al., 2002; Yaramanci et al., 2002; DOE, 2000a; DOE, 2000b; Dailey et al., 1992; Atekwana et al., 2000; Benson et al., 1997; Osiensky and Donaldson, 1995) have successfully used electrical resistivity methods to identify groundwater contamination, model changes in resistivity due to aging of hydrocarbons and background variations in resistivity values, and transient monitoring of contamination plumes or tracer injections for up to three months.

The study area of this thesis has already undergone some geophysical characterization using both surface and borehole electrical resistivity, also known as electrical resistivity tomography (McSorley, 2003). The borehole electrodes were left on site with the possibility of future monitoring. Due to this electrical resistivity tomography (ERT) is the specific electrical resistivity method that will be employed for this thesis. ERT has been cited in several publications as a good geophysical method to examine saline intrusion, infiltration, leachate recirculation, contamination and contamination remediation, and flow pathways (Wilkinson et al., 2010; Day-Lewis and Singha, 2008; Singha and Gorelick, 2005, 2006; Slater et al., 2002; Kemna et al; 2002; DOE 2000a, 2000b; Binley et al., 1996).

ERT data collected from a site before remediation and during remediation using ERT would help characterize hydrocarbon movement and changes in the geochemistry of the hydrocarbon (Atekwana et al., 2000). In order to determine what changes are occurring a transient analysis would be used on all data collected. This has been used in traditional surface resistivity arrays before (Che-Alota et al., 2009; Rein et al., 2004) and in short-term monitoring, maximum of three months, with ERT (Comfort et al., 2009; Wilkinson et al., 2004; Slater et al., 2002).

MASW was chosen because of its ability to determine depth to bedrock, areas of karst, levee leakage, hydrogeologic properties, voids, lateral velocity changes, faults/fractures, and weaknesses under asphalt in noisy urban environments as well as remote settings using (Ivanov et al., 2006; Ivanov et al., 2005; Miller et al., 2003; Miller et al., 2001; Miller et al., 1999). Most seismic methods have difficulty imaging in a geophysically noisy environment. The site chosen for this thesis is a noisy, urban environment, methods such as seismic refraction and reflection would be difficult to use due to contamination from traffic, airplanes, people, and trains. MASW was also chosen because of its ability to map bed rock, leakage, hydrologic properties, voids, lateral velocity changes, and faults. All of these items are of importance at the site chosen for this thesis.

PURPOSE OF STUDY

It is hypothesized that by using ERT and MASW geophysical methods at a site I will be able to identify stratigraphic units across the site that were seen in previously collected core data; identify preferential flow pathways or voids using shear wave

velocities from MASW analyses; determine if there are still LNAPL resistivity anomalies and, if so, have they migrated and how have they migrated; and use transient ERT to quantify any changes in resistivity that have occurred in the subsurface since the last ERT survey was acquired pre-remediation. This will be done by comparing ERT data collected in May 2010 to data collected in December 2002 in transient analyses. The geophysical data was calibrated using previously collected cores and groundwater geochemistry as well as new core and groundwater geochemistry in areas targeted by the geophysical signatures.

OBJECTIVES

1. Acquire ERT data in the chosen study area.
2. Compare ERT results with data collected eight years ago using transient analysis, and determine the changes in the electrical properties of the site during that time period.
3. Core anomalous locations based on the transient ERT data and perform geochemical tests on the cores to determine the cause of any anomalies.
4. Acquire MASW data in the chosen study area.
5. Compare the groundwater samples gathered eight years ago with samples collected in 2011 to see if there are any changes in the geochemical makeup of the LNAPL and to determine movement of the plume.

SITE HISTORY

The site chosen for this thesis is a vacant lot located at 8th Street and Broadway in Enid, Oklahoma (Figure 1). To the north of the field site is an active gas station. The UST at the station was found to be leaking in 1996 and it was excavated from the ground, however; the plume had already made its way into the groundwater. McSorley (2003) used electrical resistivity tomography to locate the LNAPL plume. Concurrently, McPhail (2003) used 16 cores to determine the stratigraphy of the site. The electrical resistivity tomography data comes from 16 monitoring wells located on the site (Figure 1). These are also the locations of cores described in McPhail (2003).

In 2002 an air sparge remediation system was installed on to help remediate the site. Air sparging is an in situ remediation technique where injection of air into the saturated zone. This causes a phase transfer of the contaminant (in this case LNAPL) from a dissolved state to a vapor state. Once this occurs the air is the vented through the saturated zone.

From 2001 to November 2009 the thickness of the LNAPL (free product) was measured in the monitoring wells on and off site. The results of these measurements are seen in Figures 2-4. From 2001 to 2009 the extent of the plume has grown in width, length, and thickness.

SITE DESCRIPTION

Stratigraphy

The generalized stratigraphy of the area is 12.8 meters of Quaternary alluvium and soil underlain by the Permian Hennessey Group (McPhail, 2003). McPhail (2003)

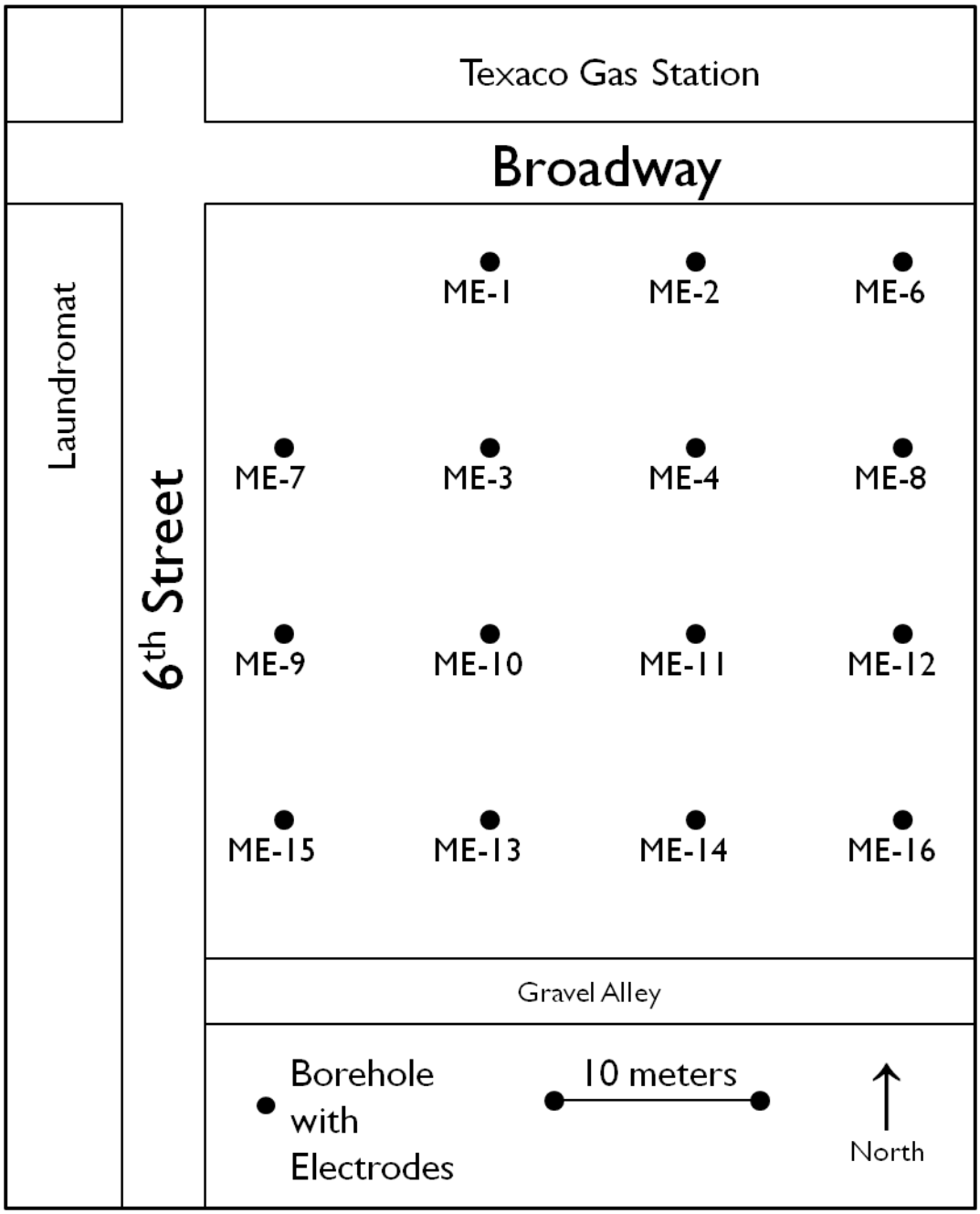

Figure 1. Site location map of field study in Enid, Oklahoma. The circles show the location of the electrodes (modified from Thorstad, 2005).

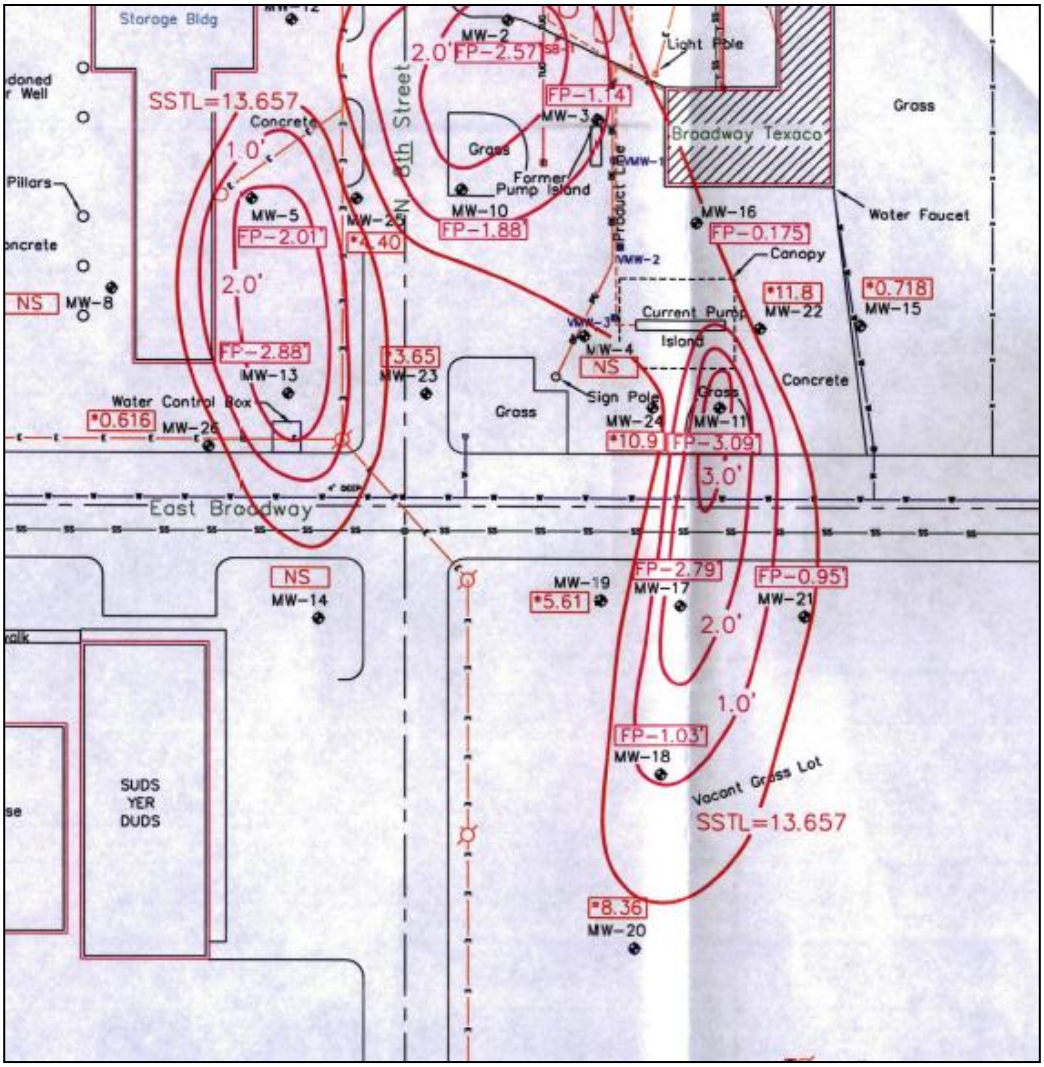

Figure 2. Map showing the thickness of the free product in July 2001. The location of this study is the vacant grass lot in the southeast corner. The red lines are one foot contours of the free product thickness. The FP-0.95 numbers in red boxes are the thickness of the free product in that monitoring well.

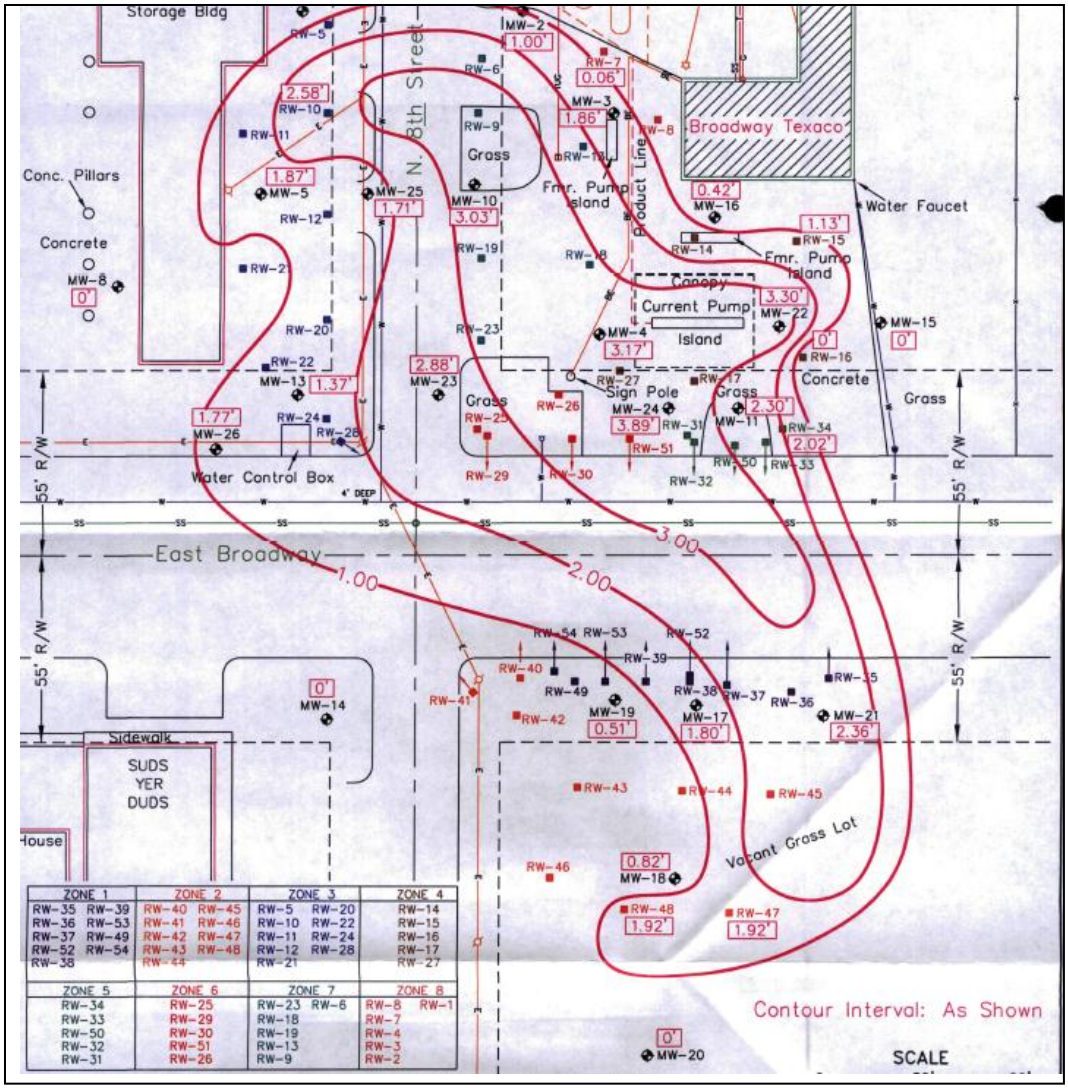

Figure 3. Map showing the thickness of the free product in July 2007. The location of this study is the vacant grass lot in the southeast corner. The red lines are one foot contours of the free product thickness. The red FP-0.95 numbers in red boxes are the thickness of the free product in that monitoring well.

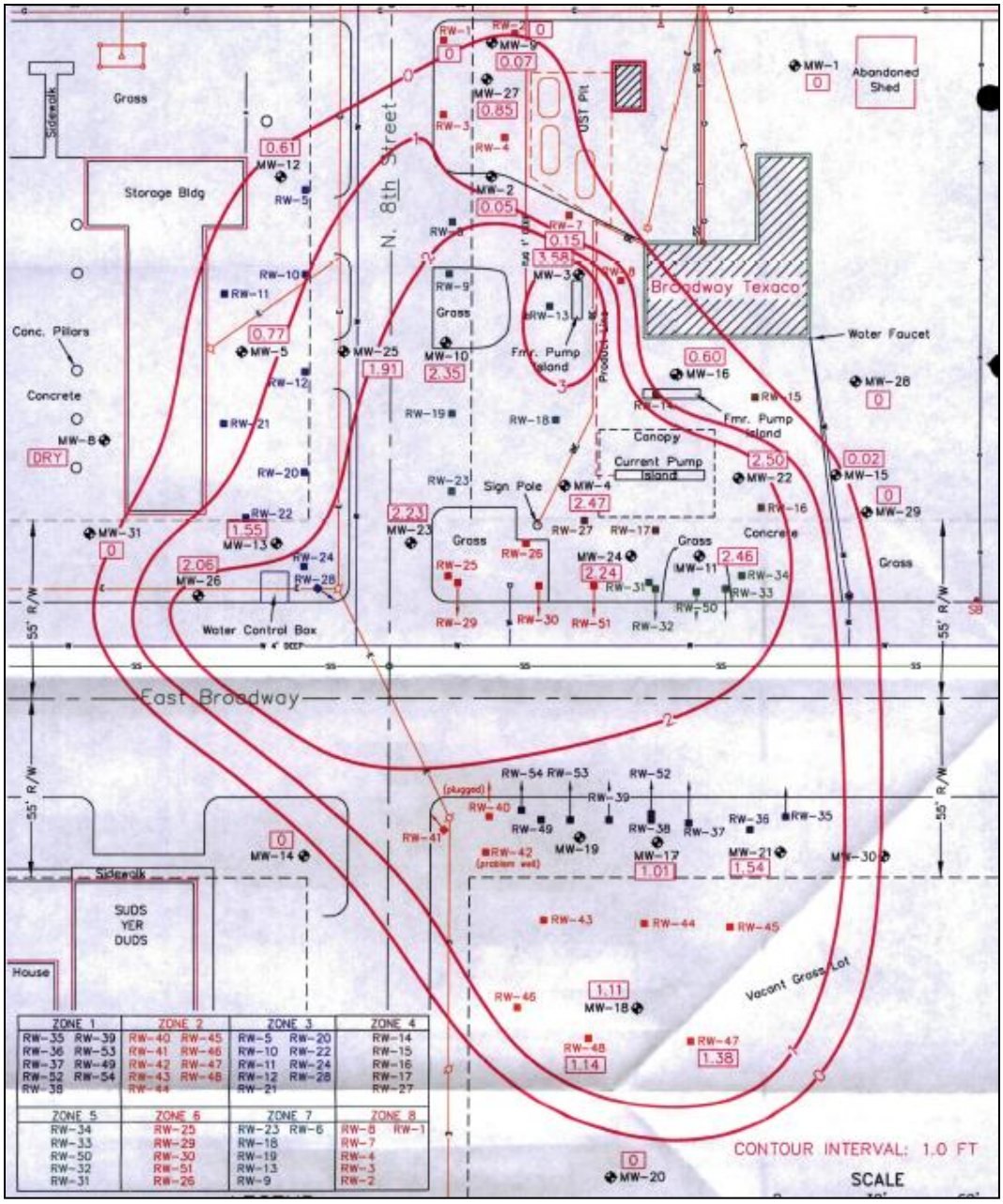

Figure 4. Map showing the thickness of the free product in August 2009. The location of this study is the vacant grass lot in the southeast corner. The red lines are one foot contours of the free product thickness. The red FP-0.95 numbers in red boxes are the thickness of the free product in that monitoring well.

Well Number: 1718 Core Numbers: 0-38 Location: 8th and Broadway

Date: 2/12//2003 Logged by: Melanie McPhail

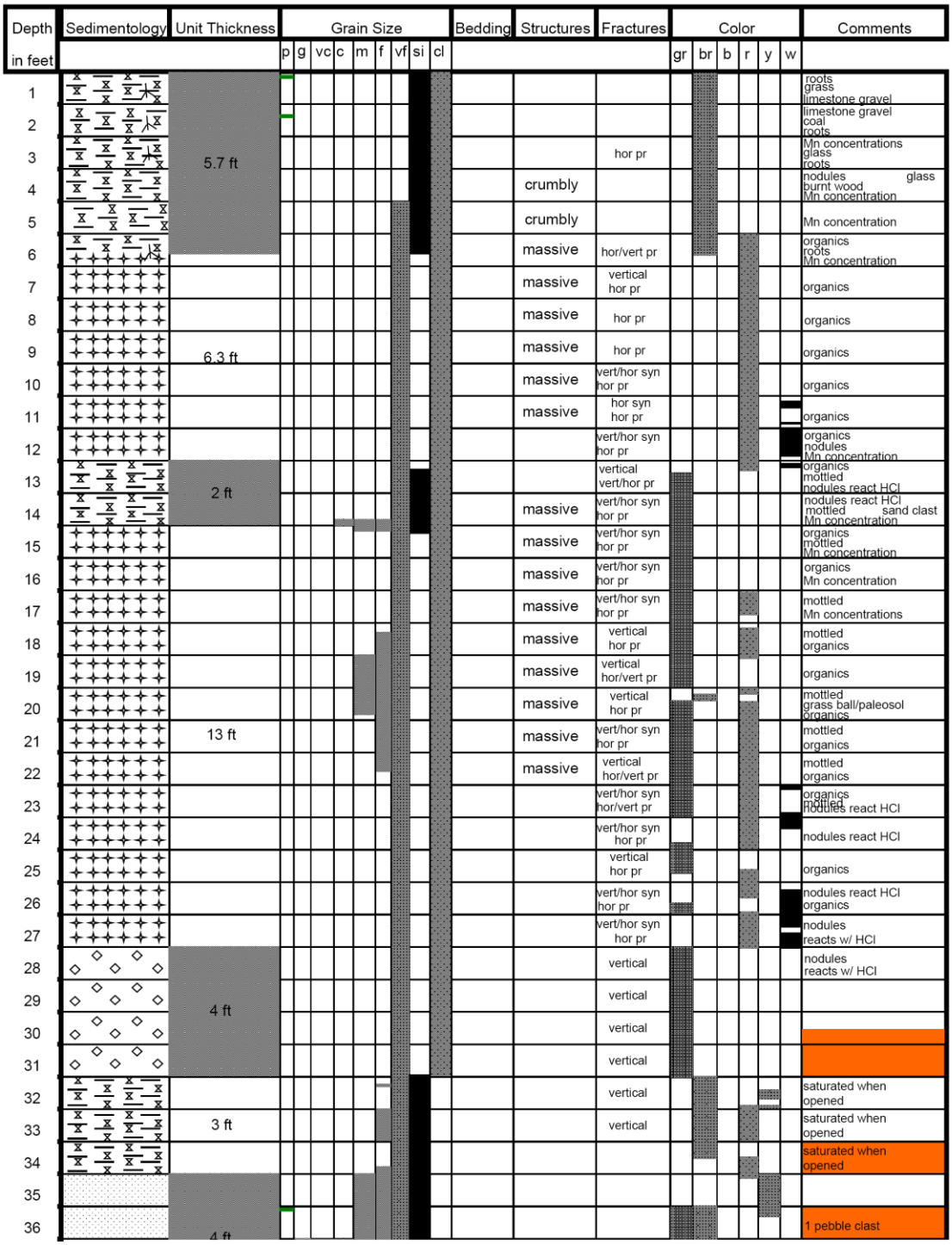

Figure 5. Core analysis for ME-06 (McPhail, 2003).

Table 1. Stratigraphy of the Enid site (modified from Thorstad, 2005).

Unit	Unit Name		Thickness (ft)	Thickness (m)	Approximate Depth (m)
C	Alluvium	Silty clay with sand	3−7	0.92−2.13	1
B		Sandy clay	25−29	7.62−8.84	9
		Gley	4−5	1.22−1.52	10
A		Sand-gravel	2.5−10.5	7.62−3.2	12
	Permian Hennessey Group		**Bedrock Aquitard**		

collected 16 cores and performed a detailed core description of the cores along with a grain size analysis. An example of one of the cores can be seen in Figure 5. Based on the results of the grain size analysis and core description McPhail (2003) subdivided the 12.8 meters of alluvium into three different units and one subunit based on grain-size analysis (Table 1).

The lowermost unit, described by Thorstad (2005) and McPhail (2003), is the Permian Hennessey Group. This group is considered to be the bedrock aquitard for the area. It is primarily shale with some sand.

Layer A, directly above the Permian Hennessey group, is a sand-pebble unit that has a thickness range from 2.4 to 10.5 feet. The grains consist of quartz and feldspar that fines upward into a well sorted fine sandstone. The majority of this unit had a hydrocarbon odor when it was cored. As the sorting changes from poorly sorted to well sorted there is a change in color because of the sandstone becoming more quartz rich than feldspar rich. In well ME-8, layer A stops at grass balls with attached roots. This indicates that this was a surface vegetation zone or soil horizon.

The contact between layer A and layer B is sharp. Layer B consists of sandy clay with a gley subunit (Layer B). Gley forms when sandy clay comes into contact with the water table. Development of the gley is related to the amount of time the pores are completely saturated. The gley is cemented by calcite. As with the previous layer, there was a hydrocarbon odor present. This layer ranges from 29 to 34 feet thick. The upper subunit of layer B contains calcite nodules, manganese concentrations, and organic remains. There were also hydrocarbon odors present and horizontal and vertical fractures.

Layer C is the surficial layer and is made of silty clay with sand that is approximately 3 to 7 feet thick. In addition, this unit contains manganese nodules and roots as well as other organic materials.

The lithology of all the wells is very similar with slight variations in dip and thickness of the horizons. From the core descriptions, McPhail (2003) created cross sections. An example of the cross sections is given along wells ME-7 through ME-8 as shown in Figure 6.

Hydrology

Halihan et al (2005) performed hydrogeologic studies on the site as well as some of the area adjacent to the site. Figure 7 shows the result of the studies. As seen on the map, the water table elevation ranges from 89.7 to 90.2 feet, based on a site datum. Notice that there is a groundwater mound located around monitoring well 25. This is likely the result of a water supply pipe that was leaking and in the process of being repaired during the time frame that Halihan et al (2005) collected the data. Based on the map (Figure 7), Halihan et al (2005) determined the flow of the groundwater, and

therefore the LNAPL. The flow paths indicated on the map show that the groundwater flow paths are to the south-southwest. Once the remediation system was installed and operational a new water level map was generated (Figure 8). Note how the gradient has changed. Groundwater flow is now converging between the study area and the Broadway Texaco gas station.

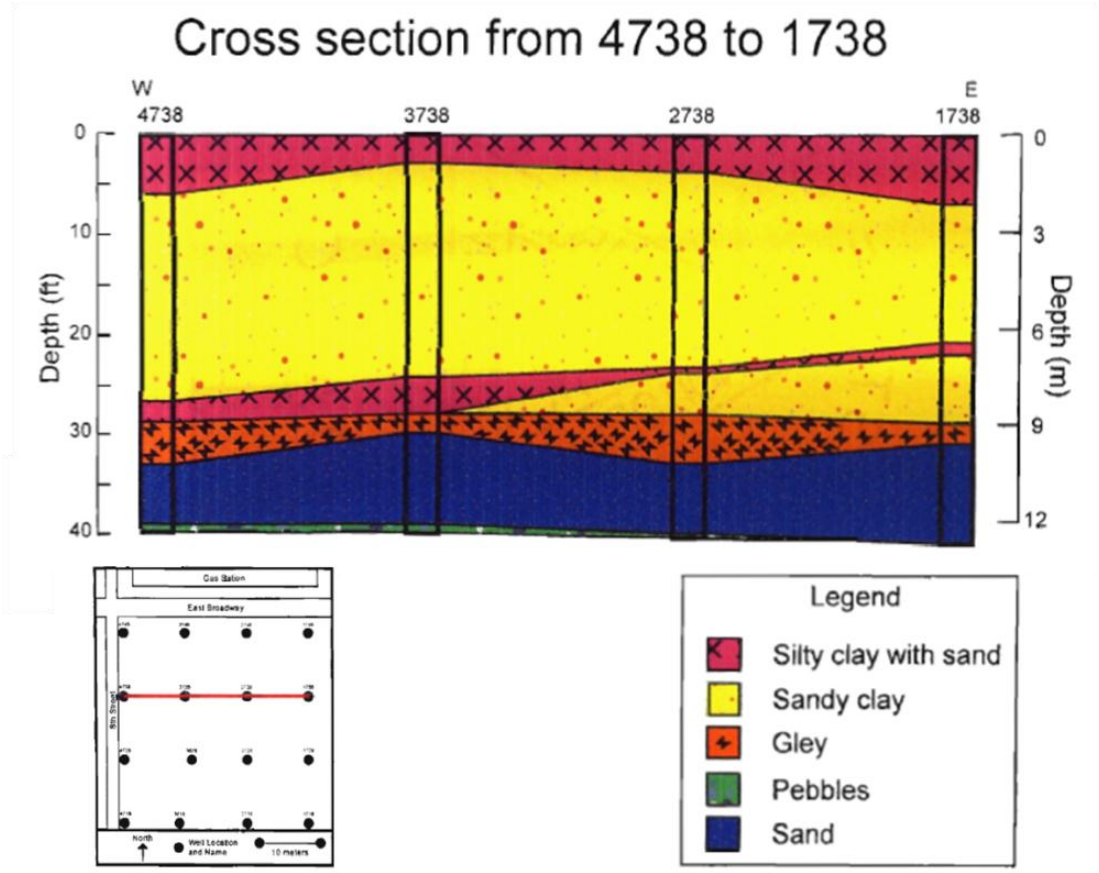

Figure 6. Cross section from soil boring wells 4738 to 1738. The soil borings labeled in this cross section as 4738, 3738, 2738, and 1738 correspond to ERT electrode string wells ME-7, ME-4, ME-3, and ME-8 respectively (modified from McPhail, 2003).

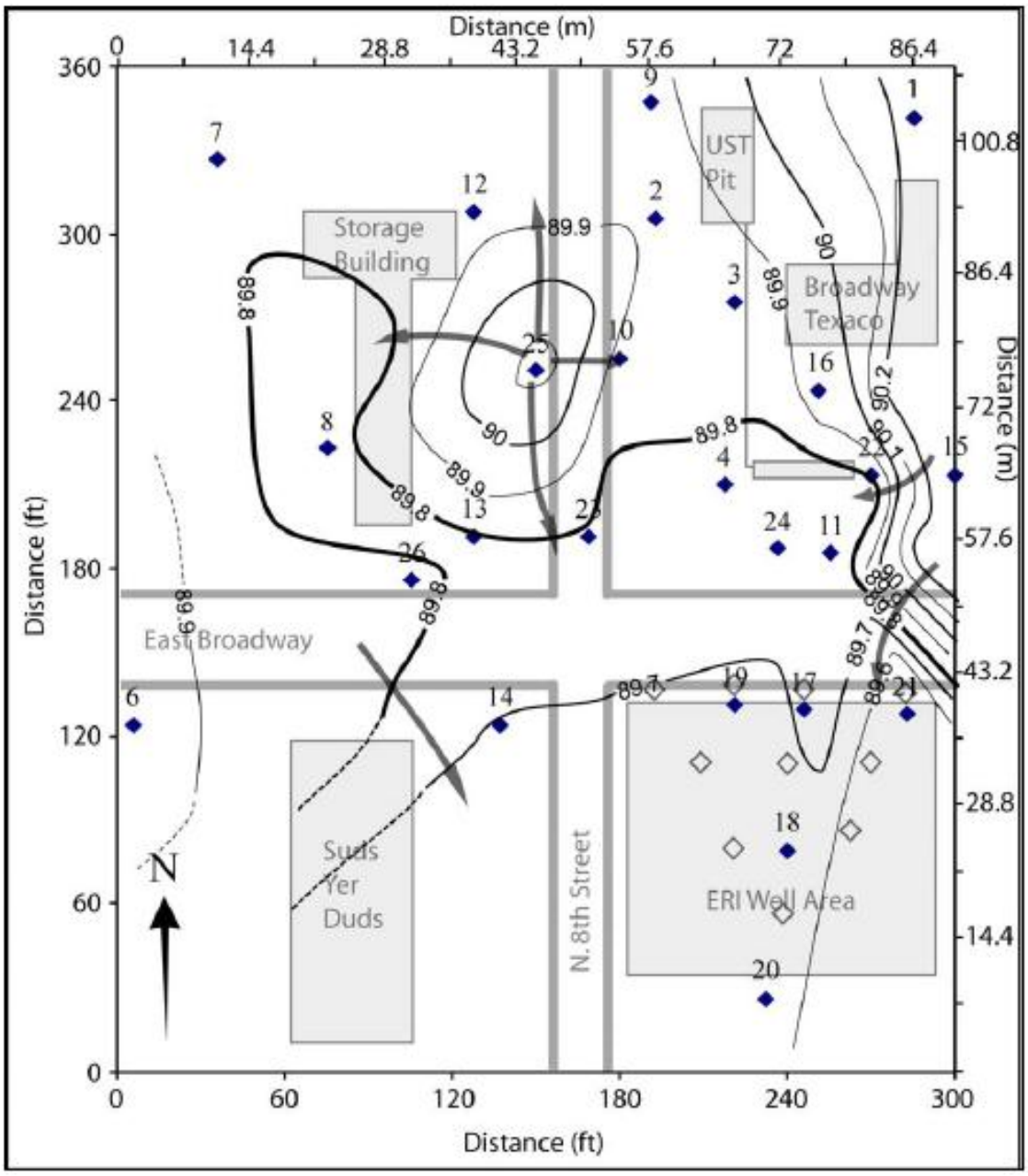

Figure 7. Water table map of area surrounding the Enid study site (SE corner). Filled diamonds are the monitoring wells that were used to create the map. The open diamonds represent planned remediation monitoring wells. As noted, the groundwater mound around well 25 is probably caused by a leaky water supply pipe that was repaired during the project (Halihan et al., 2005).

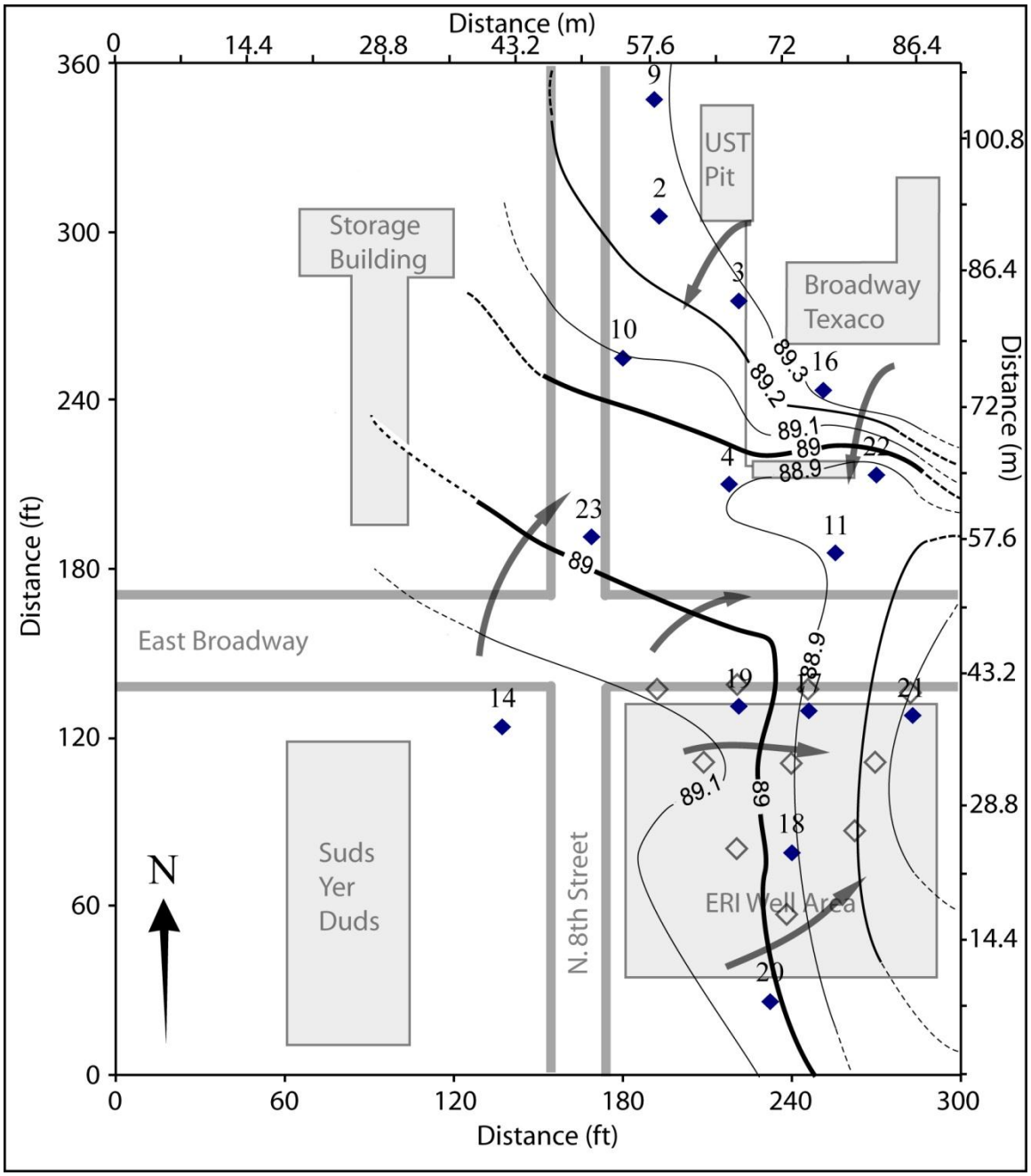

Figure 8. Water table map of the area surrounding the Enid Study site (SE corer). Filled diamonds are the monitoring wells that were used to create the map. The open diamonds represent planned remediation monitoring wells (Halihan et al., 2005).

CHAPTER II

REVIEW OF LITERATURE

Geophysics is the application of physics to the study of Earth. Numerous methods have been developed to accomplish this task. They include, but are not limited to, electrical resistivity, seismology, gravity, and magnetic. Any one of these methods, or a combination of these methods, may be used in geophysical exploration. In this literature review, electrical resistivity and the application to ERT will be evaluated along with seismic techniques, specifically surface wave seismic approaches.

ELECTRICAL RESISTIVITY

Electrical resistivity was first developed in the 1800s but did not become a popular geophysical tool until the 1970s (Reynolds, 1997). Common uses of electrical resistivity include: determination of bedrock/soil lithology; location of faults and subsurface cavities; location of groundwater; location and extent of groundwater/soil contamination; mining and oil exploration; and archaeology. For this study, electrical resistivity was used to evaluate the movement of LNAPL through the subsurface. For the purposes of this literature review the theory and development of ERT are first discussed. This is followed by discussion of summary of several works and how they relate to the scientific problems raised in Chapter I.

Theory

The basic theory of electrical resistivity can be found in most every geophysical textbook (Reynolds, 1997; Burger et al., 2006) and therefore will not be discussed here. The background theory that is important to describe in this literature review is the theory behind ERT.

ERT is a method of electrical resistivity imaging where the electrodes are located in boreholes. In ERT, two boreholes are drilled and a cable with many electrodes is inserted into both boreholes (Figure 9). The electrodes in the boreholes can be used as either current or potential electrodes. This method allows for the establishment of an electrical gradient between the two boreholes (Slater, 1996; McSorley, 2003; Day-Lewis and Singha, 2008). The basis for the use of ERT to monitor hydrologic processes and groundwater contamination is the sensitivity of the receiver's bulk conductivity (σ_b) to pore fluid conductivity (σ_f) as seen in this variation Archie's Law from Day-Lewis and Singha (2008):

$$\sigma_b = a\sigma_f\theta_t^q \qquad \text{Eqn. 3}$$

where a is the fitting parameters and θ_t^q is the total porosity raised to the cementation exponent.

Development of ERT

The use of ERT was developed for the U.S. department of Energy Office of Science and Technology by the Lawrence Livermore National Laboratory (DOE, 2000b). Over the past 20 years, ERT has been shown to be an adequate tool to detect flow, solute

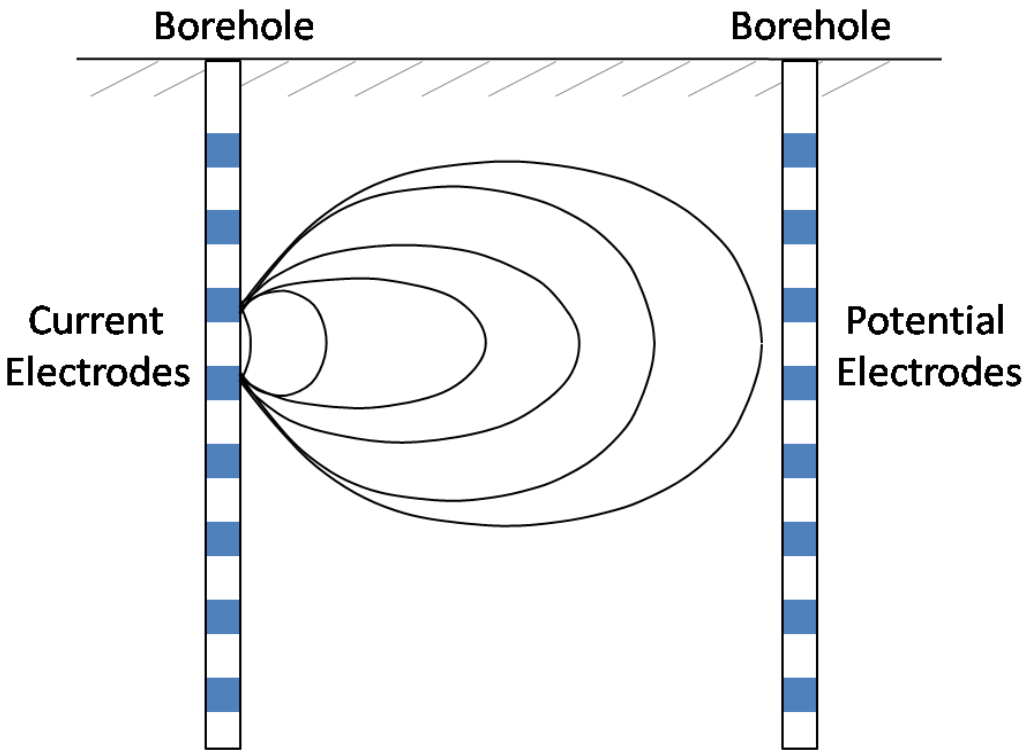

Figure 9. Multi-electrode configuration for ERT showing current flow. The blue squares represent the location of the electrodes (modified from McSorley, 2003).

transport, hydrocarbons, metals, organics, saline plumes, fluid transport, UST system leaks, steam or electrical heating during soil cleanup operations, and tracers (Dailey et al., 1992; Ramirez et al., 1993; Ramirez et al., 1995; Slater 1996; Binley, 1996; Sauck, 1998; Loh, 1999; Ramirez, 1999; Atekwana, 2000; Binley, 2002; French, 2002; Kemna, 2002; McSorley, 2003; Halihan et al., 2005a, 2005b; Singha and Gorelick, 2005, 2006; Day-Lewis and Singha, 2008; Wilkinson et al., 2010).

ERT provides increased resolution and sensitivity, lowers drilling costs, and lowers site damage by having fewer boreholes (DOE, 2000). However, the biggest advantage of ERT is the ability to leave the electrodes in the ground without harm to the environment and possibly the electrodes themselves (DOE, 2000). By leaving the

electrodes in the ground before, during, and after remediation one can determine the differences in resistivity over time. This allows for determining baseline characteristics of the bedrock and soil resistivity and observation of changes that occur during remediation (DOE, 2000).

ERT Case Studies

In this section several case studies are discussed and the importance of each to this thesis is given. The studies are from Atekwana et al. (2000). Slater et al. (2002), Comfort et al. (2009), Che-Alota et al., (2009) and Wilkinson et al. (2010).

Atekwana et al. (2000) used multiple geoelectrical methods in conjunction with soil borings to characterize a LNAPL contaminated site. The geoelectrical methods utilized were ground penetrating radar, electrical resistivity (surface and ERT), and electromagnetic induction. Because of the long time contamination at this site (50 years), one purpose of the study was to determine the change in the electrical signature of the hydrocarbon over time. In this study the ERT array was left in the ground and used to determine the changes in the vadose zone and the resistivity of the site. Geophysical data and geochemistry changes in the resistivity of the site were seen. Changes in resistivity were from resistive to conductive. Atekwana et al. (2000) attribute these as biodegradation of the LNAPL. This is important to this thesis due to the possibility of biodegradation occurring at the Enid site. If geochemical data supports this then a change in resistivity to a more conductive nature should be observed in Enid.

Slater et al (2002) performed a transient ERT study of a 9 m^3 tank that was filled with medium-grained sand (Figure 10). The lithology of the sand was broken up by two

channels, one composed of fine-grained sand in order to prevent transport through the tank, and the other filled with gravel designed to become a preferential flow pathway. Once the tank was constructed, it was saturated over several periods for 26 hours until the desired water level of 110 cm was reached. After saturation was achieved a tracer of sodium chloride was injected into the tank at the tracer injection chamber. ERT measurements and fluid conductivity data were collected from twenty observation wells prior to, during, and after injection for a period of 224 hours. The overall result of the study was that 3D ERT imaging can resolve complex flow and transport mechanisms when conducted over a period of time. This study is important to this thesis because it shows that ERT can be used to locate different types of plumes and their movement in laboratory experiments. It is therefore important to take the application described here and apply it to field settings. The next two case studies do that.

In another study performed at the former Nebraska Ordnance Plant (NOP), ERT and ERI data were gathered before, during, and after the injection of sodium permanganate over a period of 3 months (Comfort et al., 2009). The injection of sodium permanganate is for the remediation of royal demolition explosive (RDX). The results of the time-lapse data were a change from −13% to +13% from the original background data. These changes, although smaller than expected, showed that a conductive fluid was injected into the aquifer. The locations of these changes were identified to be along preferential flow paths, which did not align with the monitoring wells. The results of this study are important to this thesis because it applies the use of transient ERT to field-scale settings whereas most previous work has been in controlled laboratory settings (i.e. Slater et al., 2002). This work also uses the same processing methodology that will be

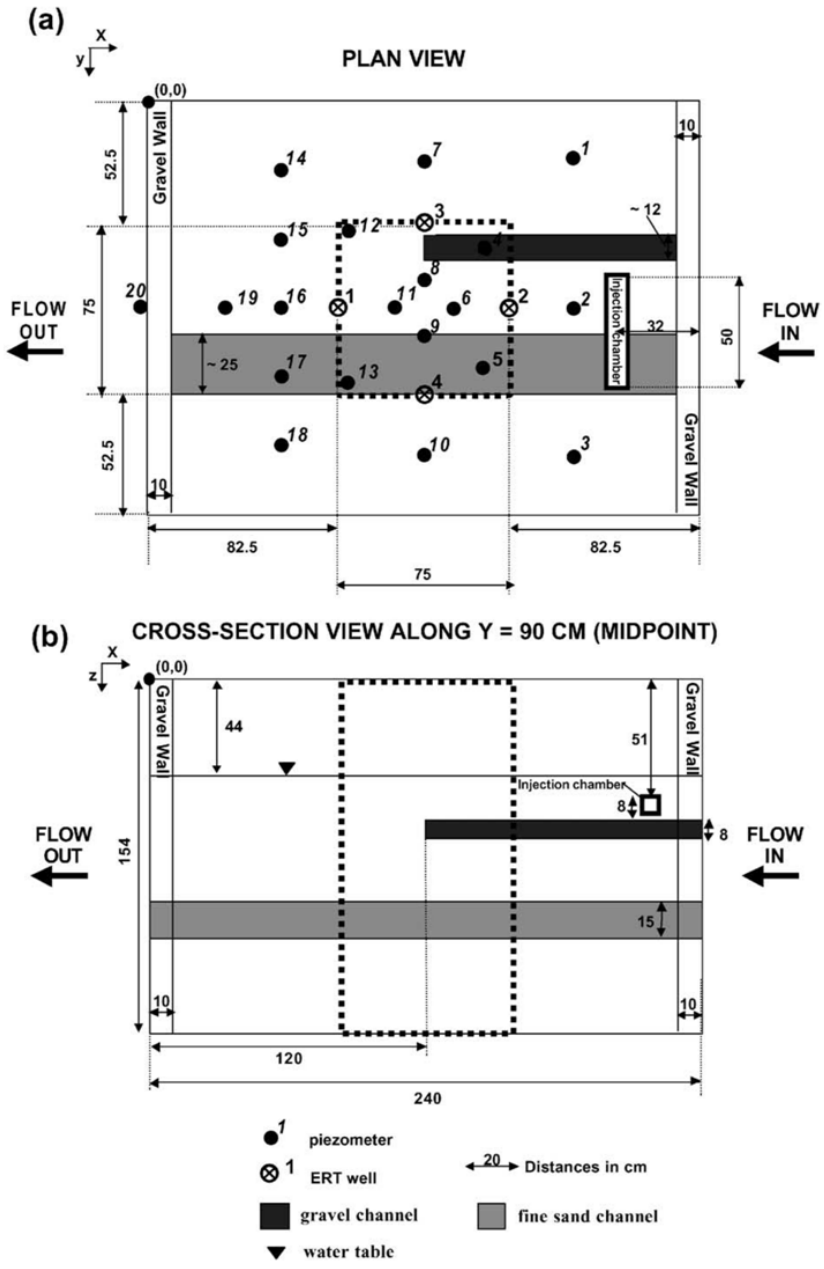

Figure 10. Geometry of the tank construction from Slater et al (2002) in a) plan view and b) cross-sectional view showing the tank structure; location of the twenty observation wells, wells with ERT arrays, injection chamber; and direction of flow (Slater et al., 2002).

described later and therefore shows that the methodology is appropriate to examine a site prior to and during remediation. How this thesis differs is the duration of time. Comfort et al. (2009) recorded data for a period of three months; pre-remediation data for the Enid site was acquired in December 2002 and during remediation data was collected in January –March 2003, May 2010, and March 2011.

A long term surface electrical resistivity array was used in Che-Alota et al. (2009) as a means for characterizing the difference geophysical signatures associated with contaminant mass remediation. In this paper the changes in the bulk electrical conductivity (inverse of resistivity) of a hydrocarbon plume are described. An illustration of the changes is seen in Figure 11. The initial hydrocarbon bulk conductivity is lower than the background site. As time goes the bulk conductivity begins to increase to a peak point that may coincide with remediation of the site. Once the contaminant mass has been reduced to almost pre-contamination levels the bulk conductivity of the site should be very similar to that of the background conductivity. This is important for this thesis because it will help identify the contamination resistivity.

The final case study to be examined used transient ERT to monitor a saline tracer test (Wilkinson et al., 2010). The study consisted of 14 boreholes with 16 electrodes each. Data were collected every four hours for 40 days. The results of this study were the ability to monitor the evolution of the saline tracer in near real-time. Wilkinson et al. (2010) were able to estimate seepage velocities that were in agreement with piezometer measurements. The importance of this study to this thesis is similar to that of Comfort et al. (2009). The authors show that contaminants affecting the electrical resistivity of the subsurface can be tracked and monitored in field-scale settings. Unlike Comfort et al.

(2009), this study gathered data in smaller intervals for a shorter amount of time. By doing so they were better able to monitor the movement of the tracer and calculate seepage velocities.

All of the above discussions are important to this thesis because they validate the use of ERT transient analyses and provide insight to the possible changes in resistivity that may occur.

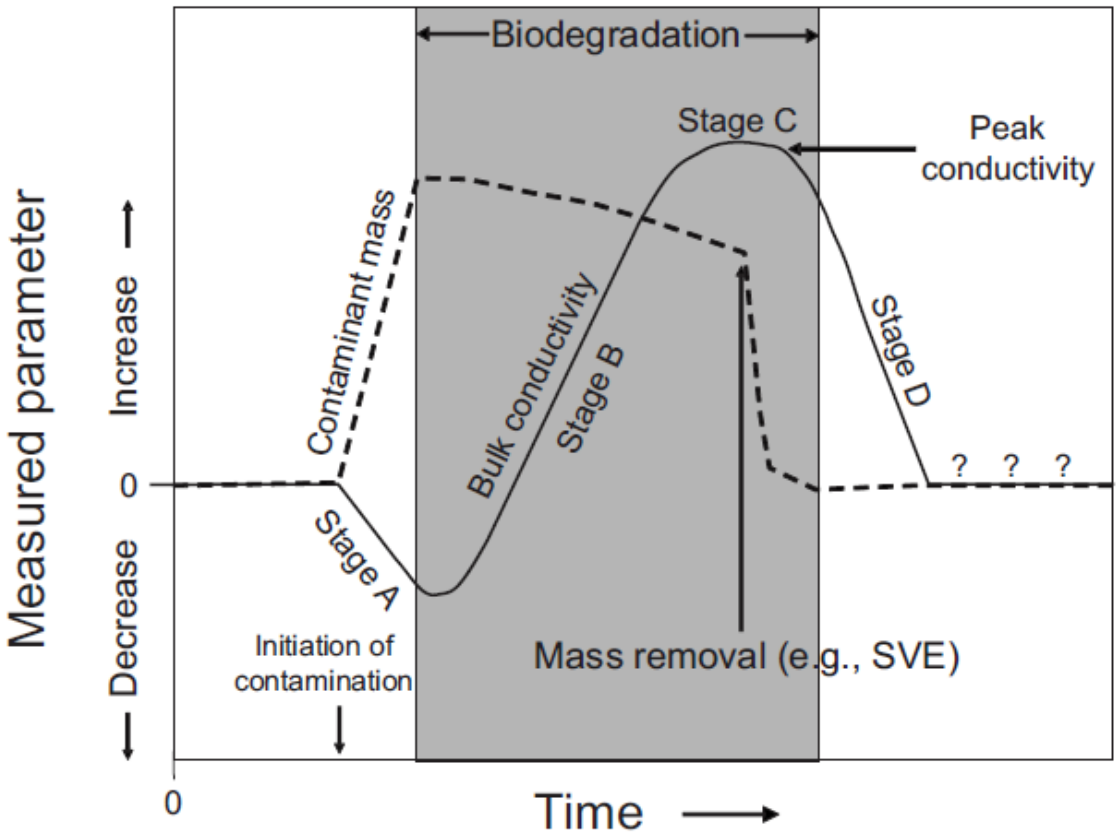

Figure 11. Conceptual model of the changes that a hydrocarbon may undergo over time and with remediation (Che-Alota et al., 2009).

SEISMIC

Seismology is a subject discussed in most geophysical textbooks. Some good examples are Sheriff and Geldart (1995), Reynolds (1997), Burger et al. (2006). For the purposes of this thesis only the theory of MASW will be described.

MASW Theory

In seismic exploration, the survey type of choice is typically reflection or refraction. However, in most seismic surveys when these surveys are used more than two-thirds of total seismic energy is transferred to Rayleigh waves (Park et al., 1999; Richart et al., 1970). In engineering, environmental, and groundwater studies surface waves have also been viewed as noise on seismic data (Miller, 1999; Steeples and Miller, 1990). Due to this another method has become utilized in the last couple of decades; multichannel analysis of surface waves. In a MASW survey the signal used is free surface waves and the noise waves are P and S; the reverse of seismic reflection and refraction. To understand the theory of MASW it is important to know what properties of surface seismic waves are being used.

The following description of surface waves is summarized from Reynolds, 1997. Rayleigh waves are the main type of free surface wave used. They propagate along the surface as ground roll with the particles moving in a retrograde elliptical motion to the direction of propagation. Due to the nature of their movement, Rayleigh waves can be said to have components of P and SV waves. Love waves move perpendicular to the direction of propagation in a shear like motion. Due to this, they are said to have components of the SH wave. In both Rayleigh and Love waves as the distance from the

ground surface (free surface) increases the amplitude and velocity of the waves decreases exponentially.

Dispersion is a property of Rayleigh waves where each frequency component has a different propagation velocity called a phase velocity (Park et al., 1999; Park et al., 2007). Due to this, each frequency propagated generates a different wavelength. MASW utilizes the dispersion property of surface waves (Park et al., 2007).

The group that has put the most research and development in using surface waves as a seismic exploration tool is Kansas Geological Survey (KGS) in Lawrence. Through their studies, they developed an algorithm and software program SurfSeis. This end result of this processing technique is a 2D shear wave velocity profile of the subsurface.

Park et al. (2007) describes the general process used in MASW as well as distinguishes between active and passive methods. Active MASW uses a source such as a viobroseis or an impulsive source such as a sledgehammer to initiate the shot record. With active MASW the maximum depth of investigation is between 10 to 30 meters (Park et al., 2007). Passive MASW uses natural or cultural sources. This provides a wider range for depth of investigation because it records lower frequencies (Park et al., 2007).

In both cases the same general process is used (Park et al., 2007). A source or noise is used to generate a multichannel record. Using dispersion SurfSeis software generates a dispersion image. Dispersion curves are extracted from this image and inverted generating a 1D shear wave velocity profile. Several of the 1D profiles can be combined to make a 2D shear wave velocity profile. Park et al. (2007) shows an illustration of this process (Figure 12).

When examining the dispersion image in Figure 12 one can see that there are several distinct curves labeled C0, C1, A, B, and E. The dispersion image is seen larger in Figure 13. This is showing what is called the fundamental mode (C0) and higher modes (C1, A, B, and E). The cause of the multiple modes is due to Rayleigh waves of different frequencies having the same velocity (Xia et al., 2003). The fundamental mode is the desirable mode for dispersion curve extraction because it provides reliable S-wave velocities with relatively small erros (Xia et al., 2007, 1999, 2000, 2002). The higher modes are considered contamination of the fundamental mode. In some instances the higher modes can be used to generate S-wave velocities when the fundamental mode is highly contaminated with body wave energy or noise (Park et al., 1999).

A useful technique in MASW is the combination of passive and active data. According to Park et al. (2007) this useful because it enlarges the analyzable frequency range of dispersion and depth of investigation as well as allowing for better identification of different modes in the dispersion curve. Figure 5 shows how the combination of active and passive dispersion curves can allow for better determination of the fundamental mode and higher modes. This therefore allows for easier extraction of a dispersion curve.

MASW Case Studies

The first case study discussed is by Ivanov et al. (2006). They used MASW to determine the subsurface geology (Ivanov et al., 2006). The area of the survey was in West Trenton, New Jersey. Previous models of the subsurface geology show dipping beds separated by a fault. The data was collected inexpensively and quickly using a 30-channel land streamer. The results of the study changed the geologic model of the area.

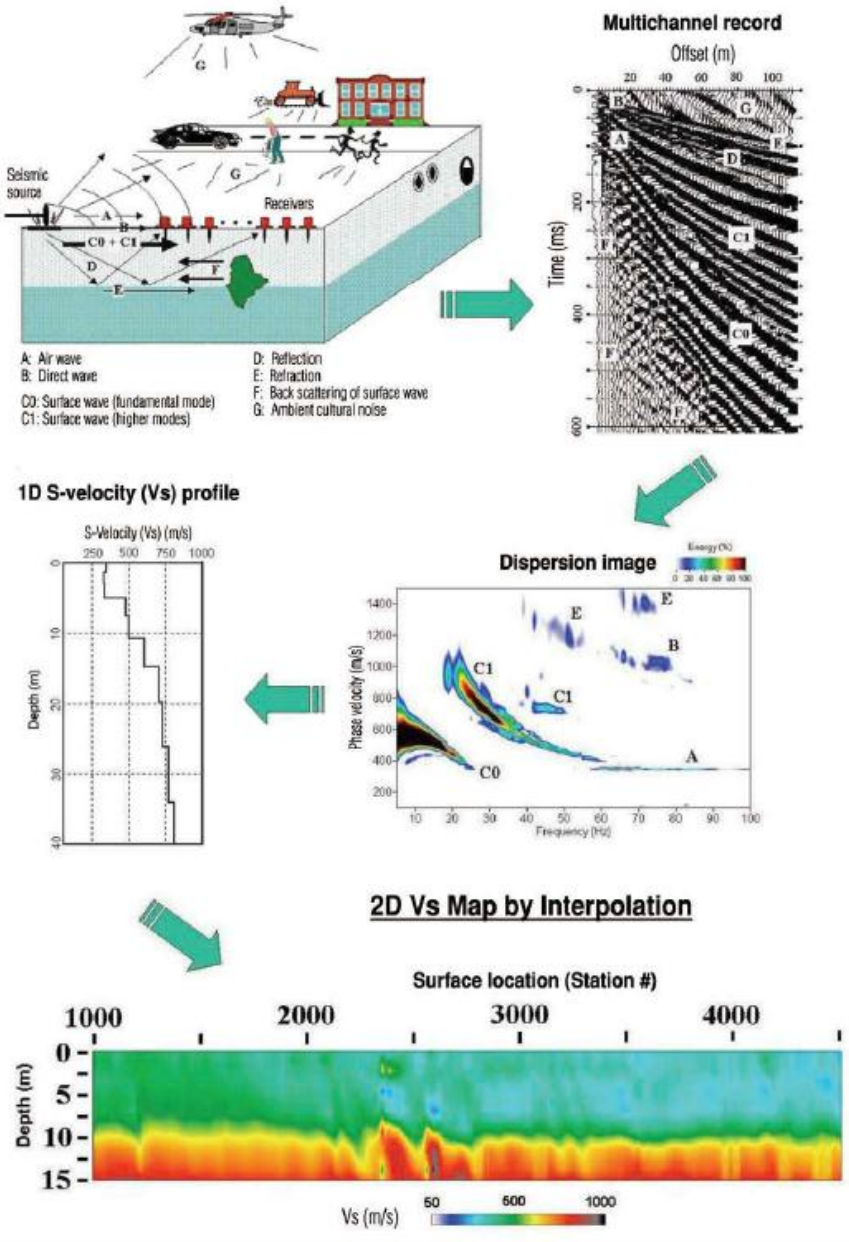

Figure 12. Illustration showing the process of MASW (Park et al., 2007).

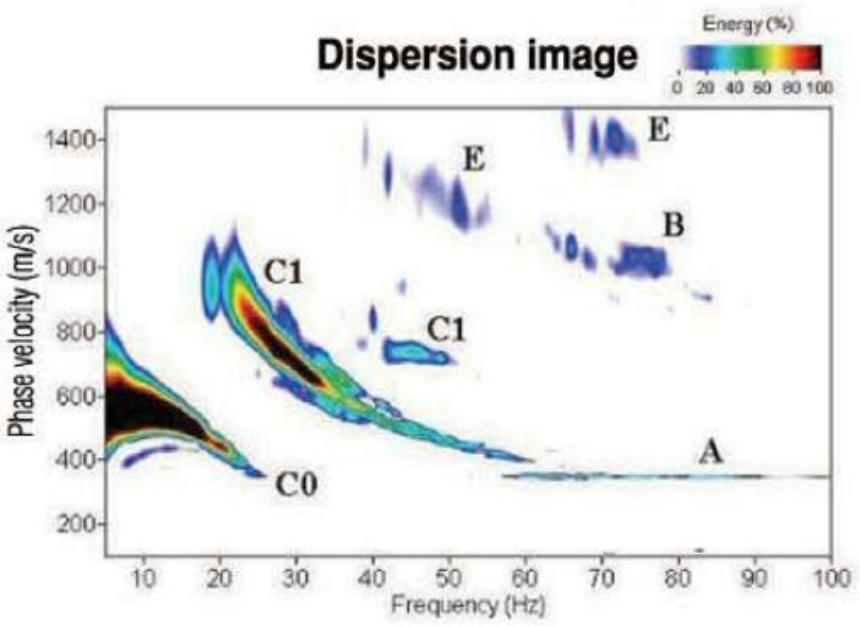

Figure 13. Enlarged dispersion image from Figure 12 (Park et al., 2007).

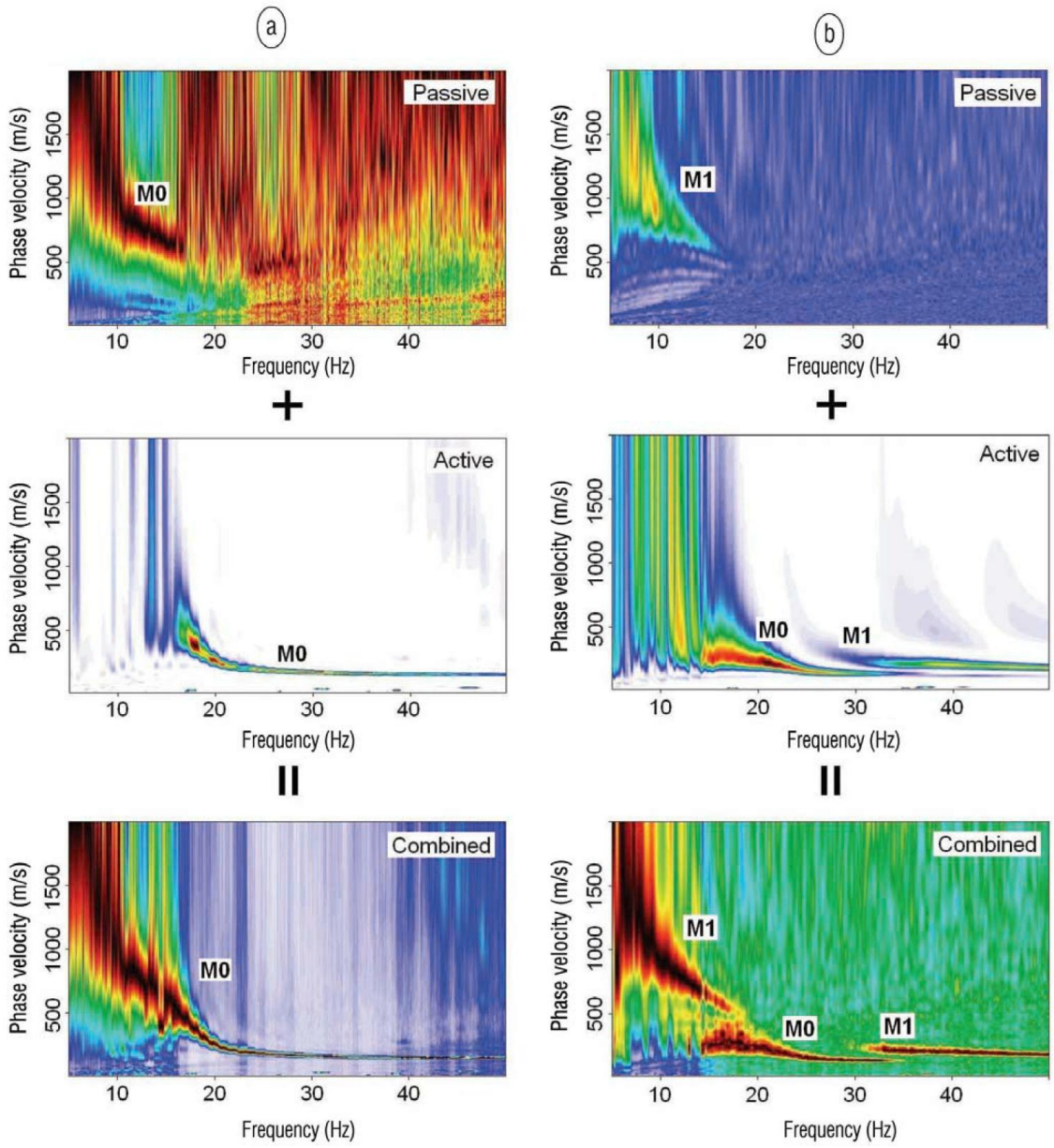

Figure 14. Dispersion images from passive (top) and active (middle) MASW surveys at the same site. When combined (bottom) they enlarge the frequency range of dispersion and allow for easier identification of the funamental mode or M0 (Park et al., 2007).

They were able to determine more exactly the location of the fault zone and the extent of the formations based on lateral variations in shear wave velocity. This study is important to this thesis because it shows that MASW is a good method to determine depth to bedrock, different stratigraphic units, and fault zones. This study also demonstrates that MASW can be used to determine lateral changes in velocity as well as vertical changes.

Another case study by Miller et al. (1999) used MASW to determine hydrogeologic properties and potential pathways or barriers to groundwater flow in Olathe, Kansas. The results of this study were identification of the top of bedrock as well as the use of lateral changes in velocity to identify fracture zones. The top of bedrock from the seismic data was consistent with borings taken prior to seismic acquisition. This study also demonstrated the insensitivity of MASW to electrical and mechanical noise from nearby industrial facilities. Based on this, it was determined that MASW would be an effective method for use in this thesis to map the top of bedrock and possible fracture zones which could serve as flow pathways for the LNAPL contamination even with the noisy urban environment this thesis studies.

The final case study examined levees in southern Texas for leakage over time (Ivanov et al., 2005). Seismic data was acquired over time to identify, delineate, and estimate the physical characteristics of material within levees during a simulated flood event and estimate the changes that occur. The results showed that shear wave velocity calculated using MASW is a sufficient way to measure the saturation of material from water. This study illustrates that soil saturation can be determined when using MASW. This is one objective of using MASW in Enid.

GROUNDWATER GEOCHEMISTRY

The gasoline that leaks from the LUSTs are made up of several different aromatic hydrocarbons that dissolve from the original hydrocarbon (gasoline) resulting in a decrease in concentration with distance from the source and time (Lipson and Siegel, 2000). The processes that cause the concentrations to decrease are adsorption, biodegradation, and volatilization (Barker and Patrick, 1987; Luhrs et al., 1992; Luhrs and Pyott, 1992; Worthington and Perez, 1993; Lipson and Siegel, 2000). The following summaries of each process are taken from Worthington and Perez (1993). Adsorption is a physio-chemical process. Hydrocarbon compounds are sorbed onto organic matter in the soil matrix causing movement of the hydrocarbon to slow. Biodegradation is a biochemical process that involves microorganisms in the subsurface metabolizing the hydrocarbon. Volatilization is another physio-chemical process where compounds such as BTEX and MTBE are adsorbed to the soil in the unsaturated zone. The vapors are then removed from the subsurface in response to natural barometric pressure changes or remediation processes.

An integral part of site characterization and monitoring during remediation are groundwater samples taken from monitoring wells on and sometimes off site geochemical analysis is performed. Several different geochemical analyses are performed on these samples. However; usually this data is presented in reports in the form of tables and plots of concentrations over time. Another way to look at this data is by using ternary plots that show the ratios between individual gasoline components such as BTEX and MTBE (Barker and Patrick, 1987; Luhrs et al., 1992; Luhrs and Pyott, 1992; Worthington and Perez, 1993; Lipson and Siegel, 2000).

Barker and Patrick (1987) examined the natural attenuation of BTEX in the laboratory and field injection experiments using ternary diagrams. In the analysis of the data no ternary diagrams were generated but the ration between benzene and xylene was closely examined. The results of the field experiment shoed that, in the case of biodegradation (natural attenuation), the xylene was removed first, then toluene, and then benzene. In the laboratory experiments the results were similar but they also showed that biodegradation of BTEX is dependent upon oxygen in the environment. Therefore, in aerobic conditions biodegradation may occur more efficiently and rapid than in anaerobic environments. The experiments conducted in this study support the ability to use rations of BTEX to determine physical and chemical processes that are occurring.

In Luhrs and Pyott (1992) uses case studies to show how ternary diagrams can show the zonation of a gasoline plume and identify the presence of multiple sources. Older plumes tend to show a ratio of benzene to xylene that is lower than a fresh spill. They illustrated this first by examining 87, 89, and 92 octane rating gasoline over the period of a week. The ternary diagrams for these results are seen in Figure 15. In the MTBE, benzene, and xylene ternary (Figure 15a), there is a definitive trend away from MTBE towards xylene. It is pertinent to note that higher octane gasoline will plot closer to the MTBE apex (Luhrs et al., 1992). In the benzene, toluene, and xylene ternary there is still a trend away from benzene but it is not distinctly towards xylene. Along with the laboratory work done, two case studies were also examined. From these case studies they determined that ternary diagrams can be used for: multiple source identification, the zonation of plumes, weathering of contaminants, relative octane rating of fresh spills, possible size of the release, and the relative age of contaminates.

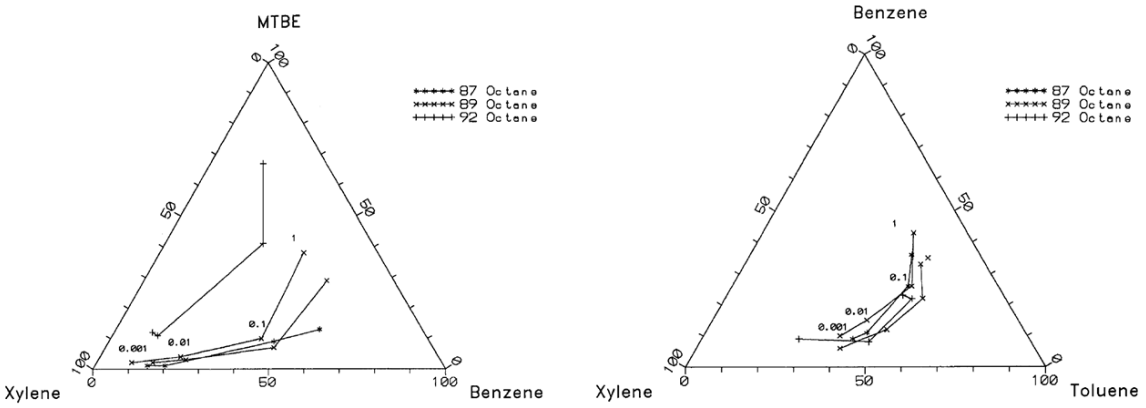

Figure 15. Ternary diagrams of a) MTBE, benzene, and xylene; b) benzene, toluene, and xylene showing the results over one week of 87, 89, and 92 octane gasoline (from Luhrs and Pyott, 1992).

Another study by Worthington and Perez (1993) shows similar results as the previous two studies. However, the authors appear to be more skeptical of the utility of ternary diagrams. They state that the analysis using ternary diagrams can only be expected to yield an approximation of the relative dates of spills due to the difficulty to understand the background concentrations, numerous possible sources and releases, the importance of different transport mechanisms, and distinguish weathering effects caused by zonation and mobility of the plume. This conclusion was drawn from five case studies performed where were known, previous site chemistry is known or easily determined, and the geologic materials are known. Note that even though Worthington and Perez are less enamored with the ternary diagrams than other authors, they do conclude that it is a useful technique.

Lipson and Siegel (2000) use mathematical modeling to show how ternary diagrams can characterize the transport processes occurring in a contaminated site. The mathematical modeling was done both in distance from the source and time since the initial spill. The results of the mathematical modeling are seen in Figures 16. Figure 16a

shows transport of BTEX by advection and dispersion of the plume over time and distance from the spill. Notice that in both case there is no trend towards any apex but concentric circles are shown with decreasing concentrations with increased distance from the source and an increase in concentration over time at the source. Biodegradation of BTEX is seen in Figure 16b; note that in both distance and time there is a very obvious trend towards benzene. In the case of volatilization (Figure 16c) there is a distinct trend away from benzene and toluene towards xylene.

All of the above studies show that ternary diagrams are an effective method for determining zonation and timing of a contamination plume both in lab and field studies.

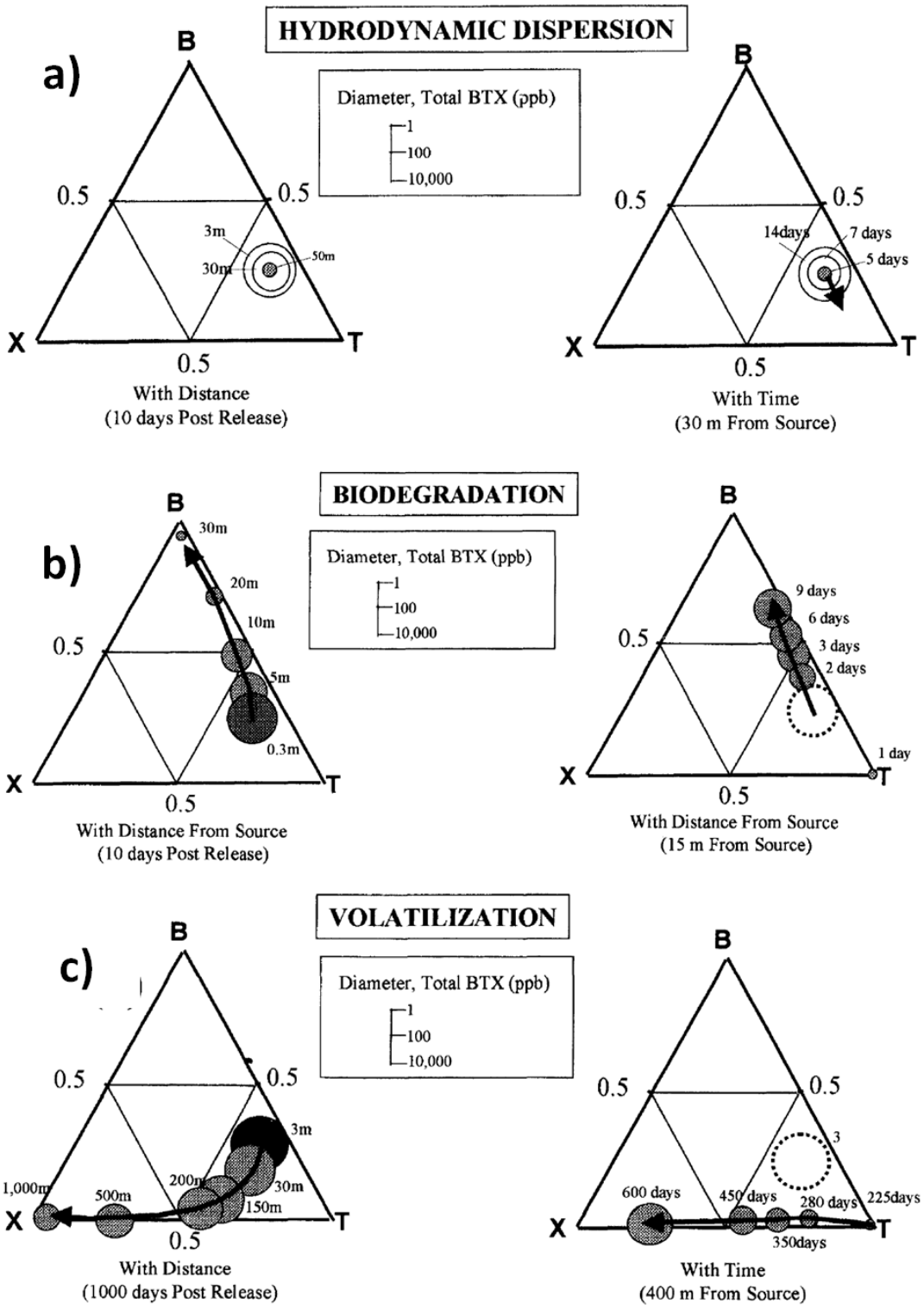

Figure 16. Theoretical ternary diagrams showing hydrodynamic dispersion (advection), biodegradation, and volatilization processes and their effects on the ration of benzene, toluene, and xylene (modified from Lipson and Siegel, 2000).

CHAPTER III

METHODOLOGY

The following chapter describes the data acquisition and processing methods that were implemented all data collected during this thesis.

ELECTRICAL RESISTIVITY

In the initial site work by McSorley (2003), electrical resistivity data were collected using both a multi-electrode surface survey and an ERT survey. To be able to perform time-lapse modeling, the parameters from McSorley (2003) were used for the ERT survey. No surface resistivity data were acquired.

Survey Design

The ERT data were collected using the electrodes and cables installed in boreholes by McSorley (2003). Each cable contains 27 graphite electrodes at 0.46 meters apart. Originally, cables were installed in fifteen boreholes in a 30 x 30 meter grid at a 10 meter spacing via a direct push installation technique (Figure 17). After the initial study in 2002–2003, there were problems with the cables in ME-1 and ME-2, therefore, they were removed. As a result, only thirteen cables were used for this study.

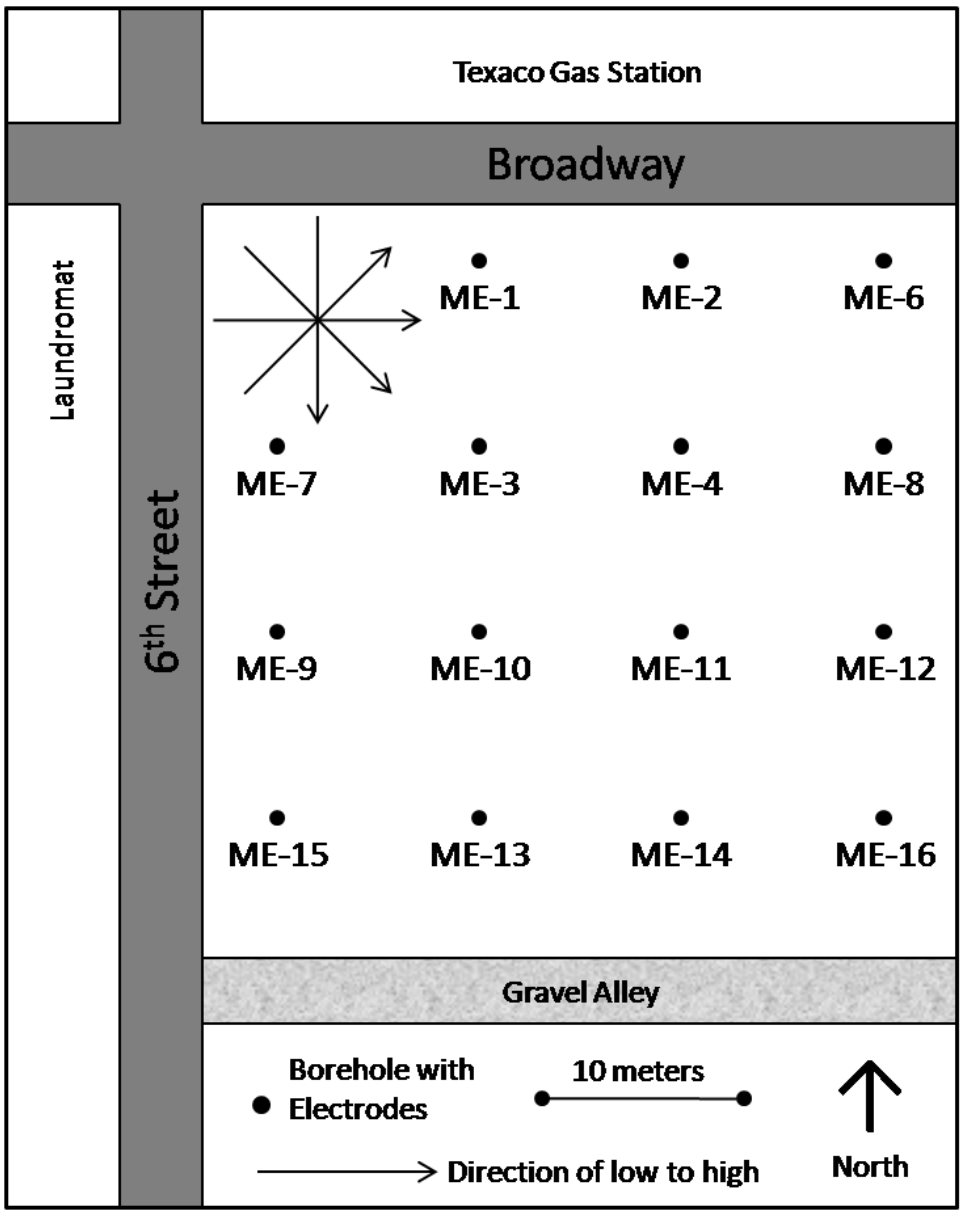

Figure 17. Initial electrode locations, Broadway Texaco Site Enid, Oklahoma. Arrows indicate the direction of low and high for the ERT survey (modified from McSorley 2003).

Data Acquisition

For this study, the ERT data were acquired using the procedures used in McSorley (2003). In order to acquire data that can be inverted to produce a two dimensional pseudo section, two cables must be used as illustrated in Figure 9. This results in a total of 54 electrodes in the array. One cable serves as the lower electrode numbers (1–27) and the other as the higher electrode numbers (28–54). The orientation for the low to high is from west to east, south to north, southwest to northeast, and northwest to southeast (Figure 17).

It is important to note that for data acquisition to occur, all of the cable connectors had to be cleaned. This was because they had been corroded (Figure 18). Figure 19 is a map showing the location of the most corroded connectors in relationship to the August 2009 free product thickness map. Based on this, it is thought that the corrosion was caused by hydrocarbon vapors escaping along the boreholes or through fractures in the clay.

Data Processing

After all the ERT data were collected they were processed using AGI Earth Imager. When the data files were loaded into Earth Imager, the screen shows the electrode configuration on the left and a raw data scatter plot on the right (Figure 20). The ERT raw data scatter plot is generated by Earth Imager by sorting the transmitting electrode pairs and receiver electrode pairs in ascending order. The color of the data point represents the apparent resistivity for that transmitting and receiver pair. Black points represent negative apparent resistivity.

Before beginning the inversion, the initial, forward modeling, and resistivity inversion settings were set. The initial settings are a max repeat error of 2%, a minimum voltage of 0.1, abs of 10^{-6}, minimum apparent resistivity of 0.01, and maximum apparent resistivity of 10^{4}. A robust inversion was used.

The final step before starting the inversion process is to note the number of data points that will be inverted. This includes noting how many data points are in the original file, how many pairs of reciprocal data were averaged, the number of data initially flagged for removal, and the number of data to be inverted. The number of data to be inverted must equal the total number of data points minus the averaged reciprocal pairs and the number of data flagged for removal. These numbers were recorded in an excel spreadsheet for each data file that was inverted.

Figure 18. Corroded ERT cable connector to SuperSting. The inside of the connectors were highly corroded.

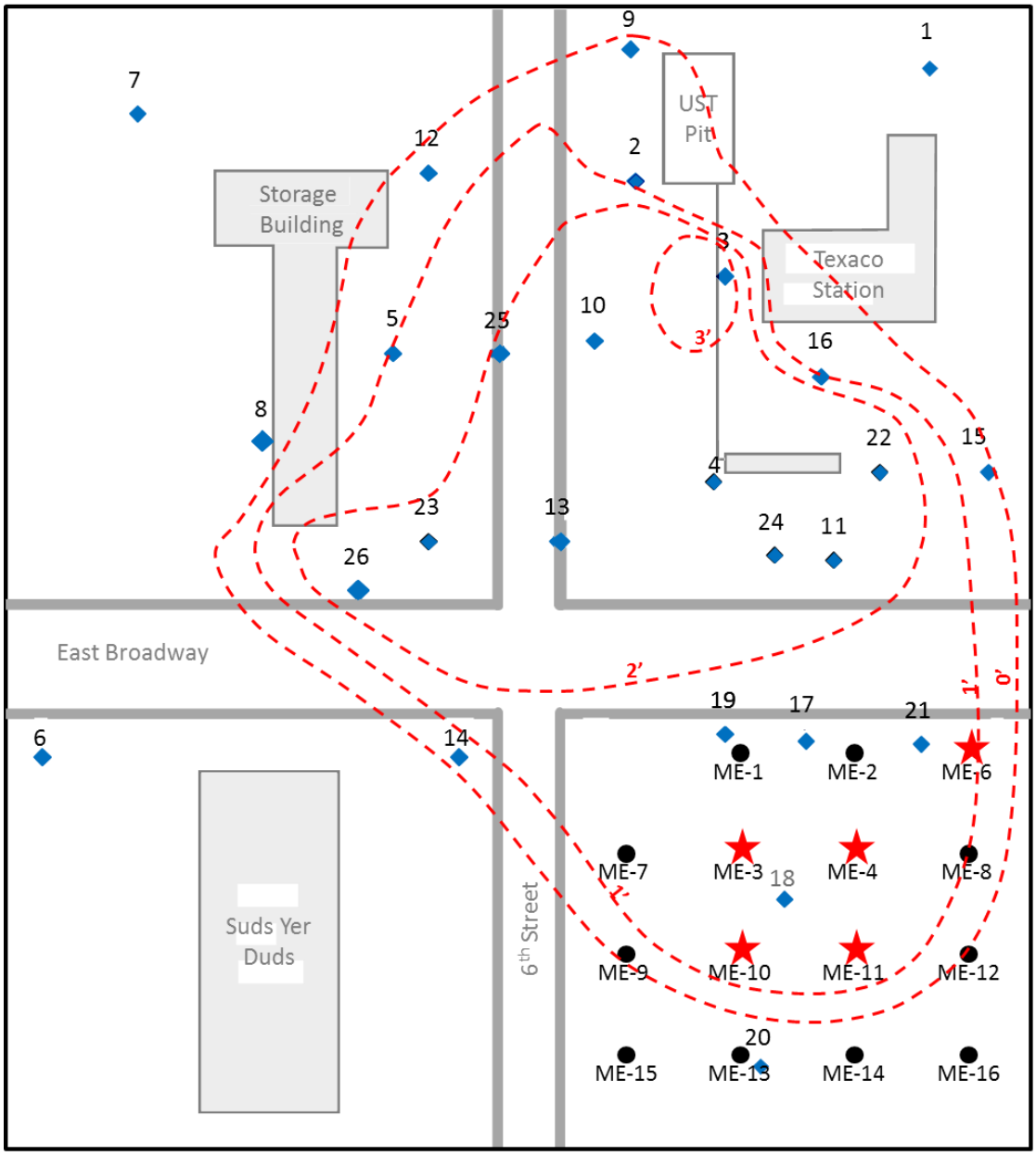

Figure 19. Map showing the location of the corroded cable connectors with red stars in relationship to the plume thickness (red dashed contours) in August 2009. Blue diamonds are monitoring wells (modified from Halihan et al., 2005).

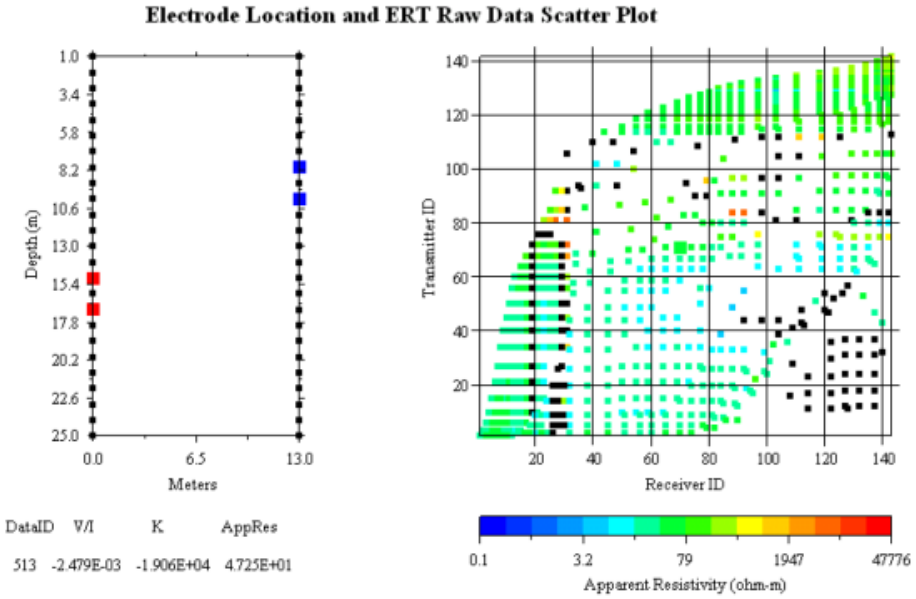

Figure 20. Electrode location and raw data scatter plot (from AGI manual, 2001).

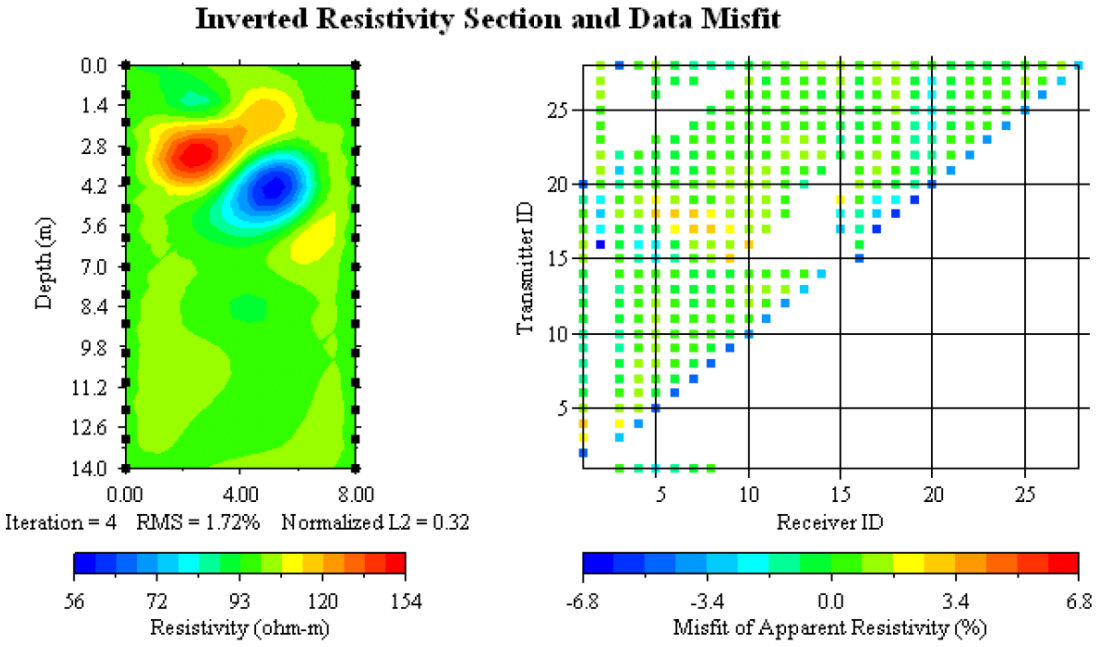

Figure 21. Resistivity and data misfit (from AGI manual).

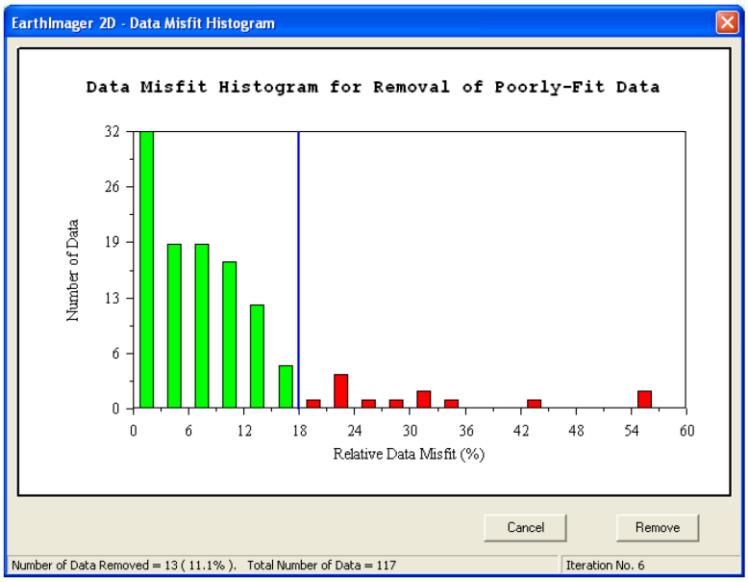

Figure 22. Data misfit histogram. The blue line represents the trim percent. The red bars show data that is being removed and the green bars show data that will continue to be inverted (from AGI manual).

SEISMIC

Two lines of surface wave seismic data were collected. The lines are 7348 and 13N (Figure 23). Seismic data were acquired and processed using MASW techniques from the Kansas Geological Society (SurfSeis/MASW Workshop, 2009).

Data Acquisition

Based on KGS guidance the following parameters were determined using the dimensions of the site:

- Forty-eight, 14 Hz geophones at one meter spacing;
- Shot points at every other geophone beginning 2 meters (twice the geophone interval) to the west or south of the first geophone; and
- A sampling interval of 0.5 ms with a 30s recording interval.

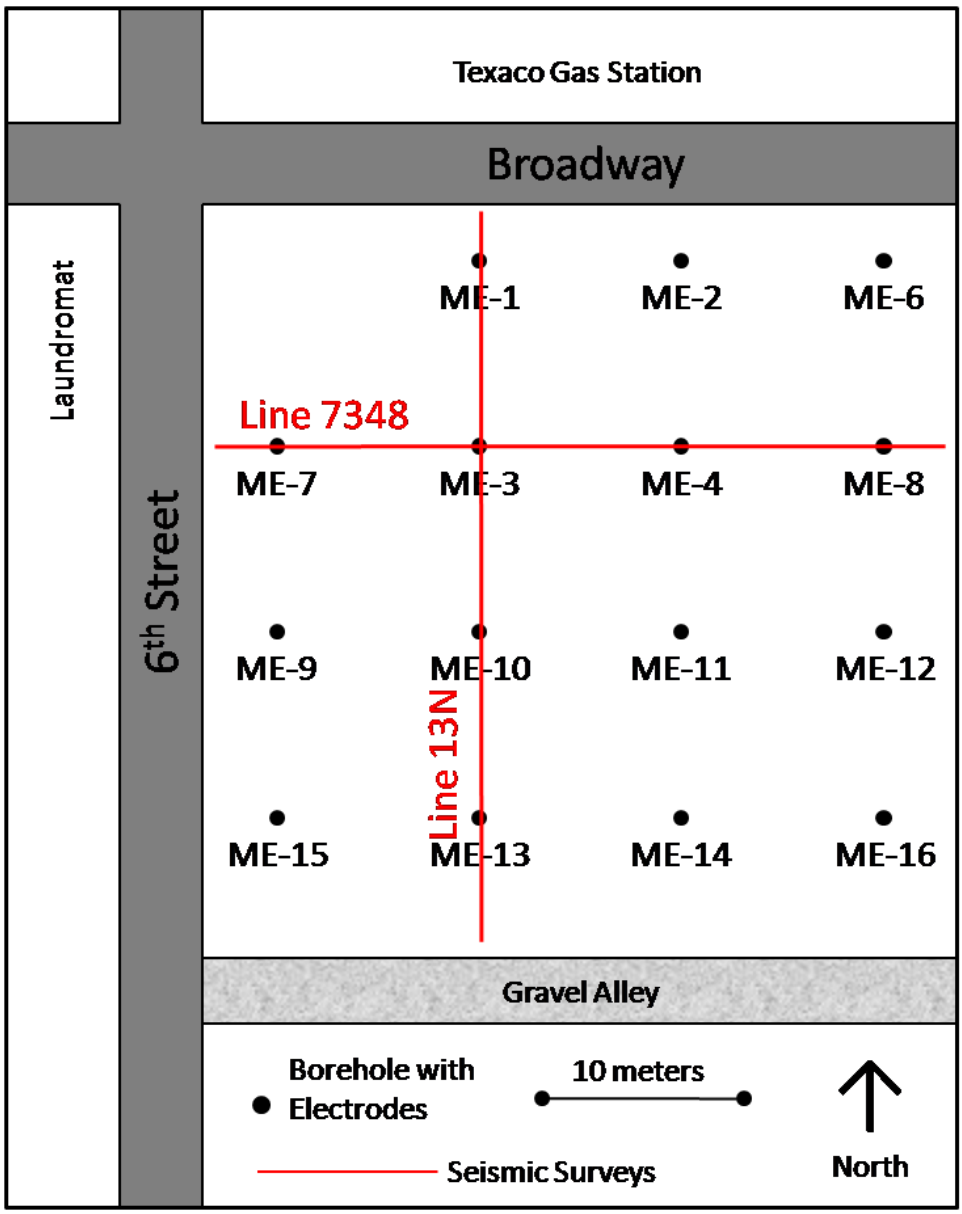

Figure 23. Site map showing the location of the seismic lines.

Data Processing

The data were processed using SurfSeis 2.05. The basic processing outline used for this data set is seen in Figure 24. When the line is acquired, a separate file is recorded for each shot point in .segy format. In order to use the KGS software the data files must be converted into a .kgs format first. Once this is done all of the shot points for each line must be compiled to a file for that line.

Once the line file was generated, the data are split into passive and active data by trimming at 2 seconds. The active data are the first two seconds of the 30 second recording time and the passive data are the last 28 seconds. The acquisition parameters are then assigned to each line. For the active data the geophone spacing, distance from the first shot to the first geophone, and the unit of measurement was input. For the passive data the geophone spacing, geophone numbers, and distance to the nearest perpendicular street were entered.

Next a dispersion analysis is conducted on each shot point for both passive and active data. This generates a graph showing phase velocity versus frequency (Figure 25). Recall from Chapter II that one property of surface waves is dispersion. Figure 25 is an active dispersion curve. Most of the dispersion curve energy is located in the lower left and you can clearly see the fundamental mode versus the higher modes.

Several of the dispersion curves had contamination from the higher modes making it difficult to determine the fundamental mode. An overtone curve is extracted from the fundamental mode, which then allows for analysis using inversion algorithms. Figure 26 shows the same shot location but is the passive dispersion curve. Note how the dispersion energy is less focused in the fundamental mode. Once an overtone curve has

been extracted for each shot point in the active and passive data they are combined. This generates a new dispersion analysis and an overtone curve is selected (Figure 26).

The last step is an inversion of each combined overtone curve, which generates a one-dimensional ten-layer velocity model at each shot location (Figure 27). Then each ten-layer model is used to generate a cross section of the shear wave velocity for the line.

For Line 7348 active, the pre-processing velocity range of 10–3000 m/s with a dominate frequency of nine Hz. The software noted that there was a high risk of contamination from higher modes in the dispersion analysis because of poor input data quality. During overtone processing the following settings were used for both the passive and active data: low contrast setting was used with a phase velocity of 5–1000 m/s and a frequency range of 5–30 Hz. Several of the shots located at the east end of the line did not have good dispersion data and an overtone curve was not selected; therefore, ~~so~~ they were not inverted and a ten-layer velocity model was not generated.

For Line 13N active, the pre-processing velocity range was 10–3000 m/s with a dominate frequency of 11 Hz. This line also had a high risk of contamination from higher modes. For processing low contrast with a phase velocity of 0–1000 m/s and a frequency range of 0–30 Hz was used. Several of the dispersion files were too noisy to pick an overtone curve and were not used for the final inversion.

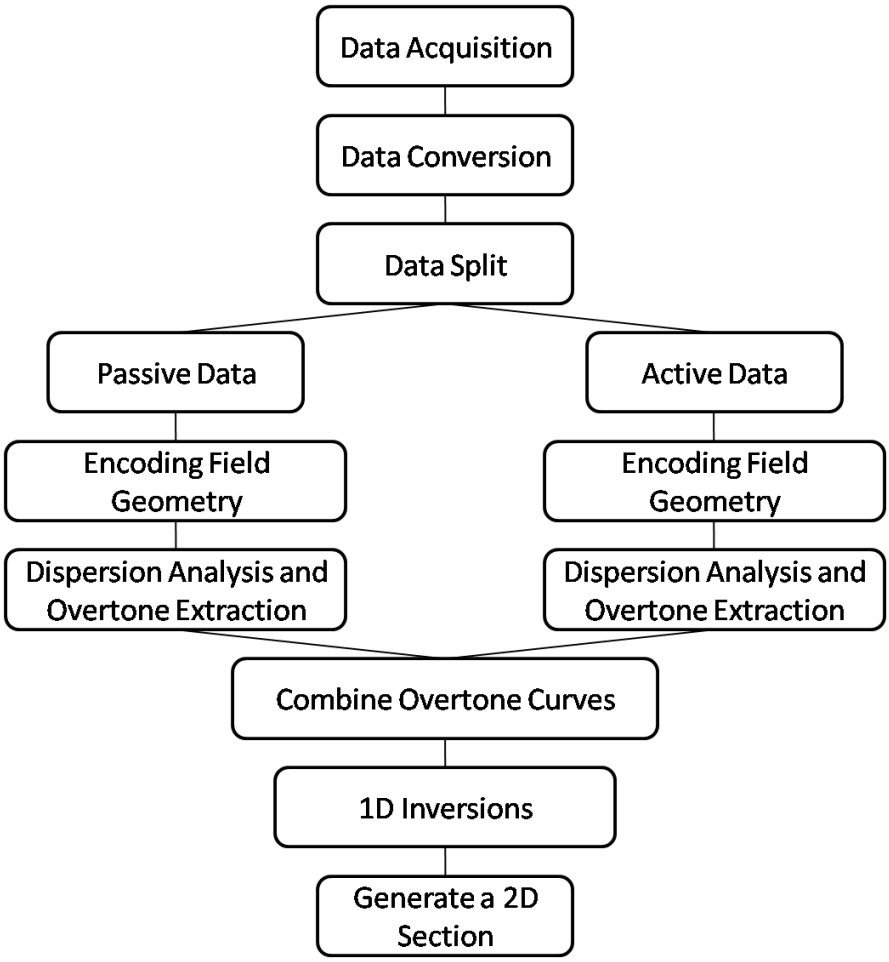

Figure 24. Outline of data processing for SurfSeis 2.05.

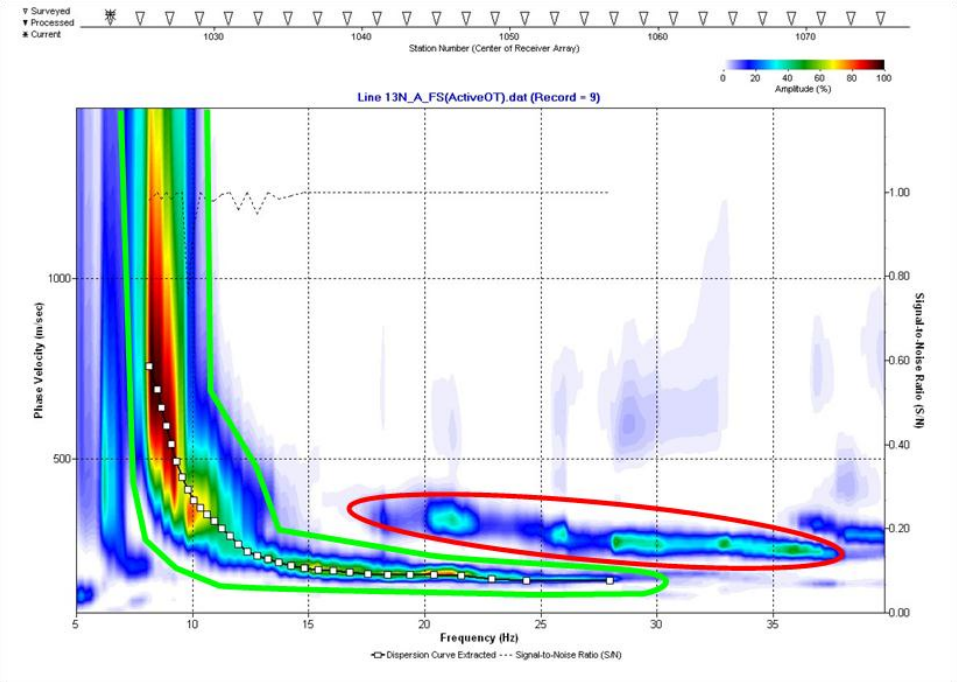

Figure 25. Active dispersion analysis and overtone curve extracted (white squares) for active data only. The area circled in green is the fundamental mode and the red circle shows the higher modes.

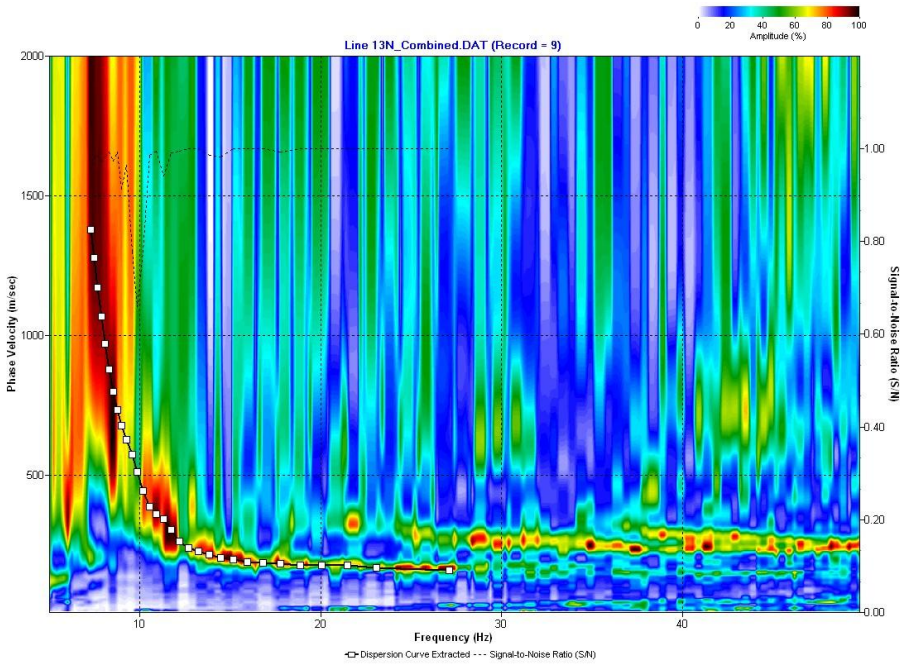

Figure 26. Combined dispersion analysis and overtone curve extracted (white squares).

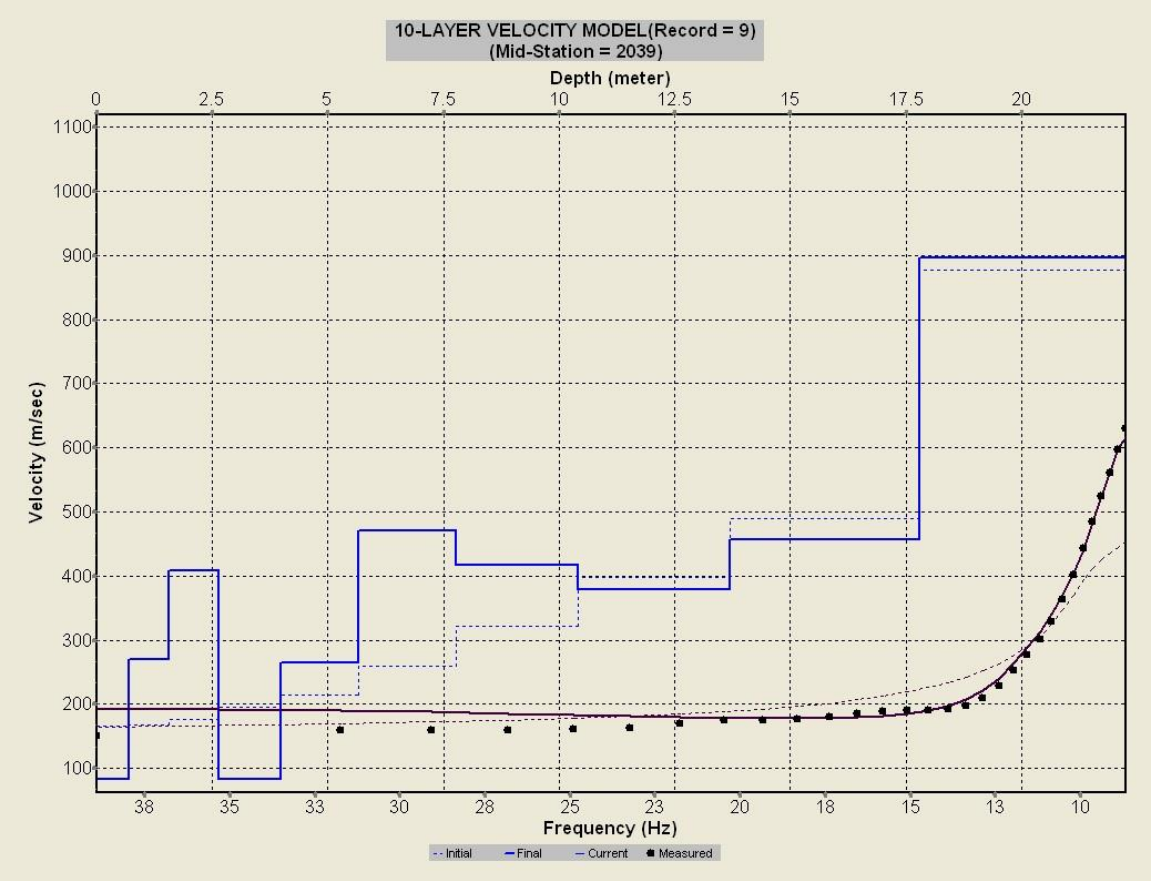

Figure 27. 1-D shear wave velocity profile of the extracted overtone curve from Figure 25.

CORE

Core Collection

Prior to core sampling, three locations were identified based on the ERT results. The cores were located halfway between ME-10 and ME-03, ME-10 and ME-14, and ME-08 and ME-06 (Figure 28). In order to collect the core, a direct push Geoprobe was used. The Geoprobe was lined up and leveled at all three locations then rod systems were pushed into the ground using the probe hydraulics and hammer (Figure 29). The cores were 1.5 inches in diameter and were gathered in continuous four-foot tubes using the Dual Tube Soil Sampler Method. Because of the swelling nature of the soil, only three feet of soil were collected per four-foot tube.

After all cores were collected, they were labeled based on the two wells they were between, arrows were drawn indicating the top, and caps were attached to the top (red) and bottom (black). Cores were collected until the lowest sand unit was reached. This gave a total core length of approximately 30–33 feet. Upon return to campus the cores were placed in a cooler to prevent volatilization of any vapors present.

Core Analysis

An analysis of the cores was completed using photoionization detection (PID), core description, and BTEX analysis.

Photoionization Detection

A photoionization detector (PID) is instrument used to determine the relative magnitude of volatile organic compounds in air samples but are unable to distinguish

between the different compounds (Daum et al., 2006). PIDs were originally designed as bench top laboratory instruments in the 1980s but the need to monitor USTs let to the design of a smaller more portable PID (Chou, 2000). This method has been used by the EPA as a general survey instrument at hazardous waste sites because of its real-time detection and ability to detect inorganic vapors (US EPA, 1994).

The following paragraphs are a description of PID and how it works. They are a summary of EPA SOP (1994), Chou (2000) and Daum et al. (2006). The basic design of a PID uses an ultraviolet light that ionizes gas molecules. The critical component of a PID is the lamp. This lamp produces photons in the ultraviolet range. The lamp is commonly a 10.6 eV lamp, this allows for gasses that have values greater than the lamp are not read. Compounds that can be read by the 10.6 eV lamp include but aren't limited to benzene, aromatic compounds, ammonia, ethanol, and acetone. These gasses include water vapor, carbon dioxide, nitrogen, and oxygen.

When sampling, a small air pump is attached to the device and held to the sample, pumping air into the PID where it passes in front of the lamp exposing it to ultraviolet radiation. Once the gas is exposed to the UV light, molecules that have an ionization potential less than that of the lamp release an ion. Within the PID there are two electrodes, one negative and once called a collector electrode. The negative electrode forces the ions to the collector electrode and a current is produced proportional to the concentration of the gas present in the chamber. The resulting output is a gas concentration displayed in parts per million.

The PID used for this project was a Thermo Environmental Instruments, Inc, Model 580B. The procedure we used was to first cut a small hole into the core tubing

using a drill, place the suction cup of the PID over the hole and record the values (Figure 30). This was repeated for every six inches of core. Calculations were performed on some of the core with swelling clays to determine the approximate half-foot locations.

Core Descriptions

The cores were not opened and filed down as done by McPhail (2003) because they are going to be analyzed for magnetic susceptibility in a sister dissertation. They were examined to ensure that the main lithological boundaries were consistent with the cross sections drawn by McPhail (2003).

Geochemistry

After the core descriptions were completed, the areas of interest based on the PID data, were sampled and sent to Environmental Testing, Inc., in Oklahoma City. A BTEX analysis was conducted.

GROUNDWATER SAMPLES

Groundwater samples were collected from three monitoring wells located on site: MW-18, MW-19, and MW-20; and two monitoring wells located north of the site and closer to the origin of the contamination: MW-2 and MW-10 (Figure 31). For each well two unfiltered liter containers were collected and four 10 mL vials were collected using a 0.45 μm filter.

The samples were obtained using a peristaltic pump located approximately two meters above the bottom of the monitoring well. Water was pumped into a flow cell

where a YSI probe was inserted. The YSI was used to collect the temperature, electrical conductivity, percent dissolved oxygen, and total dissolved solids, oxidation reduction potential, and pH of the water. The water was pumped through the flow cell until the YSI readings stabilized. Samples were then collected directly from the flow meter and the YSI values recorded. Samples were returned to the lab and refrigerated until sent to Dr. Eliot Atekwana at Oklahoma State University and Environmental Testing, Inc., in Oklahoma City for geochemical analysis.

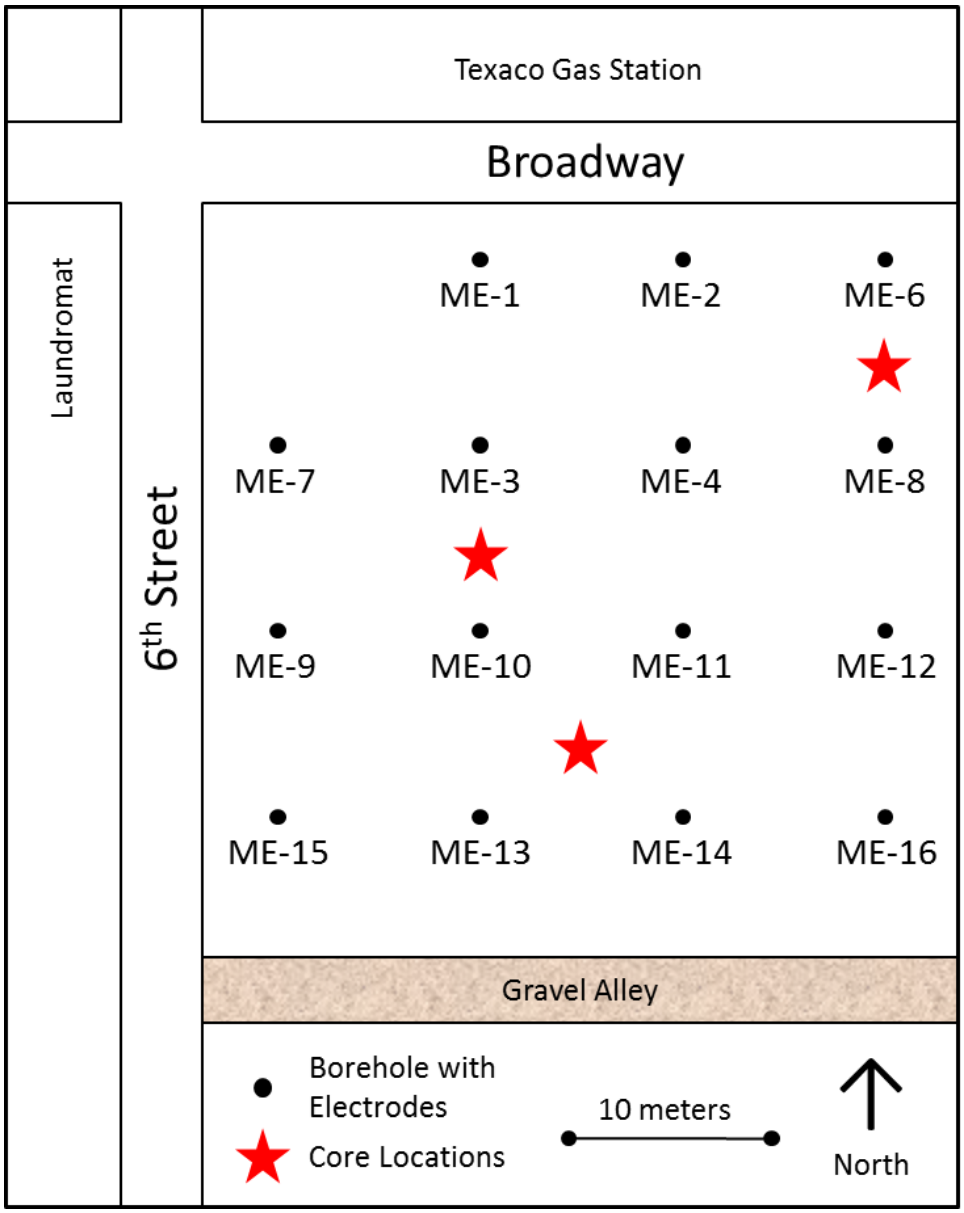

Figure 28. Map showing the location of the cores (red stars) in relationship to borehole locations (ME).

Figure 29. Geoprobe operation.

.

Figure 30. PID in use on core.

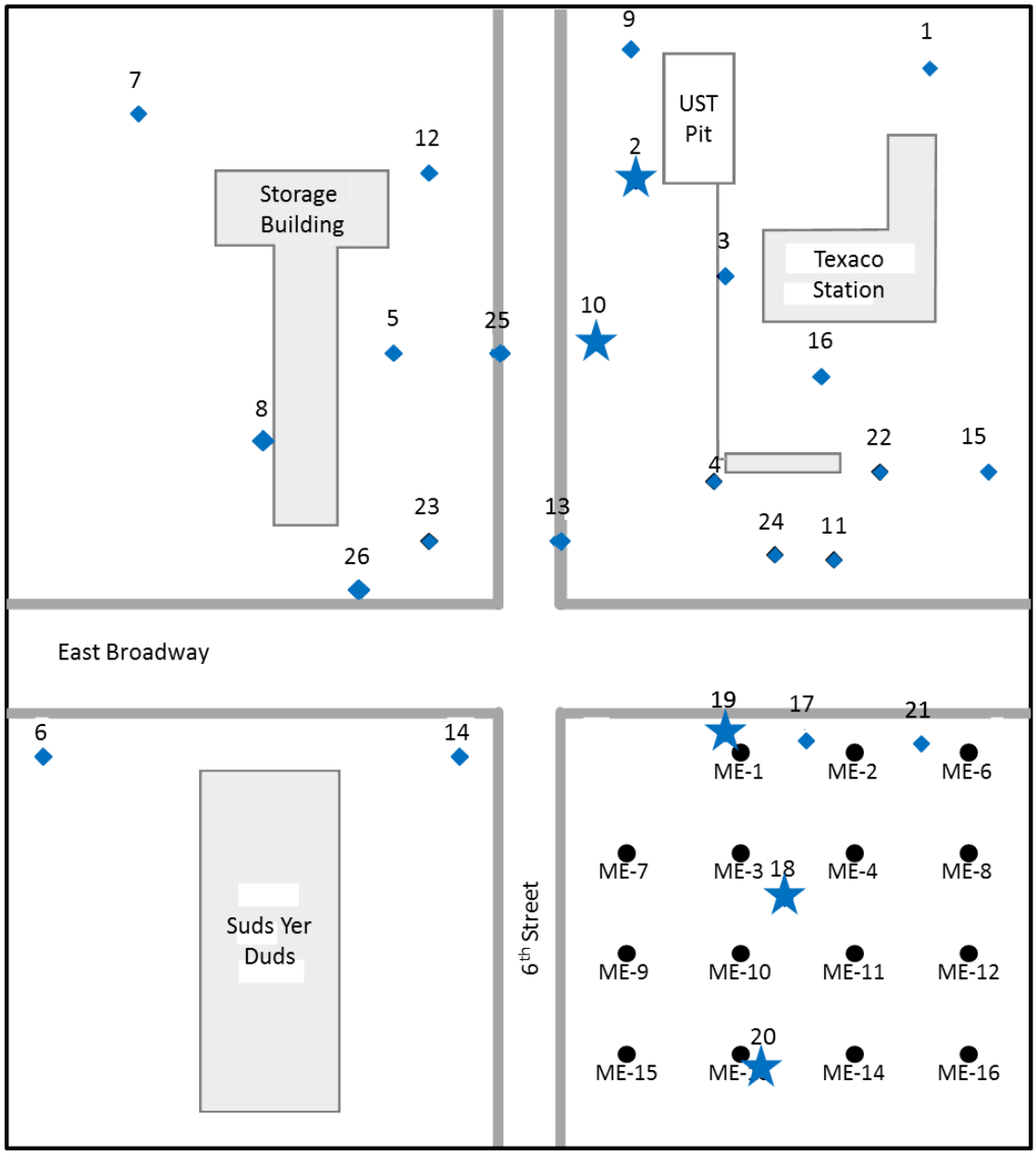

Figure 31. Site map showing the location of all monitoring wells (blue diamonds) and the sampled wells (blue diamond). The source of the LNAPL is the UST pit to the north of the site (modified from Halihan et al., 2005).

CHAPTER IV

RESULTS

ERT DATA

May 2010 ERT

The May 2010 ERT results show that overall the site consists of three geoelectrical layers. These layers are illustrated using Line 07030408 (Figure 32). The uppermost layer extends from the surface to approximately 2 meters below the surface with an apparent resistivity range of 24–56 Ω-m. The middle layer extends from approximately 2–8 meters below the surface with an apparent resistivity range of 5–16 Ω-m. Within this layer there are some high resistivity anomalies. The lowermost layer extends from approximately 8 meters to the bottom of the section (~12.5 meters). The overall resistivity of this layer is 18–26 Ω-m with some high resistivity (26–40 Ω-m) anomalies. These three layers are consistently seen throughout all of the ERT data. The individual profiles and diagonal lines can be seen in Appendix A.

When examining Line 07030408 (Figure 32), it is apparent that there are some anomalies that are located vertically next to the location of the boreholes. McSorley (2003) called these borehole effects; anomalies**,** produced as the result of air being trapped in the ground around the borehole. When one removes data points located around the boreholes**,** the majority of the borehole effects are removed from the data (Figure 33).

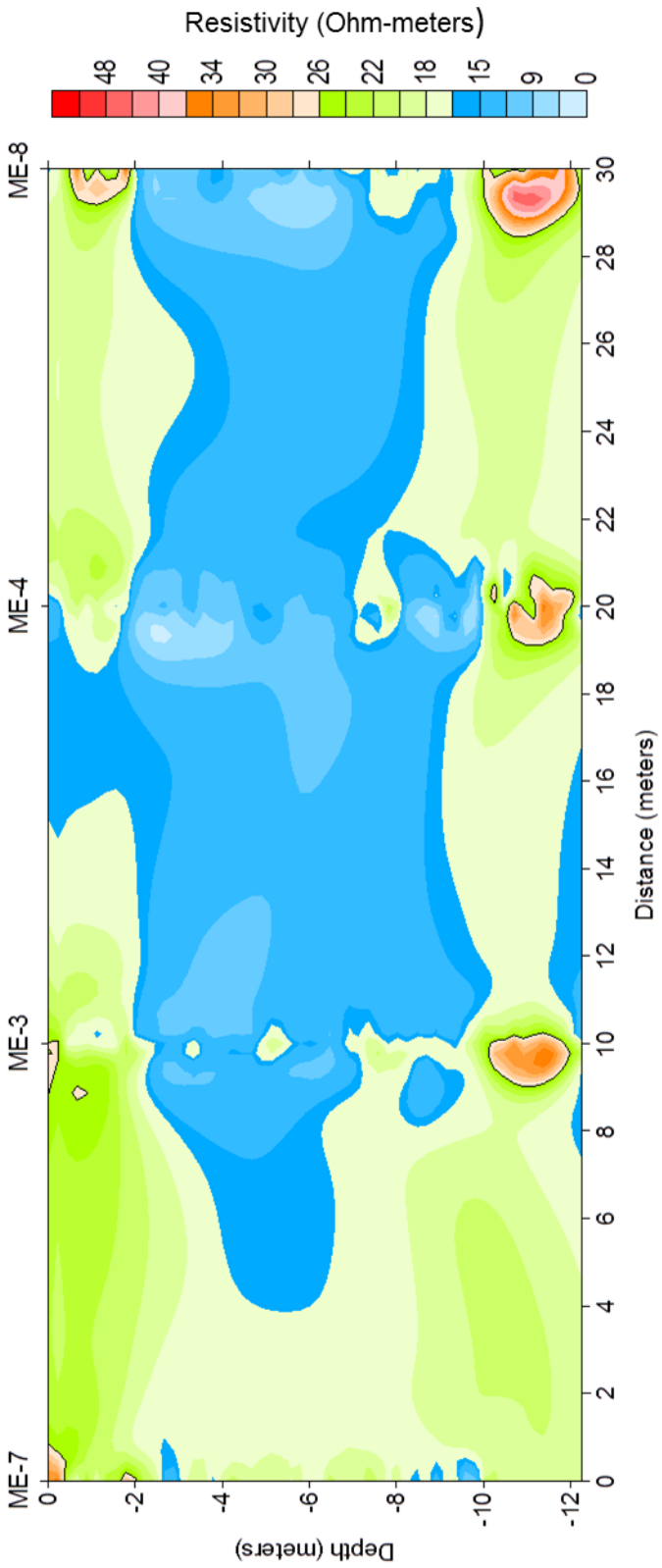

Figure 32. ERT data for Line 07030408 from May 2010.

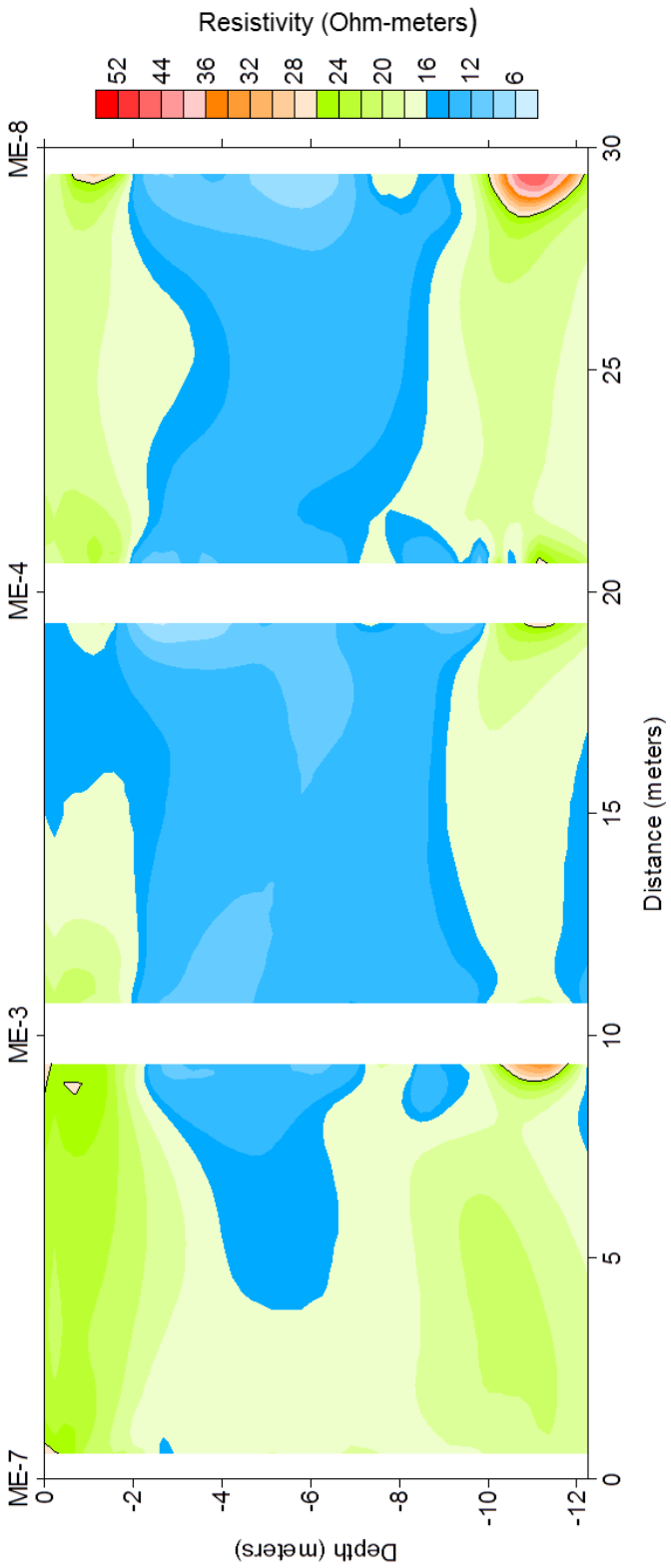

Figure 33. ERT data for Line 07030408 from May 2010 with the borehole effects removed.

March 2011 ERT

After cores were acquired, ERT data were gathered again in order to check for any changes in the subsurface electrical properties. Some additional lines were acquired because of faulty data from dirty electrode connections, which produced poor apparent resistivity profiles. The lines that were re-collected include 0806, 1416, 1509, 1510, and 1513. The results were the same three geoelectrical layers seen in the May 2010 ERT data. The lines can be seen in Appendix B.

Transient ERT

Data acquired by McSorley (2003) were used with the data collected for this study to produce a time-lapse model of the site.

December 2002 – January 2003

The first data set is from December 2002 to January 2003. The transient 2D images all show the same type of change that is illustrated with Line 07030408 (Figure 34). The change in resistivity for this line is from −15% to +15%. There are some anomalies located along the borehole for ME-10 and ME-3 that show a change from −40% to +30% resistivity change and −40% to 0% resistivity change, respectively. The remaining transient ERT images from December 2002 to January 2003 can be seen in Appendix C.

December 2002 – May 2010

The second data set is time-lapsed from December 2002 to May 2010. Some of these images vary greatly from line to line**,** but the majority of the lines show results similar to Line 07030408 (Figure 35). This transient data set typically shows three layers of resistivity changes. The uppermost layer extends from the surface to between 1.5 and 2 meters below the surface and displays a change from –40% to 0% in resistivity. The middle layer extends from the bottom of the top layer to a depth of approximately 8.5 meters with a change in resistivity from 0 to +45%. The lowermost layer extends from approximately 8.5 meters to the bottom of the section with a change in resistivity similar to that of the uppermost layer. The remaining transient ERT images can be seen in Appendix D.

May 2010 – March 2011

The third data set is time lapsed from May 2010 to March 2011. In this data set there is very little change in the resistivity, –10% to +10% (Figure 36). Of the four additional panels acquired**,** the transient results differ greatly.

In Line ME-08 to ME-06 the results are similar to those seen in transient data set one with a very small percentage change in a vertical pattern (Figure 36). There are some high percentage differences along the boreholes ranging from –30% to greater than +70%.

Lines ME-14 to ME-16 (Figure 30) and ME-15 to ME-9 show similar results. In these lines there is a horizontal variation in the percent difference of resistivity. The upper layer (same as the uppermost geoelectric layer in the May 2010 data) shows a great

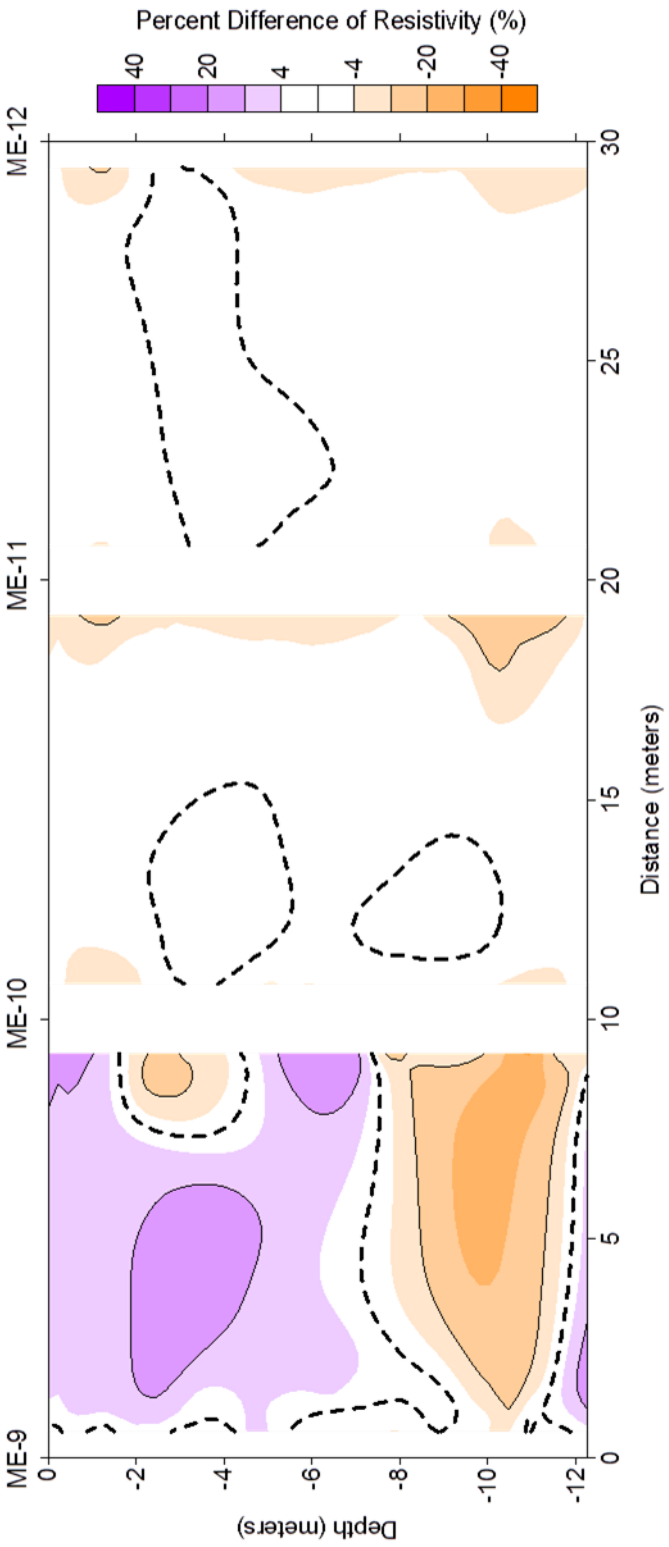

Figure 34. Transient ERT of Line 07030408 from December 2002 to January 2003 with borehole effects removed. ME-7 is to the west and ME-12 is to the east.

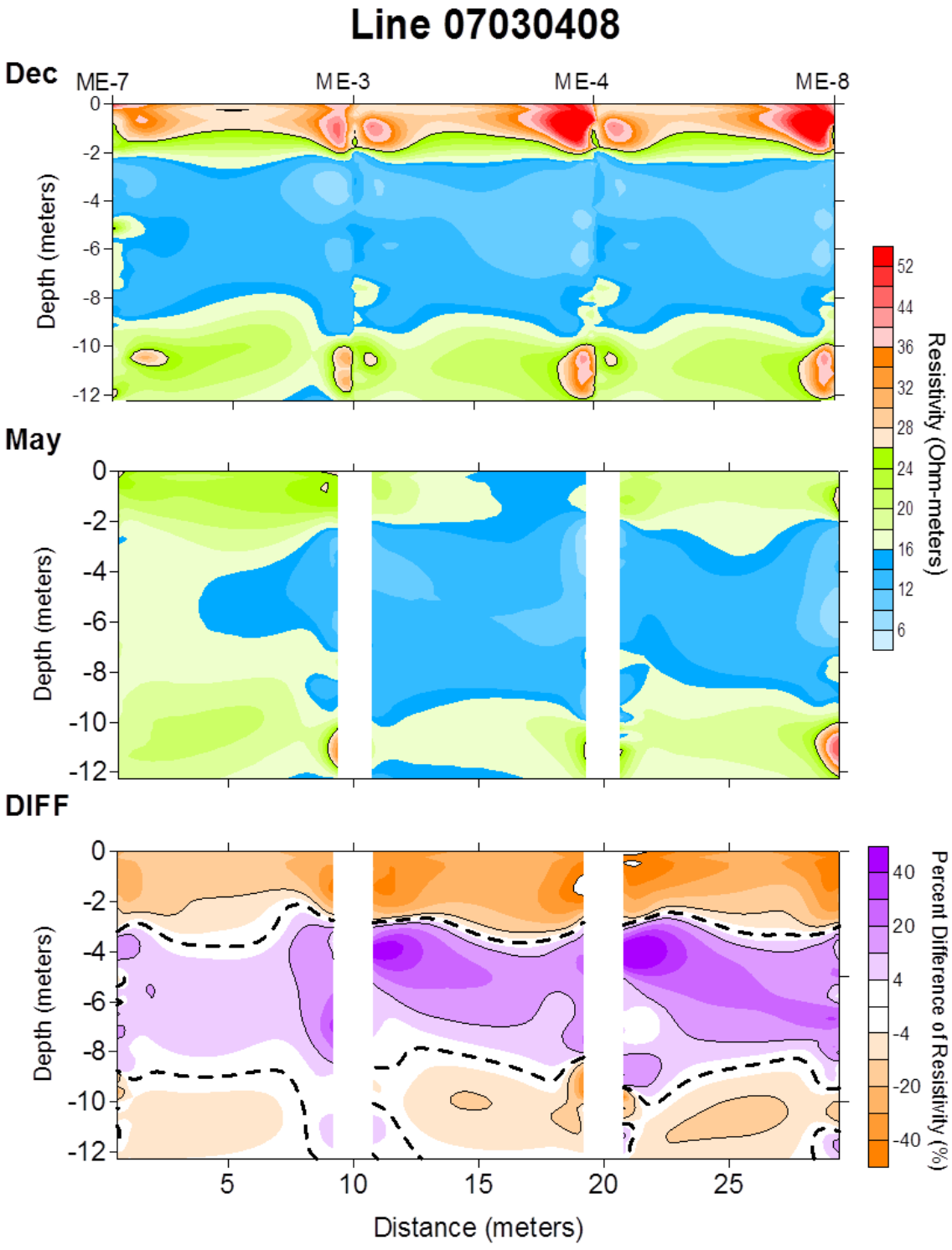

Figure 35. Transient (bottom) ERT of Line 07030408 from December 2002 (top) to May 2011 (middle) with the borehole effects removed in the May 2010 and transient images. The left of the line is west and the right side of the line is east. The heavy dashed line in the transient image represents 0% change in resistivity.

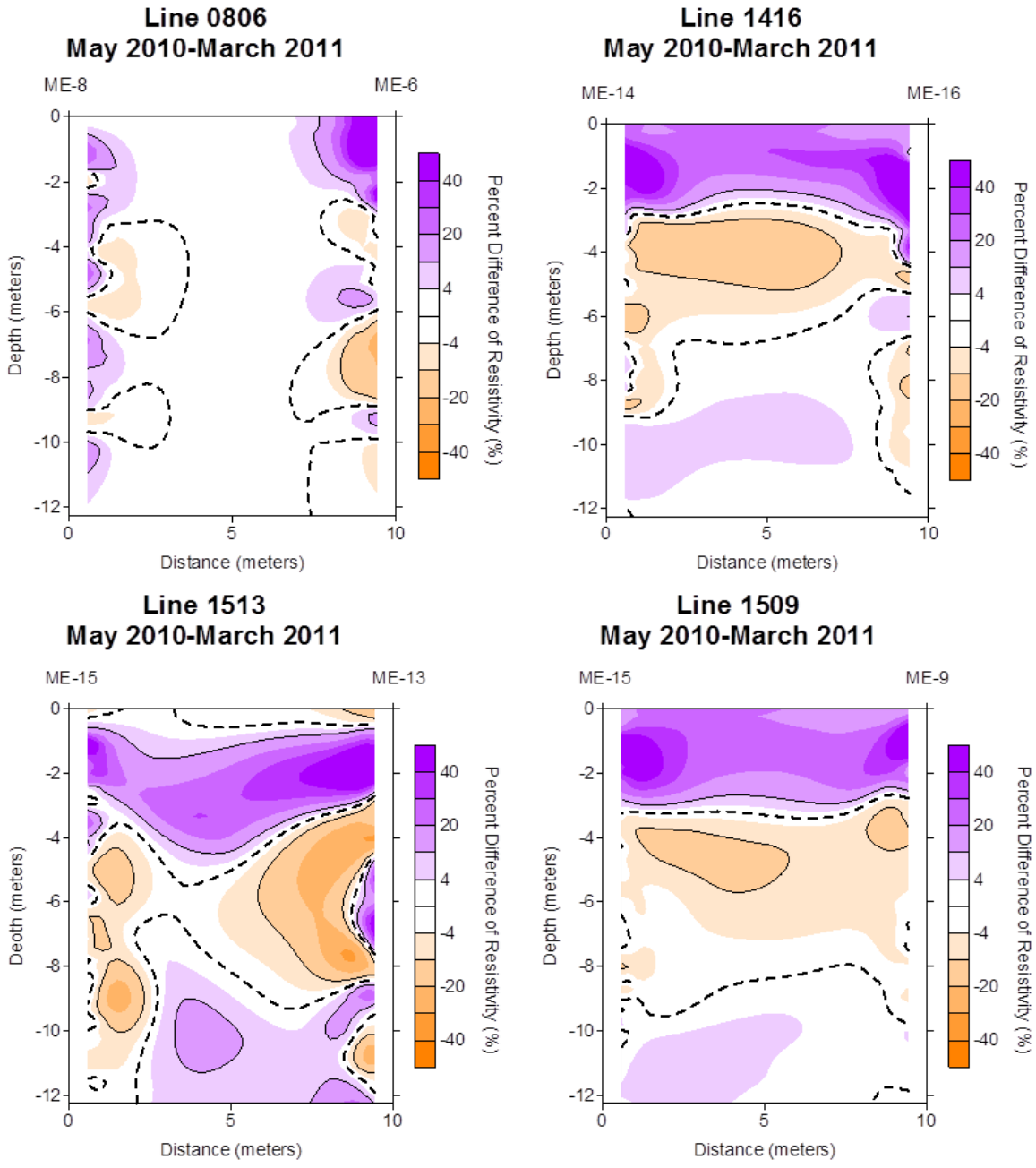

Figure 36. Transient ERT from May 2010 to March 2011 with the borehole effects removed.

range of resistivity, 0% to greater than +70% difference. The middle layer shows a resistivity change of –20% to 0%. The lowermost layer has a change in resistivity from 0% to +10%.

Line ME-15 to ME-13 shows both vertical and horizontal changes in resistivity, making it the most complicated of this data set (Figure 36). The horizontal changes occur in the center of the section and have similar resistivity ranges as those layers demonstrated in ME-14 to ME-16 with the exception of layer two. Layer two shows a higher negative percent change to –40%. The vertical changes occur around the boreholes of ME-14 and ME-16 with the changes ranging from –30% to greater than +70%.

MASW DATA

Line 7348 was aquired west to east approximately 20 meters south of Broadway street (Figure 37). The line is 30 meters long, extending from ME-7 in the west to ME-8 in the east. The cross section can be broken into thee main velocity layers. The first layer extends from about 1 meter in depth to approximately 7 meters and has an average velocity ranging from 200–300 m/s. Within the first layer there are localized velocity pockets of 100 and 300 m/s. The second layer is directly beneath the first and has an average velocity from 300 to 450 m/s and extends to a depth of approximately 17.5 meters. The lowermost velocity zone extends from 17.5 meters to the bottom of the data with a velocity range of 450 m/s to 900 m/s. There is a localized area that has a shear wave velocity greater than 500 m/s. Thre are two anomalous features located in the second layer centered at approximately 2.5 meters horizontal distance. The first, more

shallow anamoly is centered at 10 meters depth and has a higher velocity than layer two. The second is centerd at 16.5 meters with a velocuty that is lower than layer two. The contact between the layers is an undulating surface. Also, note the sharp angle in layer two on the eastern end of the line. This is most likely the result of poor data quality caused by contamination of the fundamental mode as described in the Methods chapter.

Line 13N was acquired south to north (Figure 38). The line is 30 meters long and extends from ME-13 in the south and ends at ME-8. The same three velocity zones from Line 7348 are seen in this line but the depths are different. The first velocity zone still extends from the surface to approximately 7 meters in depth and has the same velocity range as in the other line. The second velocity zone is not as thick as in the previous line. The depth for layer two is from approximately 7 meters to 13 meters. The third velocity zone extends from 13 meters to the total depth of the data. There three anomalies in this line The first is a very concentric higher velocity zone centered at 15 meters distance and 4 meters depth. The second anomaly is a lower velocity zone in layer three. It is centered at 18 meters depth and 10 meters distance.

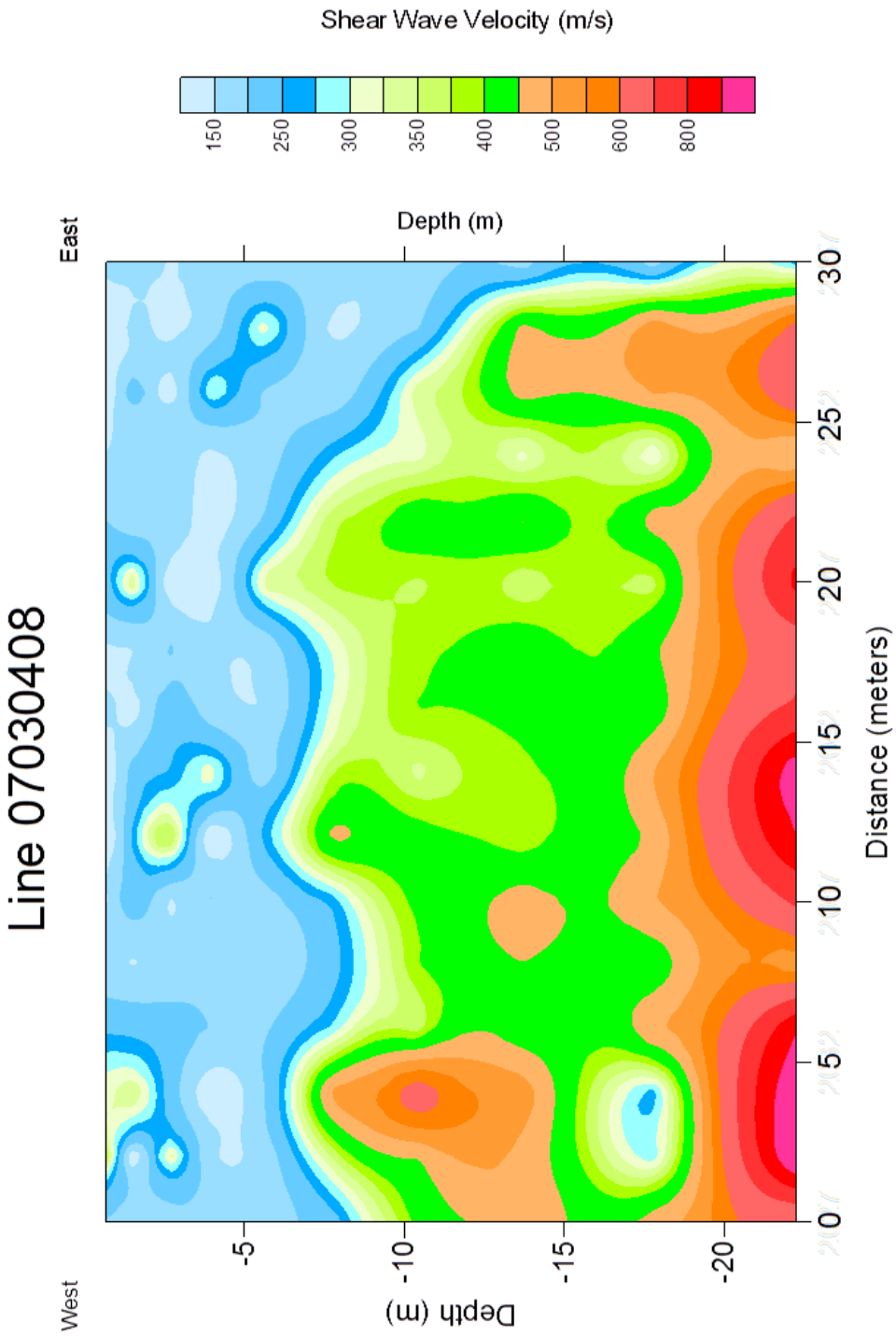

Figure 37. MASW results of Line 7348. Electrode boreholes are located at the following distances: ME-7 is located at 0 meters, ME-3 at 10 meters, ME-5 at 20 meters, and ME-8 at 30 meters. A 1-D profile for this line can be seen in Figure 26.

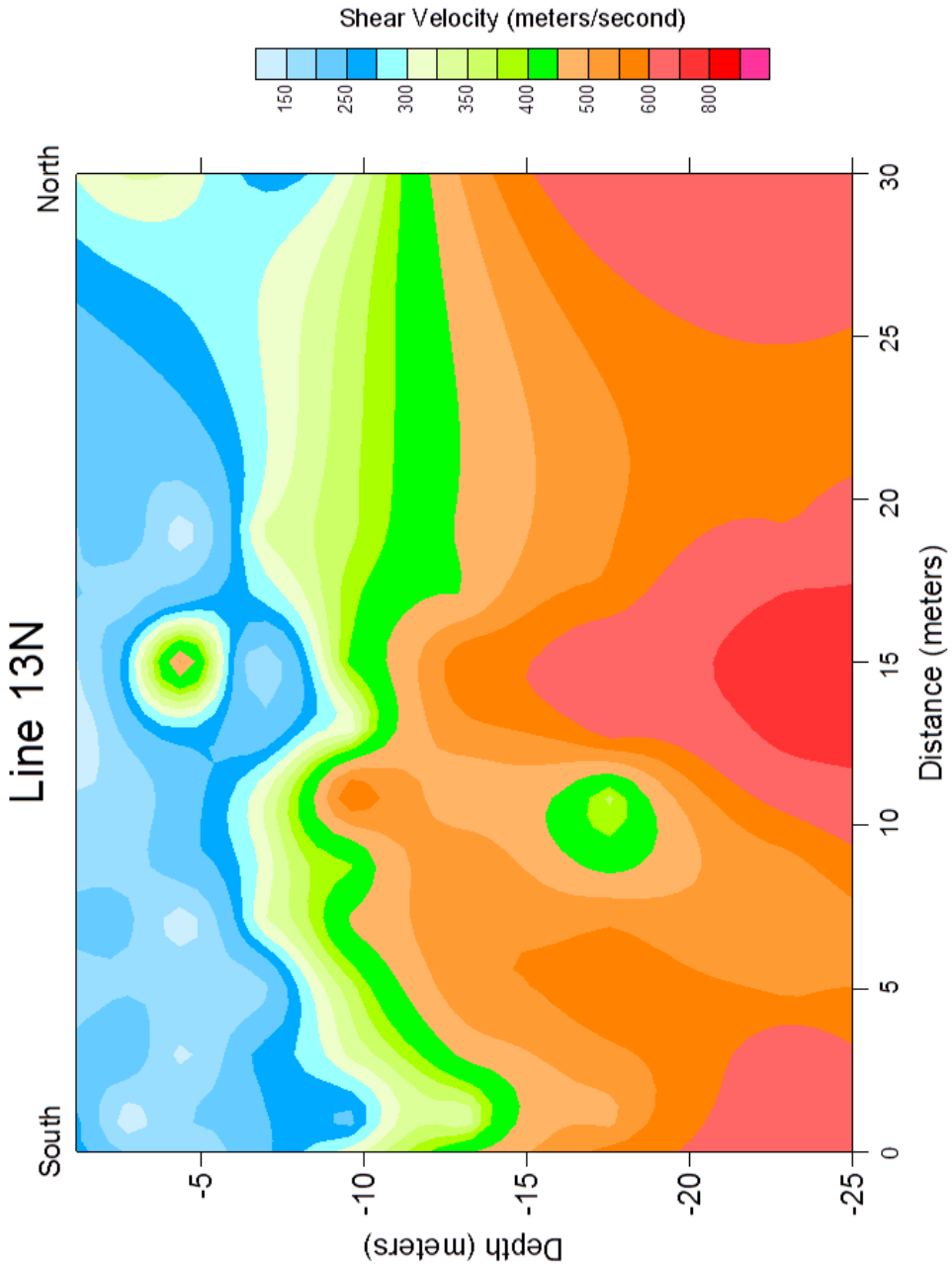

Figure 38. MASW Line 13N. Electrode boreholes for ME-13, ME-10, ME-3, and ME-2 are located at 0, 10, 20, and 30 meters respectively.

CORE SAMPLES

The lithology of the cores was consistent with that of McPhail (2003) data and cross sections; therefore, a detailed grain analysis was not performed.

PID Results

Photoionization detection (PID) was used approximately every six inches along the core. The results were plotted as depth versus value in Figure 39. The peaks were used to determine the locations of core samples for BTEX analysis. In the core between ME-08 and ME-06 the PID values are negligible until a depth of 24 feet is reached. The values then oscillate between highs and lows with the highest value at 29.5 feet. The core between ME-10 and ME-03 had no detectable values until a depth of 26 feet. The values then increased to a maximum value at 33 feet then decreased to background. The final core, between EM-10 and ME-14 was negligible until 30.5 feet and reached peak value at 31.5 feet.

Geochemistry Results

The cores were analyzed for BTEX content at different depths (Table 2) based on the PID data. Two samples at depths of 15–15.5 feet and 29–29.5 feet for core 0806, and for core 1003, three samples at depths of 15–15.5, 29–29.5, and 34–35 feet were analyzed. Two samples from Core 1014 were analyzed at 15– 15.5, 31.5–32 feet. For all three cores, the shallowest sample (at 15–15.5 feet) showed less than 0.025 mg/Kg of BTEX, which was the detection limit. All of the deeper samples showed some BTEX (refer to Table 2 for values).

Table 2. Core sample geochemistry separated by core location and depth.

Core	Core Depth (feet)	Benzene (mg/Kg)	Toluene (mg/Kg)	Ethylbenzene (mg/Kg)	Xylene (mg/Kg)
0806	15–15.5	<0.025	<0.025	<0.025	<0.025
	29–29.5	1.92	5.61	5.14	28.9
1003	15–15.5	<0.025	<0.025	<0.025	<0.025
	29–29.5	0.484	5.52	4.99	29.2
	34–35	0.683	0.676	0.121	0.57
1014	15–15.5	<0.025	<0.025	<0.025	<0.025
	31.5–32	0.734	2.17	4.55	20.4

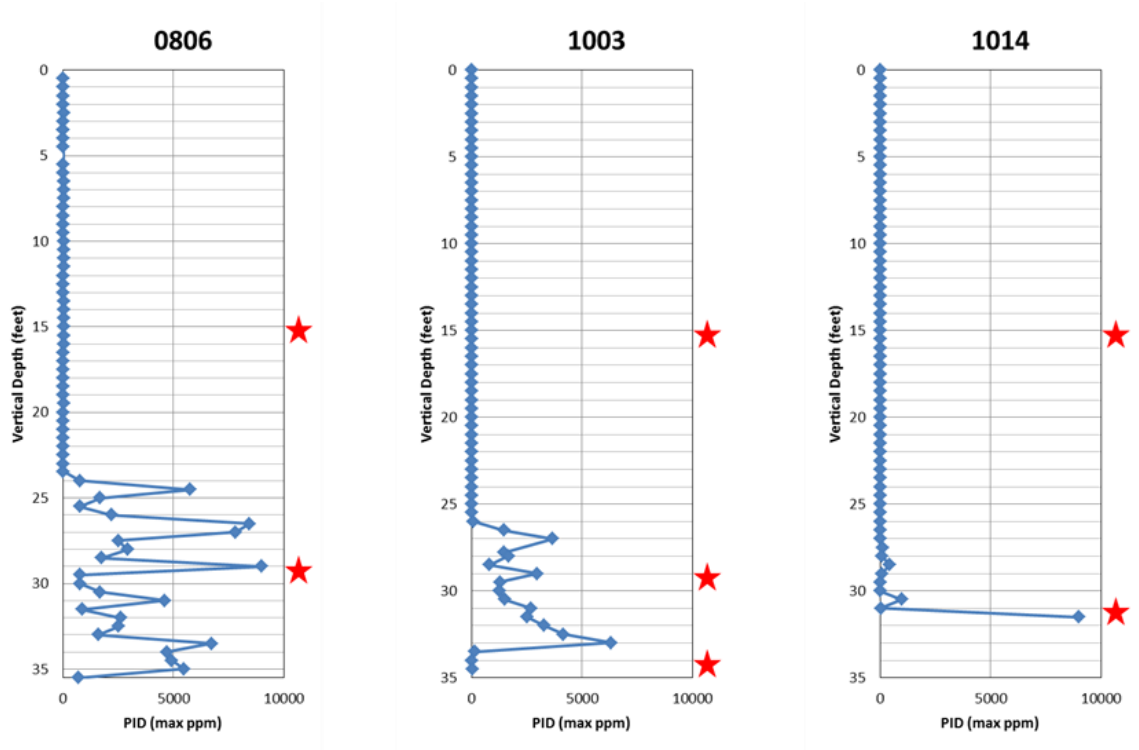

Figure 39. PID results of the cores from Enid, Oklahoma. The red stars indicate the depths of samples that were sent to Oilab in Oklahoma City.

GROUNDWATER DATA

The results of the groundwater BTEX samples are shown in Table 3. The highest overall values were seen in MW-18 and the lowest overall values were seen in MW-19. For locations of the monitoring wells refer to Figure 31.

The results from Dr. Eliot Atekwana are seen in Table 4. The results from groundwater samples taken in December 2002 are seen in table 5. This sample geochemistry for these samples was also performed by Dr. Eliot Atekwana. These results were used to look for any major changes in the February 2011 groundwater geochemistry. This was difficult due to the different wells that were sampled in 2011 versus 2002.

Table 3. Groundwater geochemistry from Environmental Testing Inc..

Well	MTBE (mg/L)	Benzene (mg/L)	Toluene (mg/L)	Ethylbenzene (mg/L)	Xylene (mg/L)
MW-02	0.093	0.54	0.109	0.005	0.225
MW-10	0.5	5.76	12.9	1.88	20
MW-18	0.363	3.41	9.53	2.33	17.4
MW-19	0.027	0.738	0.006	0.005	0.055
MW-20	4.56	8.79	0.05	0.063	0.122

Table 4. Groundwater geochemistry from Oklahoma State University for February 2011.

Well	WL (m)	EC (µS)	COND (µS/cm)	TDS (g/l)	DO %	DO (mg/l)	pH	ORP(mV)	C (mg/L)	SO4 (mg/L)	ALK (mg/L)	Na (mg/L)	K (mg/L)	Mg (mg/L)	Ca (mg/L)
MW-10	9.313	821	1390	0.904	36.0	16.00	5.9	-65.0	42.573	1.803	600	197.477	8.343	21.080	103.139
MW-18	9.210	951	1477	0.949	77.3	6.20	6.2	22.0	16.806	1.000	830	282.452	7.582	20.025	110.371
MW-19	9.280	864	1455	0.946	9.4	0.86	6.2	737.1	117.447	97.613	457	165.156	5.529	25.723	144.337
MW-2	9.310	254	1020	0.696	50.0	4.09	6.0	-110.5	22.740	5.299	359	79.688	5.931	14.985	80.193
MW-20	9.130	1031	1413	0.919	3.3	0.31	5.7	-1328.0	48.458	0.549	678	195.162	5.993	24.377	134.638

Table 5. Groundwater geochemistry from Oklahoma State University for December 2002.

Well	Date	Temp (C)	EC (µS/cm)	TDS (g/l)	DO (mg/l)	pH	C (mg/L)	SO4 (mg/L)	ALK (mg/L)	Na (mg/L)	K (mg/L)	mg/L (mg/L)	Ca (mg/L)
MW-4	12/1/02						87.34	37.54					
MW-6	12/1/02	21.94	1.283	0.826	3.11	6.88	103.58	127.11	404	149.64	4.67	18.65	119.33
MW-8	12/1/02	20.94	1.694	1.083	1.32	6.52	124.31	1.75	769	169.40	2.22	28.75	176.97
MW-12	12/1/02	26.29	2.313	1.485	0.57	6.74	136.99	3.43	1073	349.55	3.83	32.7	161.79
MW-14	12/1/02	23.51	1.695	1.087	0.37	6.69	32.48	177.08	604	262.21	4.35	18.71	107.94
MW-15	12/1/02	19.95	1.560	0.999	0.41	6.51	30.36	2.07	550	99.44	3.85	27.84	173.56
MW-16	12/1/02	20.19	1.589	1.017	0.70	6.74	113.05	2.15	641	247.38	3.03	17.22	100.31
MW-17	12/1/02	20.89	1.358	0.868	1.81	6.56	104.81	4.11	519	176.58	2.29	21.19	120.22
MW-19	12/1/02	21.28	1.572	1.007	2.90	6.59	181.32	212.52	413	174.57	3.28	25.19	153.15
MW-20	12/1/02	19.25	1.507	0.965	1.49	6.54	95.26	10.68	45	211.06	2.55	19.77	112.04
MW-22	12/1/02	20.18	2.617	1.033	0.52	6.52	174.19	83.84	528	171.24	2.46	24.68	146.02
MW-23	12/1/02	20.88	1.514	0.971	0.83	6.72	133.47	118.91	472	146.60	2.63	22.60	144.06
MW-24	12/1/02	21.21	1.626	1.041	0.90	6.65	158.39	221.64	409	161.36	3.31	24.85	145.08
MW-25	12/1/02	21.20	1.854	1.182	2.16	6.48	149.62	108.27	579	185.10	2.44	25.76	158.68
MW-26	12/1/02	20.84	1.754	1.116	0.44	6.7	145.34	106.46	594	212.47	2.49	23.32	133.8

CHAPTER V

DISCUSSION

GROUNDWATER GEOCHEMISTRY

Using the method from Lipson and Siegel (2000), Luhrs and Pyott, Worthington and Perez (1993), and (1992); several ternary diagrams of the Enid site geochemistry were generated by year and by distance away from the source. In the ternaries in Figures 40-42, the red circles are labeled with the monitoring well (MW) number, and its distance from the UST pit (source) or the date the samples collected. A blue circle represents a signature similar to the source. Pink arrows indicate biodegradation and green arrows indicated volatilization. The ternaries, when compared to the literature, allowed for determination of processes affecting the LNAPL at this site.

Figure 40 shows the data divided by year. The first samples, collected in 2000, were determined to represent the source contamination signature. As the years have passed, there is a distinct signature in the data indicating biodegradation and volatilization. Figure 41 illustrates the site geochemistry for 2011. This is the data set collected and presented in Chapter IV. As seen with the previous years' data, there is a movement toward biodegradation in some wells and toward volatilization in others.

Unfortunately, a more complete data set is unavailable for this site because of the testing parameters used by the consulting company. Data from other years can be found in the OCC report, case number 064-2182. Because of this, there are only a few wells that have consistent data for the site; one of these is MW-20. The data for this monitoring well is presented in Figure 42 and shows a definite biodegradation signature. When multiple wells are plotted in ternary diagrams a map can be generated showing areas of biodegradation and volatilization (Figure 43). The ternary diagrams for each well used to make the map are located in Appendix E.

The other geochemical data from Dr. Eliot Atekwana at Oklahoma State University do not appear to have been the cause of the changes in resistivity. The values are similar to the data collected in 2002. The main changes observed were in the EC measurements and the TDS in MW-19 and MW-20, which are the only two wells sampled both years. The increase in TDS and EC can be explained using Atekwana et al., 2004a and 2004b. In these papers an increase in TDS and EC was due to the presence of hydrocarbons undergoing biodegradation. Thus, the groundwater chemistry and ternary diagrams are both consistent with biodegradation of LNAPL occurring on the site.

ERT

The May 2010 and March 2011 data sets can be interpreted using the same three geoelectrical layers. The data sets also exhibit the same anomalies. The three layers can be interpreted showing the site stratigraphy (Figure 44). The first layer has a resistivity

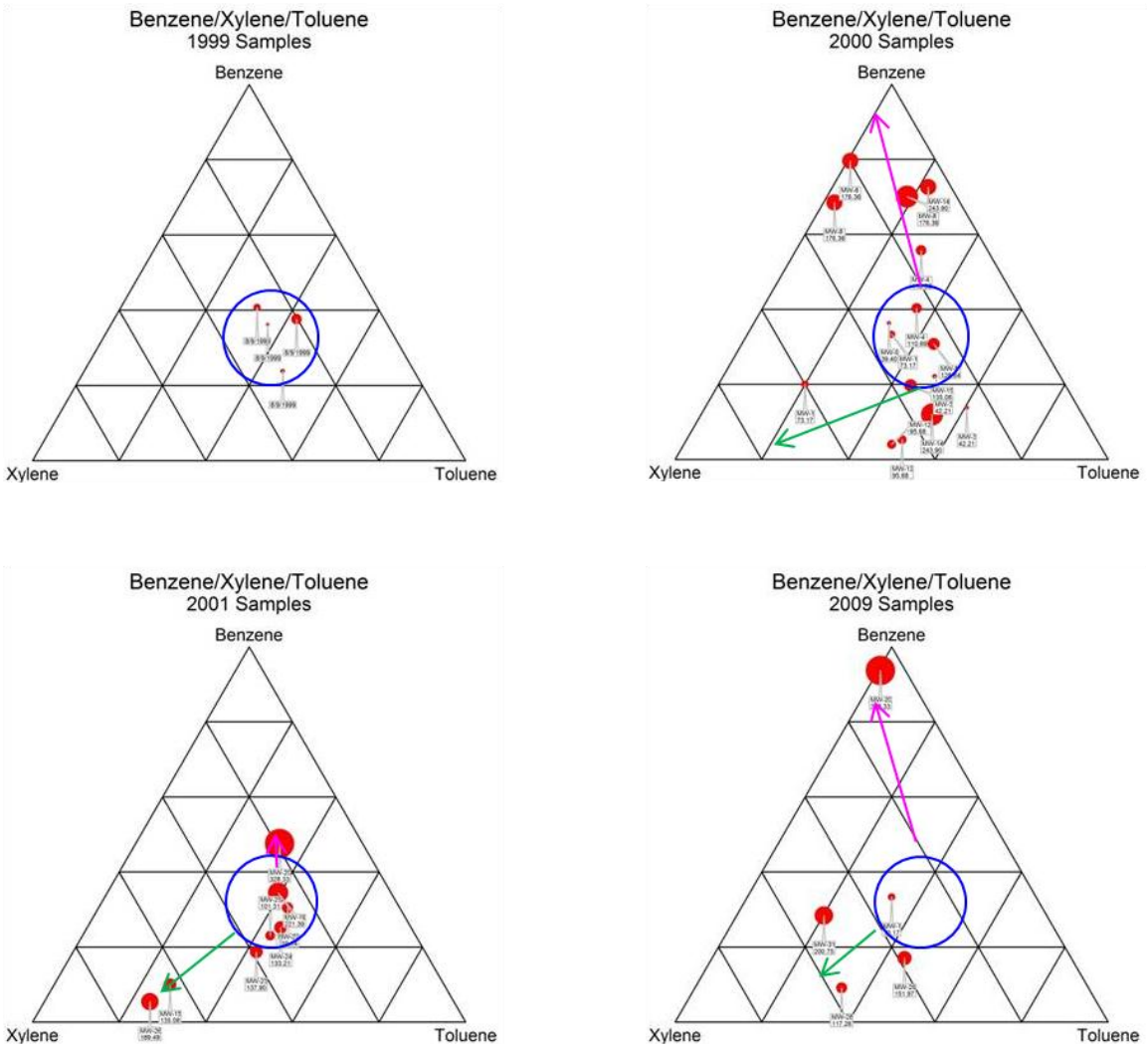

Figure 40. Groundwater geochemistry of Enid, Oklahoma groundwater samples divided by year. The source contamination signature is indicated by a blue circle. The pink arrows represent a move toward biodegradation, the green represents a move toward volatilization, and there is no movement toward pure advection.

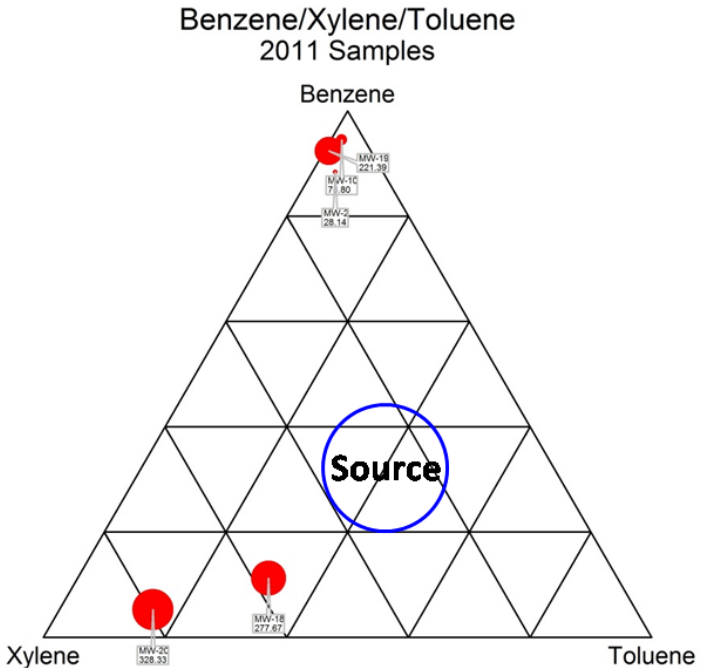

Figure 41. Groundwater geochemistry for March 2011. Each red circle is labeled with the name of the monitoring well and the distance from the UST pit where contamination originated.

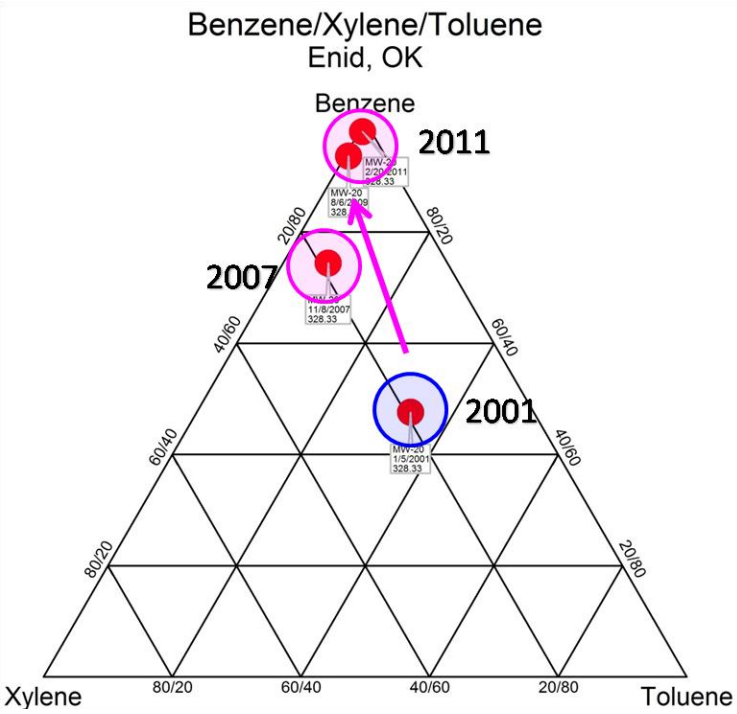

Figure 42. Geochemical analysis of MW-20.

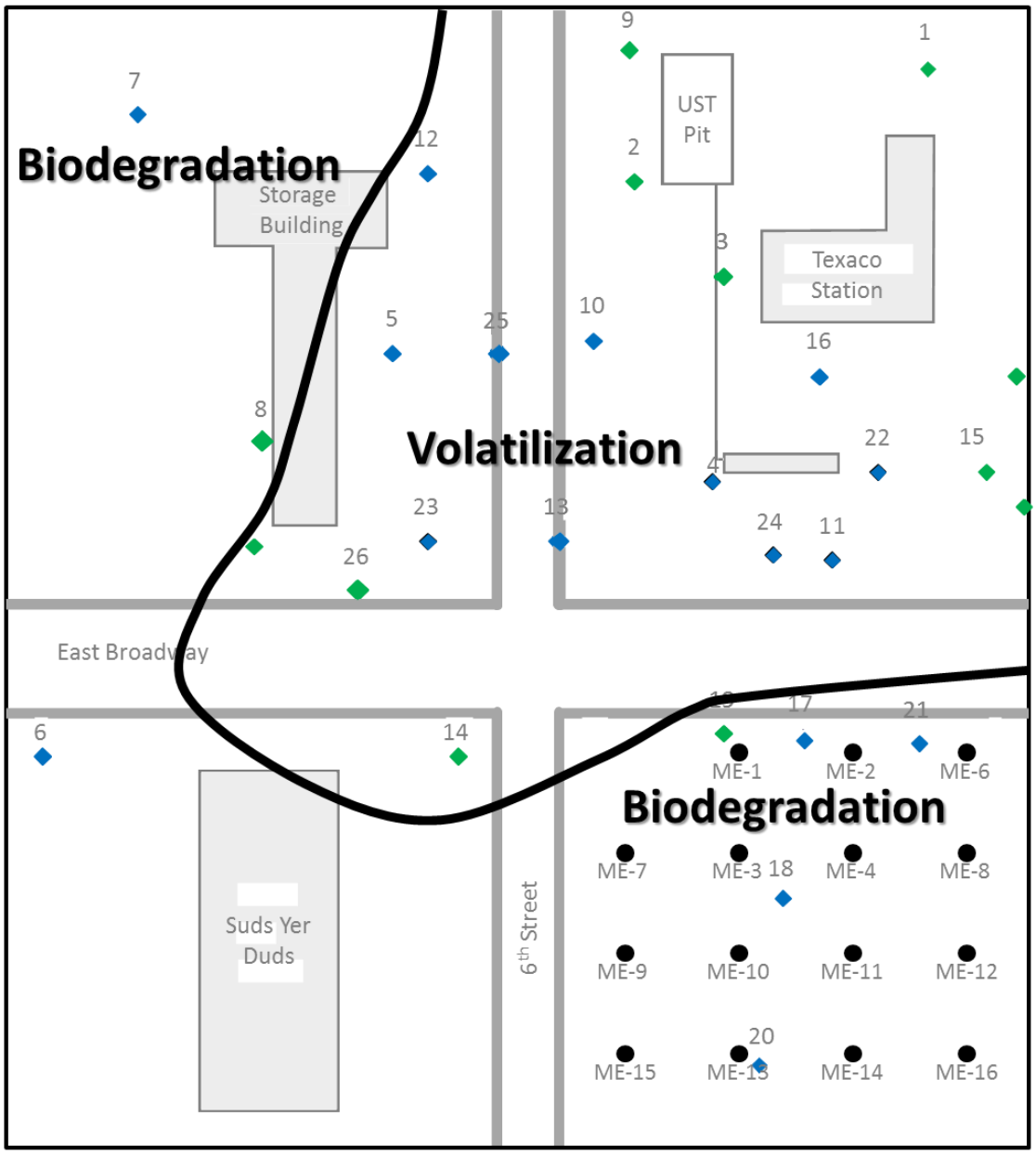

Figure 43. Map generated from ternary diagrams showing where biodegradation and volatilization is occurring on the site and areas adjacent to the site. The wells used are highlighted with green diamonds (modified from Halihan et al., 2005).

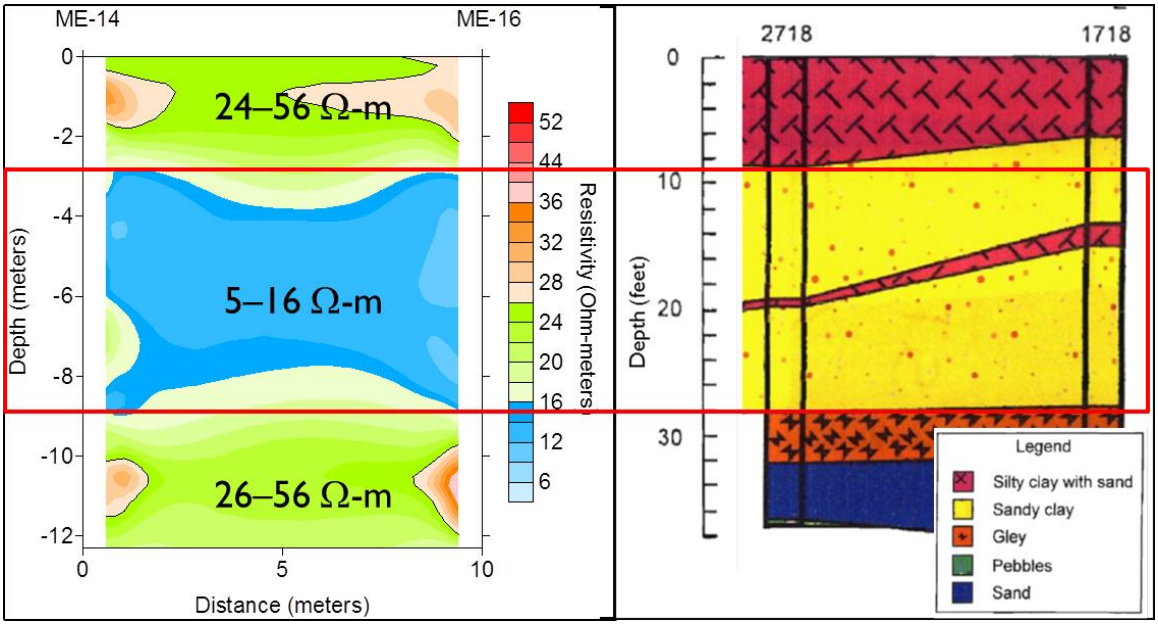

Figure 44. May 2010 ERT on the left with the resistivity range and a stratigraphic cross section from McPhail (2003) on the right; 2718 is the same as ME-14 and 1718 is the same as ME-16.

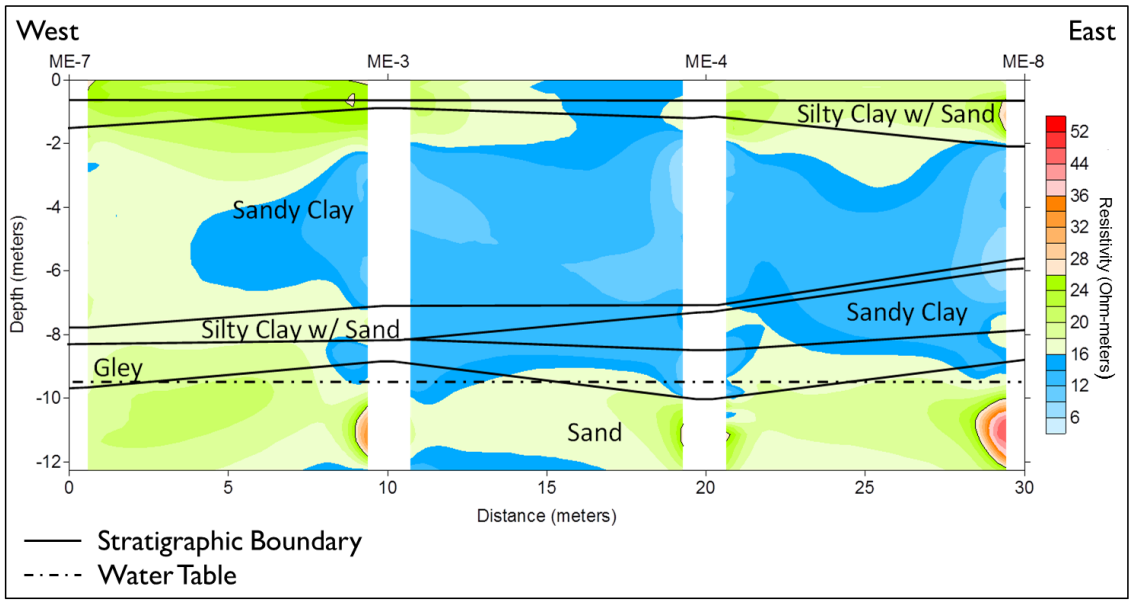

Figure 45. Line 07030408 from the May 2010 dataset with stratigraphic boundaries (solid line) and water table elevation (dashed line).

range of 24–56 Ω-m; this is consistent with dry silty clay that contains some sand. The second layer, 5–16 Ω-m, is a lower resistivity layer because of higher clay content than the upper and lower layers. The lowest layer, 26–56 Ω-m, is consistent with a sand or sandy-clay layer. The interpretation of the ERT data is consistent with units A-C of the alluvium identified by McPhail (2003). To better see how the resistivity shows the stratigraphy of the site an overlay of stratigraphic boundaries from McPhail (2003) and the elevation of the water table at the time of collection is seen in Figure 45.

Even though resistivity values are the result of the site stratigraphy there are some anomalies that can't be explained by stratigraphy alone. Mcorley (2003) also identified these anomalies as LNAPL. Halihan et al. (2005) and McSorley (2003) used a cutoff value for LNAPL resistivity greater than 46 Ω-m value based on the groundwater geochemistry (Figure 46). Halihan et al. (2005) and McSorley (2003) determined that the LNAPL at this site does not form a traditional plume as depicted in Figure 5, but is in the form of blobs (Figure 46). When the same value is used on the May 2010 dataset some areas of LNAPL are observed (Figure 47). A comparison of the same ERT line from December 2002 and May 2010 appears to indicate a decrease in the amount of LNAPL present, which would suggest that the site has been mostly remediated. However, results from the groundwater samples and core samples indicate that this is not the case. Using 46 Ω-m shells eight years after initial contamination fails to account for compositional and concentration changes in the hydrocarbons that occur over time and distance from the source.

Che-Alota et al. (2009) provided a conceptual model in which hydrocarbons become more conductive (minimum resistivity) over time with remediation (Figure 11).

Using this conceptual model there are two possible scenarios that could be occurring. The first possibility is that the bulk conductivity is increasing (decrease in resistivity) and the second is a decrease in bulk conductivity (increase in resistivity). The second case is unlikely. When a higher resistivity cut off is used, few to no blobs are indicated. This is inconsistent with both groundwater and core geochemistry data from the site (Tables 2 and 3). Therefore it is likely that the bulk conductivity of the site still has not reached the maximum value that is determined based on observation of the contaminated area. When a cut off value of 26 Ω-m is used there are still areas of hydrocarbon contamination indicated in Figure 48. In McSorley (2003) 36 Ω-m and 26 Ω-m represented 20,000 mg/kg total petroleum hydrocarbons and 600 mg/kg total petroleum hydrocarbons respectively. Using the conceptual model from Che-Alota (2009), it is possible that either 26 or 36 Ω-m could represent the LNAPL plumes. Note that several of the 36 Ω-m areas are in similar locations as the 46 Ω-m areas in the December 2002 data.

Over the past eight years, the electrical signature of the site has changed, both in increasing and decreasing resistivity values. These are the result of changes in moisture content and, most importantly, the change in the electrical signature of LNAPL over time. Since the resistivity of the contaminated layer has changed the same parameters used to define the extent of the LNAPL by Halihan et al. (2005) and McSorley (2003) can no longer be used to identify the location of LNAPL. By using 36 and 26 Ω-m cut-off values the extent of the LNAPL was identified in the 2D resistivity sections.

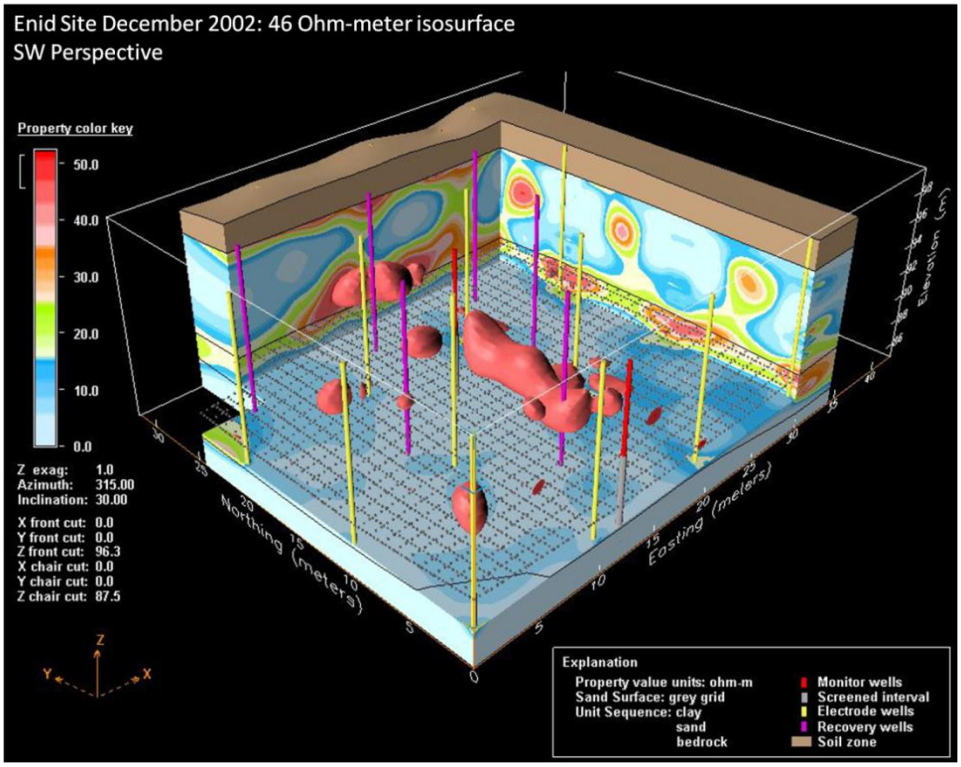

Figure 46. Enid Site 46 Ohm-m isosurface from December 2002, pre-remediation (McSorley, 2003).

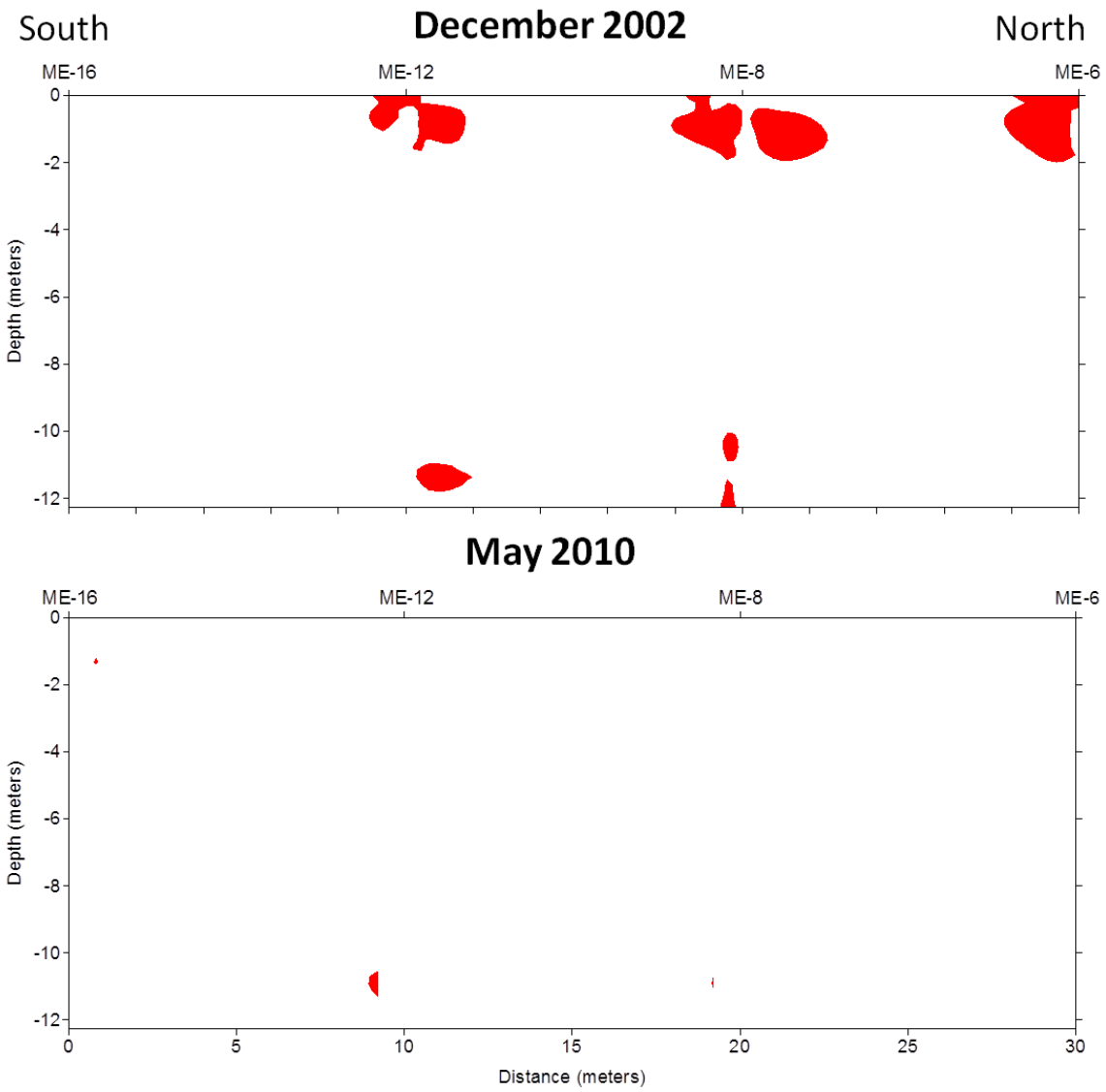

Figure 47. Comparison of 46 Ohm-m resistivity sections for December 2002 and May 2010.

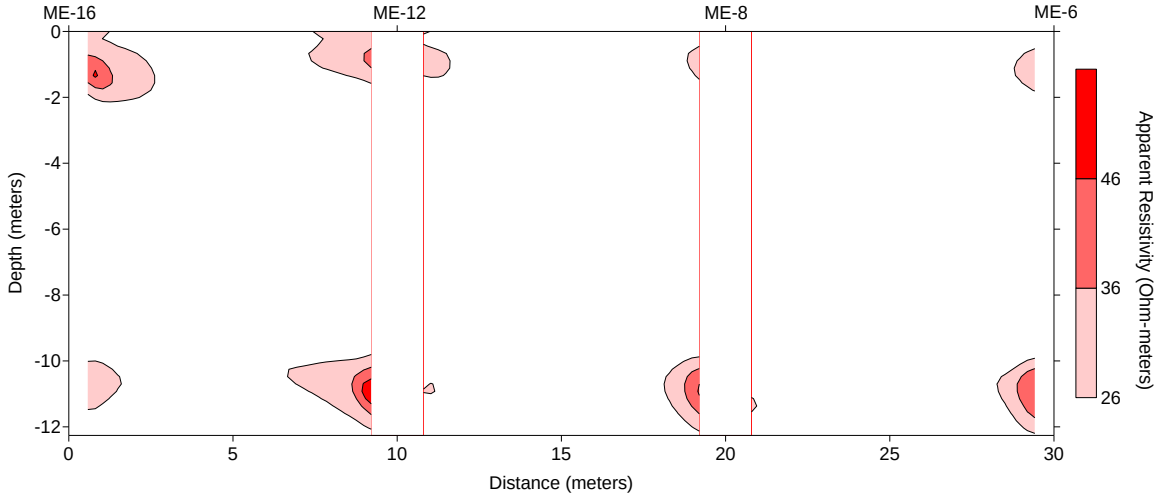

Figure 48. May 2010 ERT data showing 26, 36, and 46 Ω-m shells.

TRANSIENT ERT

According the Earth Imager manual a negative change in resistivity indicates that the site is becoming more resistive or that the resistivity in that area has increased. In the case of positive changes in resistivity the area is becoming more conductive or the resistivity has decreased.

December 2002–January 2003

For this dataset there appears to be little (−10% to +10%) change (Figure 49). The nature of the observed changes is a vertical pattern with the most change occurring along the borehole and decreasing towards the center of each section. This is caused by borehole effects or the subsurface around the boreholes settling after being disturbed during drilling. When examining the transient image with the December 2002 and January 2003 image there appears there is no resistivity difference associated with the

stratigraphy at the site. This is consistent with the conclusions in Atekwana et al. (2000); through the use of transient electrical resistivity, the effects bedrock has on resistivity values are eliminated and only changes in moisture content or contamination are seen.

December 2002–May 2011

One main characteristic of the December 2002 to May 2010 data is the stronger horizontal changes and weaker vertical changes in resistivity when compared to the December 2002 to January 2003 dataset. This is the result of changes in resistivity occurring within the different stratigraphic zones, which were characterized as the three different geoelectrical layers.

Based on this transient data, it appears that the uppermost geoelectrical layer has become less resistive (Figure 50). According to Rein et al. (2004) a decrease in resistivity could be caused by a decrease in the moisture content of the upper two meters of the sediment.

The middle layer has become, on average, more resistive from December 2002 to May 2010. This is strongly seen between ME-7 and ME-3 where the resistivity has increased from an average of 12 Ω-m to an average of 18 Ω-m. This increase in resistivity could be caused by vaporization of the LNAPL. At the time of collection for the 2002 data the water table was at approximately -8.8 meters. The water table for the May 2010 dataset was at approximately -9 meters. Thus, the second layer is above the water table, so that there is the possibility of vapor phase. This would also coincide with the air sparge remediation system in place.

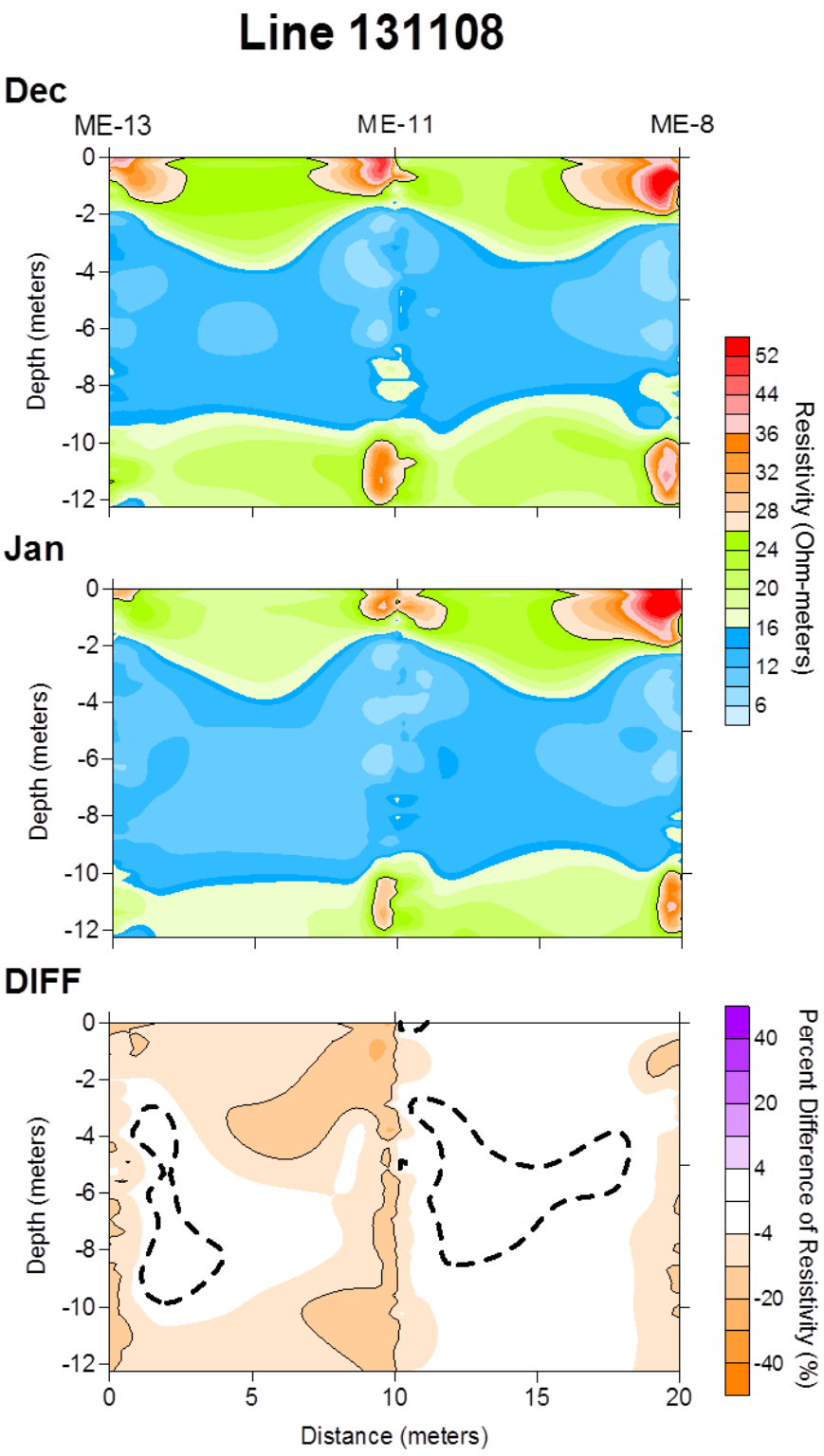

Figure 49. Composite image showing December 2002 (top), January 2003 (middle) and the transient (bottom) images for Line 131108. The left side of the lines is the southwest and the right is the northeast. In the difference image, the heavy dashed line represents 0% change of resistivity.

Another possibility, as with layer 1, would be changes in the moisture content as cited by Rein et al. (2004). Core samples were also acquired within this layer. As seen in Table 2, all of the BTEX values were below detection. Therefore, of the two possibilities, it is more likely that the observed change in resistivity has been caused by a change in moisture content due to prolonged drying of the subsurface above the water table.

The lowermost layer has become more conductive over time. Using the water level readings, this layer is located beneath the water table. Using the conceptual model presented by Che-Alota (2009) and the analysis of the ternary diagrams of the groundwater geochemistry, it is possible that this increase in conductivity is due to biodegradation of the LNAPL. Two other studies, (Atekwana et al., 2004a, b), concluded that contaminated areas with higher total dissolved solids that are undergoing biodegradation have higher conductivities when compared to uncontaminated locations, consistent with the observations at this site.

May 2010–March 2011

This data set shows similar characteristics as the background transient data set. In the ten months between the two data sets**,** very little change occurred in resistivity. The observed changes occur in the vertical direction, indicating that the responsible processes occurring are occurring adjacent to the boreholes.

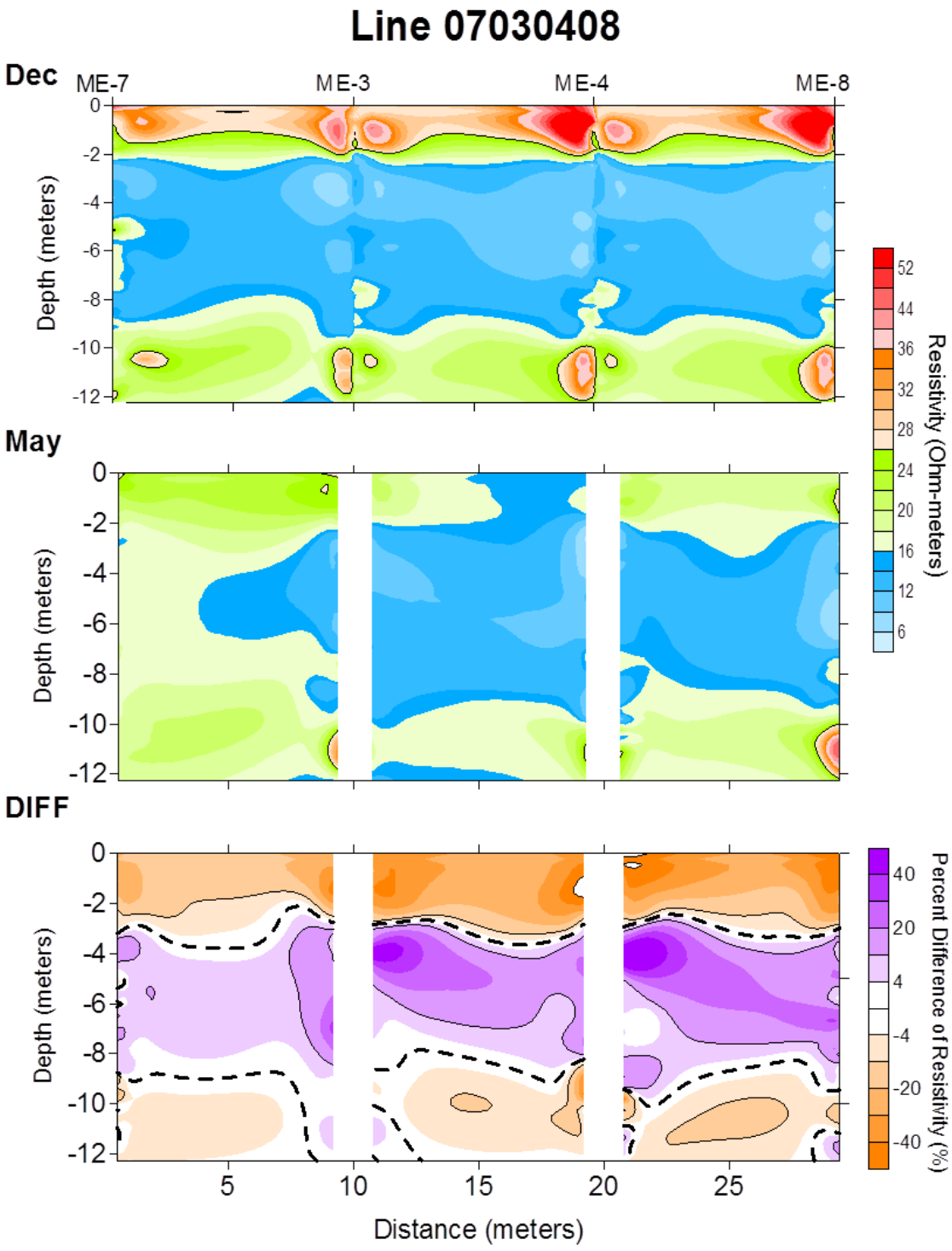

Figure 50. Composite image showing December 2002 (top), May 2010 (middle) and the transient (bottom) images for Line 131108. The left side of the line is the southwest and the right is the northeast. In the difference image, the heavy dashed line represents 0% change of resistivity.

MASW

The MASW velocities show two distinct different velocity zones. The velocities found in these zones are representative of clay rich soil on top of sand and the Hennessey Group below. Figure 51 shows Line 7348 and Line 13N with an overlay of the geologic cross section from McPhail (2003). Figure 52 shows MASW line 7348 with a 1D shear wave velocity profile, stratigraphic overlay, and water table elevation. When examining the location of the 1D shear wave velocity profile in the 2D line it is evident that there are approximately two different velocity zones with several anomalies, one of which is located in the 1D profile.

The uppermost velocity zone corresponds to the silty clay with sand stratigraphic layer defined by McPhail (2003). Within this layer are several anomalies. The two high velocity anomalies located in the uppermost velocity layer are located approximately 2.5 meters east of ME-7 and 2 meters depth and 2 meters east of ME-3. The first correlates to the location of a trench that was constructed during installation of the remediation system. The second anomaly is most likely a foundation or basement. When removed the basement was in filled with sediment. If this sediment is more permeable than the surrounding material then it could serve as a vapor flow pathway.

In the high velocity layer (layer 2) there is a very high velocity anomaly located 4.5 meters east of ME-7 and centered around 10 meters depth, indicates there is a possibility of an artifact. However, no drilling was conducted to determine the validity of this assumption.

One of the purposes of using MASW at this site was to determine if there were any lateral changes in velocity that could serve as flow pathways.

However, given the data resolution and quality determination of flow pathways was not possible.

Overall, there were subsurface anomalies more likely false positives than actual anomalies. This is based on lack of correlation to site stratigraphy. Possibilities for these false anomalies include equipment failure, non-optimum equipment, and numerous buried objects. All of these are discussed below.

After this data were processed, it was decided that a second trip to the site to reacquire the same lines would be needed to validate the observed anomalies. During the second trip, it was discovered that some electrical issues existed with the equipment. It is unknown if these issues affected the first data acquisition or had occurred since the initial visit. However, during the first visit there were some technical difficulties with the same piece of equipment that failed the second time.

Park et al. (1999) determined the optimal field parameters for MASW data acquisition. In this paper three different sources and three different geophones of different Hz ratings were analyzed. Based on the results the best combination was a rubber-band-aided-weight-drop (RAWD) and 4.5 Hz geophones. Due to the capabilities of the university a 20 pound sledge hammer and 14 Hz geophones were used for this study. While these were not the optimum conditions, Park et al. (1999) provided several dispersion images that show good data can be collected with a 20 pound sledge hammer and higher Hz geophones. Therefore, the poor data quality is not due to the use of non-optimum equipment.

The third possibility for poor-quality MASW data is buried objects. This site has numerous buried obstacles including sewer lines, electrical lines, remediation equipment

and the foundation or basement of a house (Figure 16). The presence of these buried obstacles may have caused excess ringing that did not allow for good signal clarification, which ultimately impacts the signal-to-noise ratio. During processing, the software noted poor data quality because of noise contamination. it was believed that MASW would be unaffected by electrical and mechanical noise, it was believed that MASW would be a good technique to use at this site. Even though MASW did not work for this site, there have been numerous other studies where it has been a useful method for determination of near surface stratigraphy, faults, and fluid pathways.

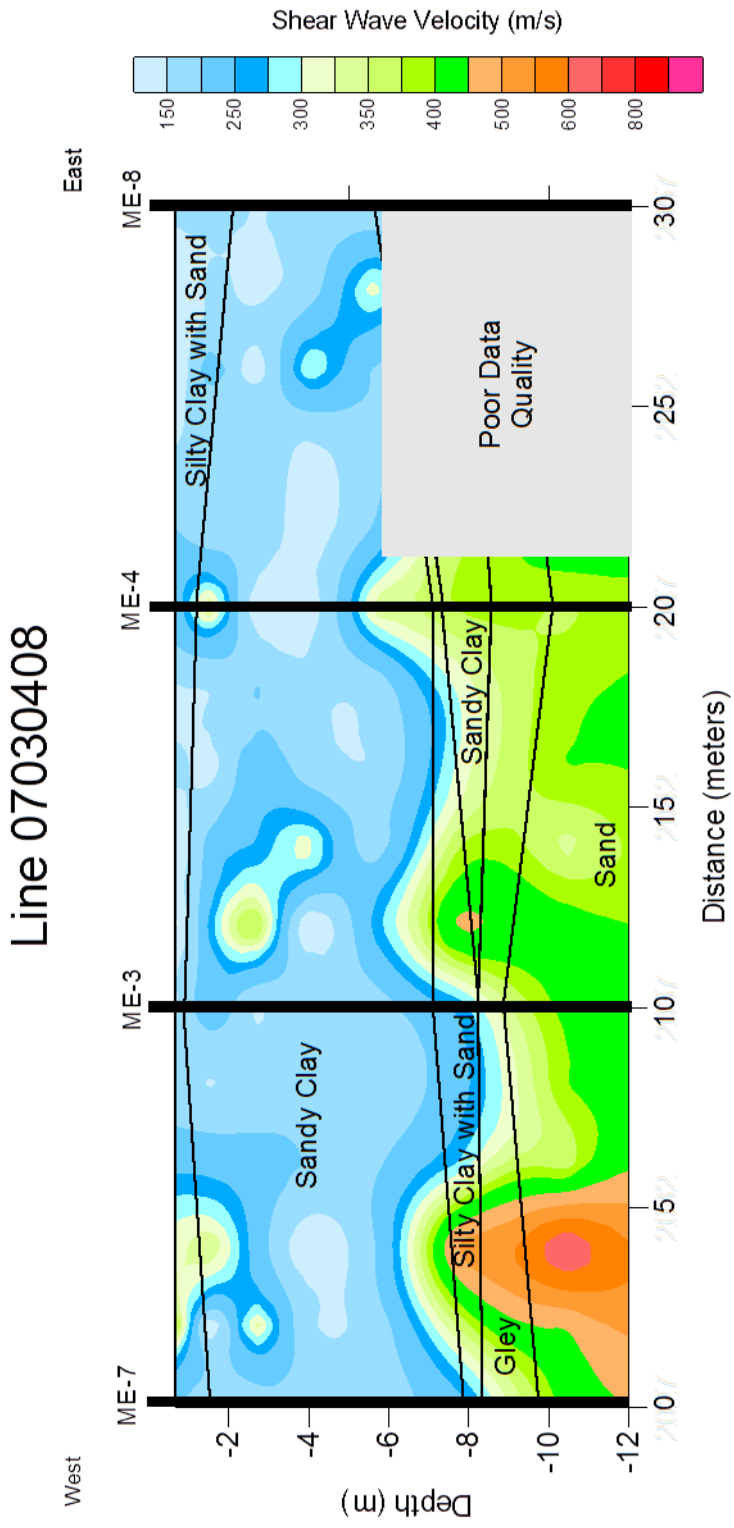

Figure 51. MASW Line 07030408 with a stratigraphic overlay from McPhail (2003). Note how only some of the stratigraphic surfaces are confirmed with the seismic data. The poor data quality block to the left represents an area where the dispersions curves were contaminated by higher modes.

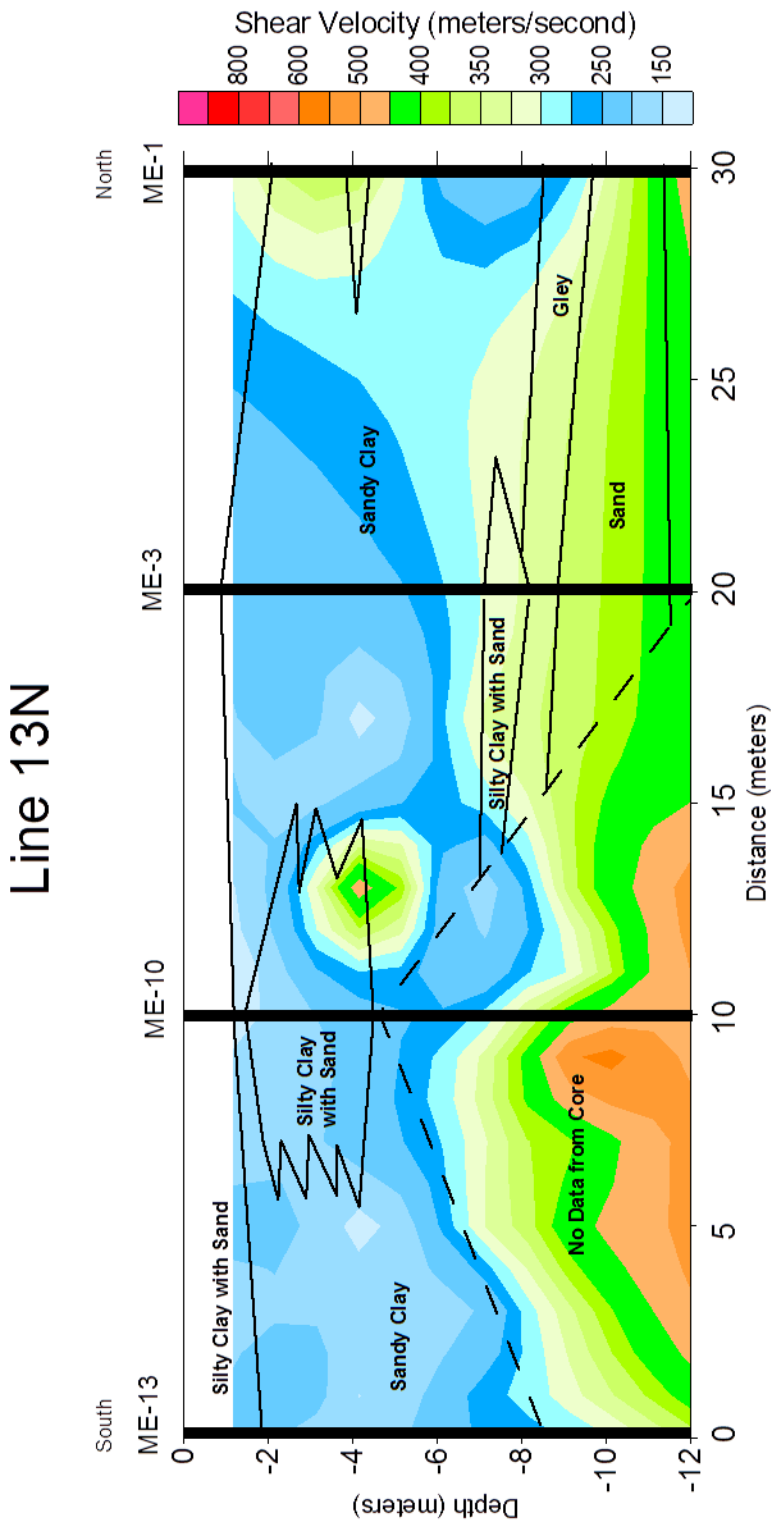

Figure 52. MASW Line 13N with a stratigraphic overlay from McPhail (2003). Note that the stratigraphic boundaries do not match the varying velocities.

CHAPTER VI

CONCLUSIONS

The purpose of this study was to use multiple geophysical methods to better delineate contamination and possible flow pathways. To do this MASW and transient ERT were used. Based on the geophysical results core and groundwater geochemistry was also used. The integration of these techniques indicate that:

1. The site is still contaminated with LNAPL (gasoline). This is clearly observed in the groundwater and core geochemistry. The transient ERT data from December 2002 to May 2010 indicates that Layer 3 became more conductive with time, likely caused by a change in hydrocarbon composition. These observations are consistent with the conceptual models of Lipson and Siegel (2000) for the groundwater geochemistry and by Che-Alota et al. (2009) for the transient ERT data.
2. By using a ternary diagram analysis on the groundwater geochemistry it was concluded that the site is undergoing both biodegradation and volatilization.
3. The increase in resistivity in Layer 1 is due to seasonal moisture changes within the sediment above the water table, as described by Rein et al. (2004).

4. The changes in resistivity in Layer 2 are most likely due to a seasonal decrease in moisture content, as for Layer 1. Layer 2 is also located above the water table. However, these changes could also be attributed to movement of the LNAPL into the vapor phase by the air sparge remediation system in place on the site. The core data from this layer has no measurable BTEX, making it unlikely that vapor phase hydrocarbons are the cause. However, BTEX concentrations may not be the best method to determine if vapor phase is present. Corrosion of the borehole electrode cables (Figure 19) also supports the hypothesis that the resistivity increase is due to vapor phase BTEX compounds.
5. ERT has proven to be an effective tool for long-term monitoring of an LNAPL contaminated site. Although there has been some corrosion of the cable connections, the cables and electrodes are still in good condition to acquire additional data.
6. MASW, although adequate for many urban environments, is not a valuable tool for this site. The data only approximated some of the stratigraphic units from McPhail (2003) and didn't image others. In order to fully determine the applicability of MASW at this site further work should be done using the optimum source and receiver combinations.

REFERENCES

Advanced Geosciences, Inc., 2001, Instruction Manual for the SuperSting R8/IP and Swift, pp. 1−50.

Andrews R. J., Barker, R., and Heng, L. M., 1995, The Application of Electrical Tomography in the Study of the Unsaturated Zone in Chalk ant Three Sites in Cambridgeshire, United Kingdom, Hydrogeology Journal, v. 3, no. 4, p. 17−31.

Atekwana, E. A., Sauck, W. A., and Werkema Jr., D. D., 2000, Investigations of Geoelectrical Signatures at a Hydrocarbon Contaminated Site, Journal of Applied Geophysics, v. 44, p. 167−180.

Barker, J.F. and Patrick, G.C., 1987, Natural Attenuation of Aromatic Hydrocarbons in a Shallow Sand Aquifer, Ground Water Monitoring & Remediation, vol. 7, no. 1, pp. 64-71.

Atekwana, E.A., Atekwana, E.A., Legall, F.D., and Krishnamurthy, R.V., 2004a, Field evidence for geophysical detection of subsurface zones of enhanced microbial activity, Geophysical research letters, v. 31, L23603.

Atekwana, E.A., Atekwana, E.A., Rowe, R.S., Werkema Jr., D.D., and Legall, F.D., 2004b, The relationship of total dissolved solids measurements to bulk electrical conductivity in an aquifer contaminated with hydrocarbon, Journal of Applied Geophysics, v. 56, pp. 281-294.

Benson, A.K., Pyne, K.L., Stubben, M.A., 1997, Mapping groundwater contamination using dc resistivity and VLF geophysical methods – A case study, Geophysics, vol. 62, pp. 80-86.

Berryman, J. G., 1999, Origin of Gassmann's Equations, Stanford Exploration Project, Report 102, p. 187−192.

Braile, L., 2004, Seismic Wave Demonstrations and Animations, in *Seismic Wave Demo*, Downloaded November 27, 2010, from http://www.web.ics.purdue.edu /~braile/edumod/waves/WaveDemo.htm.

Bullen, K. E., 1963, An introduction to the theory of seismology: Cambridge University Press, 381 p.

Che-Alota, V., Atekwana, E.A., Atekwana, E.A., Sauck, W.A., and Werkema Jr., D.D., 2009, Temporal Geophysical Signatures from Contaminant-Mass Remediation, Geophysics, vol. 74, no. 4, pp. B113-B123.

Chou, J., 2000, Photoionization Detectors *in* Hazardous gas monitors: a practical guide to selection, operation, and applications, McGraw-Hill, pp. 73-81.

Comfort, S., Zlotnik, V., and Halihan, T., 2009, Final Report: Using Electrical Resistivity Imaging to Evaluate Permanganate Performance During an In Situ Treatment of a RDX-Contaminated Aquifer, ESTCP Project ER-0635.

Dailey, W., Ramirez, A., LaBrecque, D., and Barber, W., 1995, Electrical Resistance Tomography at the Oregon Graduate Institute Experiment, Journal of Applied Geophysics, v. 33, p. 227−237.

Daum, K.A., Watrous, M.G., Neptune, M.D., Michael, D.I., Hull, K.J., and Evans, J.D., 2006, Data for First Responder Use of Photoionization Detectors for Vapor Chemical Constituents, prepared for the DOE.

Day-Lewis, F. D., and Singha, K., 2008, Geoelectrical Inference of Mass Transfer Parameters Using Temporal Moments, Water Resources Research, vol. 44, W05201.

DOE Environmental Management, 2000a, Tomographic Site Characterization Using CPT, ERT, and GPR, Innovative Technology Summary Report, OST/TMS ID 284.

DOE Environmental Management, 2000b, Electrical Resistance Tomography for Subsurface Imaging, Innovative Technology Summary Report, OST/TMS ID 17.

Gassmann, F., 1951, Elastic Waves through a Packing of Spheres: Geophysics, no. 16, p. 673−685.

George, L. A., Dewoolkar, M., and Znidarcic, D., 2009, Simultaneous Laboratory Measurement of Acoustic and Hydraulic Properties of Unsaturated Soils, Vadose Zone Journal, vol. 8, no. 3, p. 633−642.

Graham, I. A., 2007, Electrical Resistivity Imaging Using Vertical and Surface Electrodes Conjunctionally at a Post-Remediated Site in Golden, Oklahoma, Master of Science Thesis, Oklahoma State University, Stillwater, Oklahoma.

Halihan, T., Paxton, S., McPhail, M., McSorley, H., and Riley, M., 2005a, Final Report for: Environmental Characterization and Monitoring of LNAPL Using Electrical Resistivity Tomography (ERT) and Hydraulic Push Techniques, Oklahoma Corporation Commission.

Halihan, T., Paxton, S., Graham, I., Fenstemaker, T., and Riley, M., 2005b, Post-Remediation Evaluation of a LNAPL Site Using Electrical Resistivity Imaging, Journal of Environmental Monitoring, v. 7, p. 1−6.

Han, D. H., and Batzle, M.L., 2004, Gassmann's Equation and Fluid-Saturation Effects on Seismic Velocities, Geophysics, vol. 69, p. 398-405

Ivanov, I., Miller, R.D., Ballard Jr., R.F., Dunbar, J.B., Smullen, S., 2005, Time-lapse seismic study of levees in southern Texas, SEG Expanded Abstract, p. 1121−1124.

Ivanov, J., Miller, R.D., Lacombe, P., Johnson, C.D., & Lane Jr., J.W., 2006, Delineating a shallow fault zone and dipping bedrock strata using multichannel analysis of surface waves with a land streamer, Geophysics, vol. 17, no. 5, pgs. A39−A42.

Lipson, D. and Siegel, D.J., 2000, Using Ternary Diagrams to Characterize Transport and Attenuation of BTX, Groundwater, vol. 28, no. 1, pp. 106-113.

Luhrs, R.C., and Pyott, J.C., 1992, Trilinear plots: A powerful new application for mapping gasoline contamination, In *Proceedings of National Ground Water Association Conference on Hydrocarbons and Organic Chemicals Found in Ground Water: Prevention, Detection, and Restoration*, October 13-15, pp. 2-15, Dublin, Ohio: NGWA.

Luhrs, R.C., Stewart, N., and Pyott, C.J., Graphical Evaluation of Gasoline Contaminated Water: A powerful new approach, In *Proceedings of the NGWA Focus Conference on Eastern Regional Ground Water Issues*, October 1992.

McPhail, M., 2003. Geological Controls on the Location and Distribution of an LNAPL Plume at a Site in Enid, Oklahoma, Master of Science Thesis, Oklahoma State University, Stillwater, Oklahoma.

McSorley, J., 2003, Direct Push Electrical Resistivity Tomography to Detect LNAPL, Master of Science Thesis, Oklahoma State University. Stillwater, Oklahoma.

Miller, R.D., Ivanov, J., and Park, C. 2003. After Action Review Otay Mesa, California, Tunnel Search Mission. Kansas Geological Survey Open Report #2003-61. Kansas Geological Survey. Lawrence, Kansas.

Miller, R.D., Xia, J., Park, C.B., Ivanov, J. 1999. Multichannel Analysis of Surface Waves to Map Bedrock. The Leading Edge. Vol. 18, no. 12, pp. 1392-1396.

Miller, R.D., Xia, J., Park, C.B., and Ivanov, J., 2001, Shear wave velocity field to detect anomalies under asphalt: Proceedings of the 52nd Highway Geology Symposium, May 16, Baltimore, Maryland.

Osiensky, J.L., and Donaldson, P.R., 1995, Electrical Flow Through an Aquifer for Contaminant Source Leak Detection and Delineation of Plume Evolution, Journal of Hydrology, vol. 169, pp. 243-263.

Park, C.B., Miller, R.D., Xia, J., 1997, Multi-Channel Analysis of Surface Waves (MASW): A summary report of technical aspects, experimental results, and perspective, Kansas Geological Survey Open-File Report 97−10, 27 p.

Park, C.B., Miller, R.D., and Xia, J., 1999, Multichannel analysis of surface waves (MASW); Geophysics, 64, 800−808.

Park, C.B., Miller, R.D., Xia, J., Ivanov, J., 2007, Multichannel analysis of surface waves (MASW)-active and passive methods, The Leading Edge, pp. 60-64.

Pride, S. R., 2005, Relationships between Seismic and Hydrological Properties, in Hydrogeophysics, Springer, Netherlands, p. 253−291.

Rein, A., Hoffmann, R., and Dietrich, P., 2004, Influence of natural time-dependent variations of electrical conductivity on DC resistivity measurements, Journal of Hydrology, pp. 215-232.

Reynolds, J. M., 1997, An Introduction to Applied and Environmental Geophysics. John Wiley & Sons, New York, 796 p.

Richert, R.D., Hall, J.R., and Woods, R.D., 1970 Vibrations of soils and foundations: Prentice Hall, Inc.

Samoeilian, S., Cousin, I., Richard, G., Tabbagh, A., and Bruand, A., 2003, Electrical Resistivity Imaging for Detecting Soil Cracking at the Centimeter Scale, Soil Science Society of America Journal, vol. 67, no. 5, p. 1319−1326.

Singha, K.F. and Gorelick, S.M., 2005, Saline tracer visualized with three-dimensional electrical resistivity tomography: Field scale moment analysis, Water Resources Research, vol. 41, W05023.

Singha, K.F., and Gorelick, S.M., 2006, Effects of spatially variable resolution on field-scale estimates of tracer concentration for electrical inversions using Archie's law, Geophysics, vol. 71, no. 3, pp. G83-G91.

Slater, L.D., Brown, D., Binley, A., 1996, Determination of hydraulically conductive pathways in fractured limestone using cross-borehole electrical resistivity tomography. European Journal of Environmental and Engineering Geophysics, v. 1, p. 35-52.

Slater, L., Binley, A., Versteeg, R., Cassiani, G., Birken, G., Birken, R., and Sandberg, S., 2002, A 3D Study of Solute Transport in a Large Experimental Tank, Journal of Applied Geophysics, vol. 49, p. 211−229.

SurfSeis/MASW Workshop, 2009, Kansas Geological Survey, November 18-19, 2009, Lawrence, Kansas.

Thorstad, J. L., 2007, Influence of Borehole Construction on LNAPL Thickness Measurements, Master of Science Thesis, Oklahoma State University, Stillwater, Oklahoma.

US EPA, 2010, www.epa.gov/storagetanks/html, downloaded in May, 2010.

US EPA, 1994, Photoionization Detector (PID) HNU, SOP# 2114.

Wilkinson, P.B., Meldrum, P.I., Kuras, O., Chambers, J.E., Holyoake, S.J., Ogilvy, R.D., 2010, High-resolution electrical resistivity tomography monitoring of a tracer test in a confined aquifer, Journal of Applied Geophysics, vol. 70, pp268-276.

Worthington, M.A., and Perez, E.J., 1993, Dating gasoline releases using ground-water chemical analyses: case studies, In *Proceedings of the 1993 Petroleum Hydrocarbons and Organic Chemicals in Ground Water: Prevention, Detection, and Restoration*, pp. 203-217, Dublin, Ohio, NGWA.

Xia, J., Chen, C., Li, P.H., and Lewis, M.J., 2004, Delineation of a collapse feature in a noisy environment using a multichannel surface wave technique: Geotechnique, v. 54, n. 1, p. 17−27.

Xia, J., Miller, R.D., and Park, CB., 1999, Estimation of near-surface shear-wave velocity by inversion of Rayleigh waves, Geophysics, vol. 64, no. 3, pp. 691-700.

Xia, J., R.D. Miller, and C.B. Park, 2000, Multichannel analysis of surface wave theory and applications: Kansas Geological Survey Open-file Report 2000-25.

Xia, J., Miller, R.D., Park, C.B., Hunter, J.A., Harris, J.B., and Ivanov, J., 2002, Comparing shear-wave velocity profiles inverted from multichannel surface wave with borehole measurements: Soil dynamics and Earthquake Engineering (SDEE), v. 22, p. 181-190.

Xia, J., J.E. Nyquist, Y. Xu, M.J.S. Roth, and R.D. Miller, 2007, Feasibility of detecting near-surface feature with Rayleigh-wave diffraction: Journal of Applied Geophysics, 62(3), 244-253.

Yarmanci, U., Lange, G., and Hertrich, M., 2002, Aquifer Characterisation using Surface NMR Jointly with other Geophysical Techniques at the Nauen/Berlin Test Site, Journal of Applied Geophysics, vol. 50, pp. 47-65.

APPENDICES

APPENDIX A
ERT IMAGES (MAY 2011)

This data set contains all the 2-D inverted images from the May 2010 ERT survey. All images run from west to east or south to north. Refer to Figure 1 for locations of lines.

Line 0903

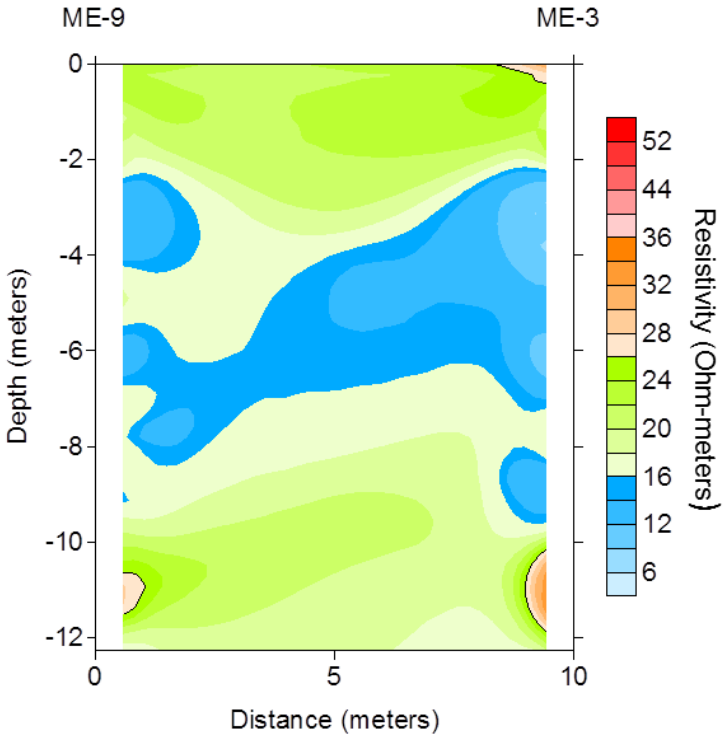

Line 0913

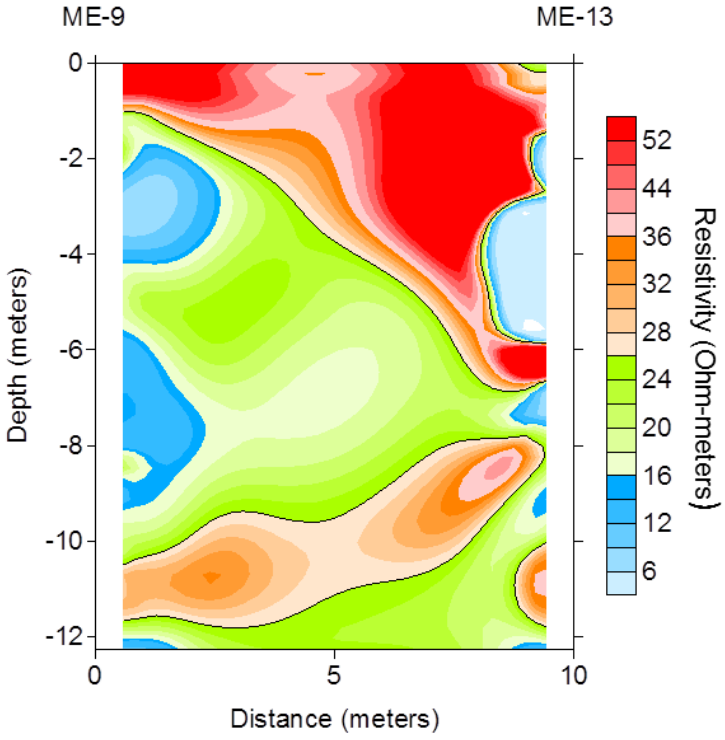

Line 0412

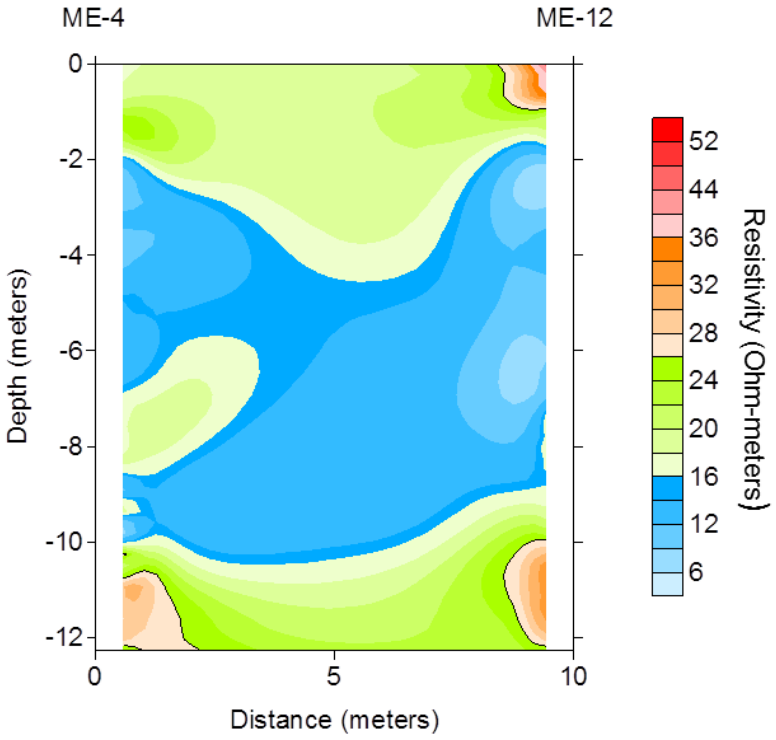

Line 1416

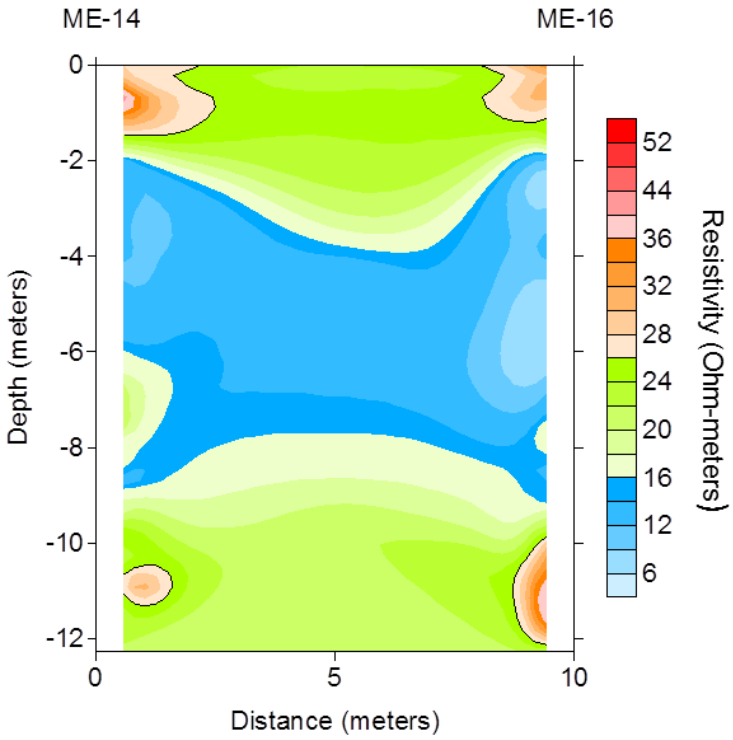

Line 150907

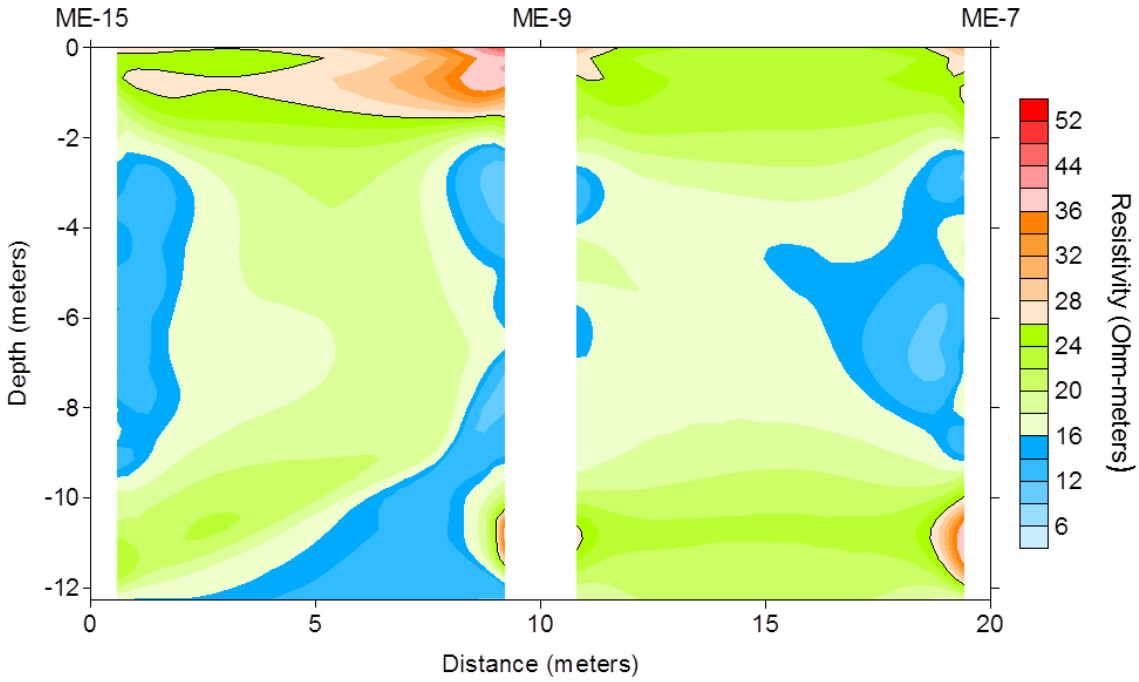

Line 141104

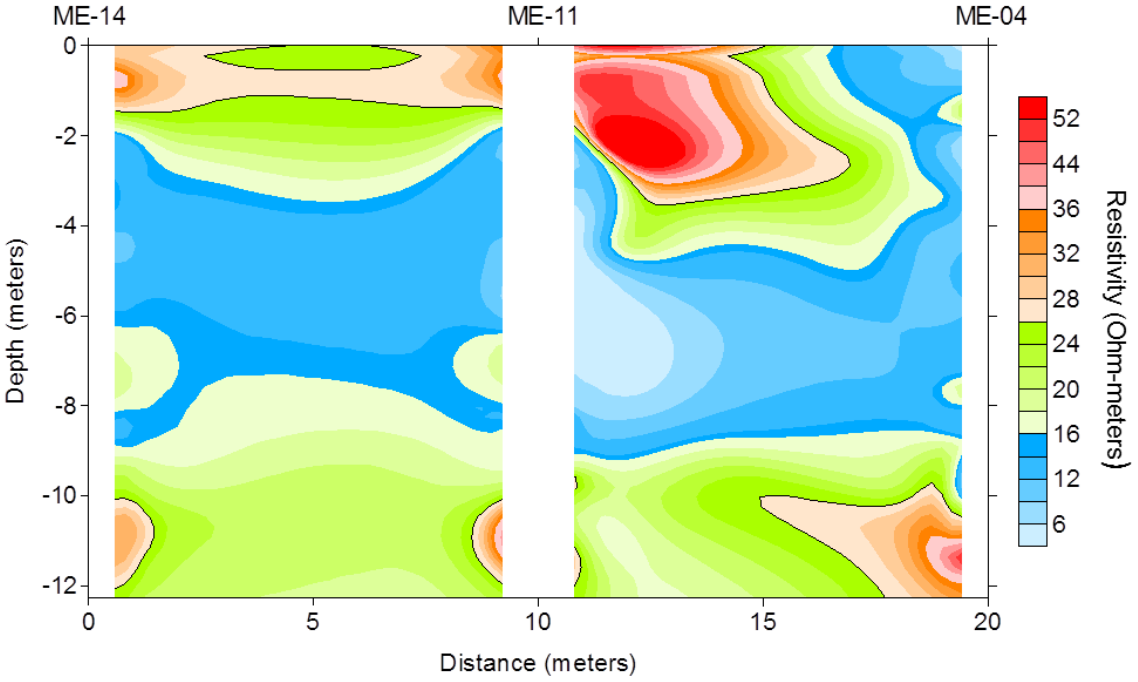

Line 131003

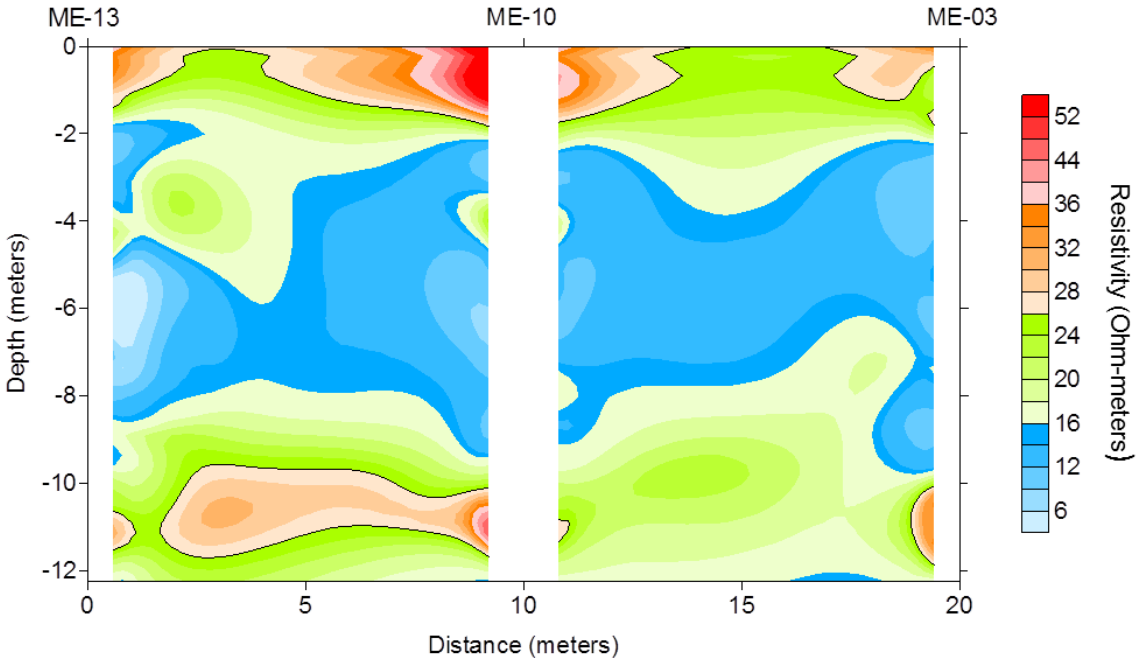

Line 131108

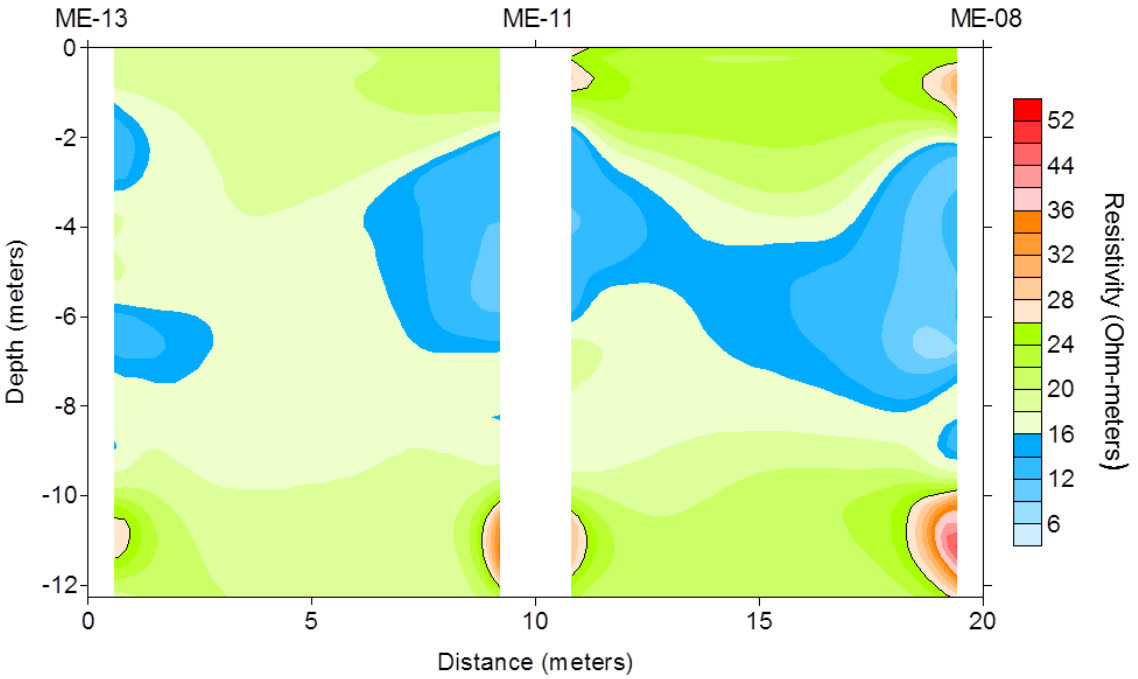

Line 031116

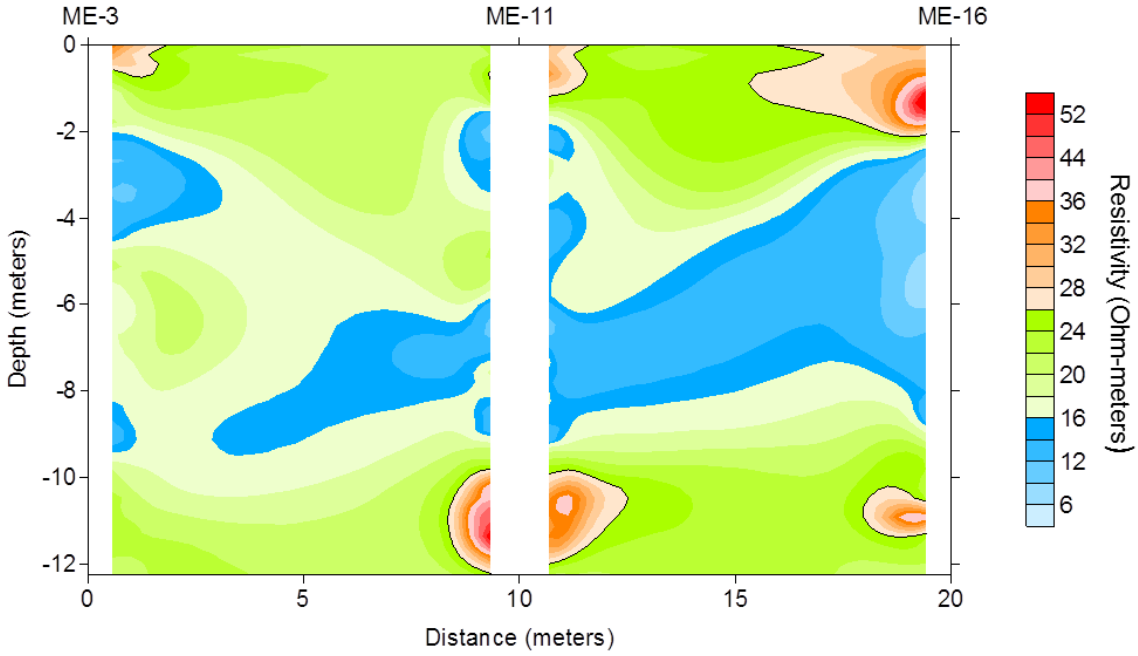

Line 071014

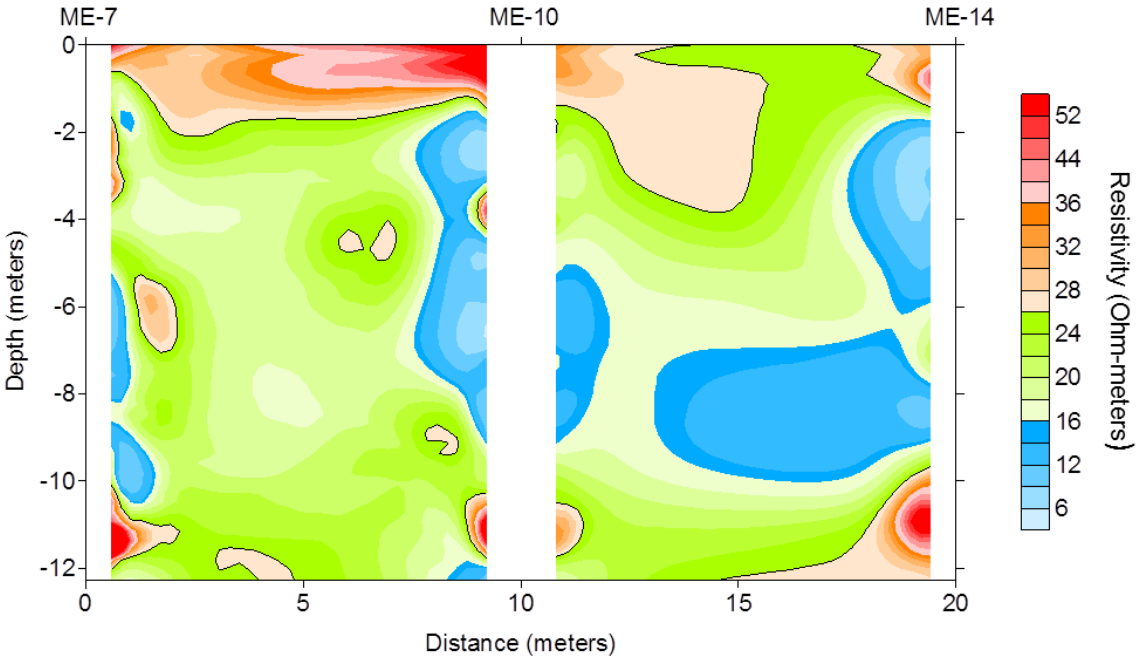

Line 16120806

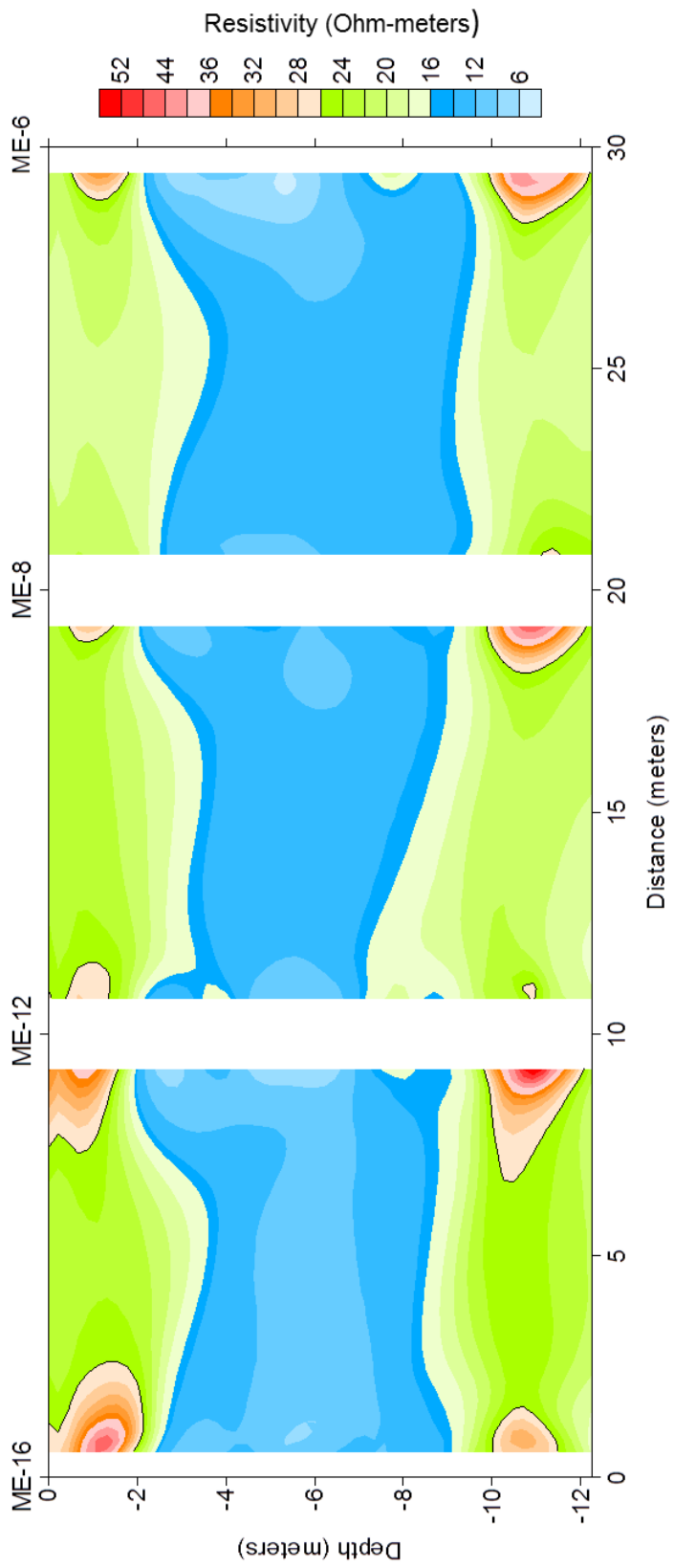

Line 15131416

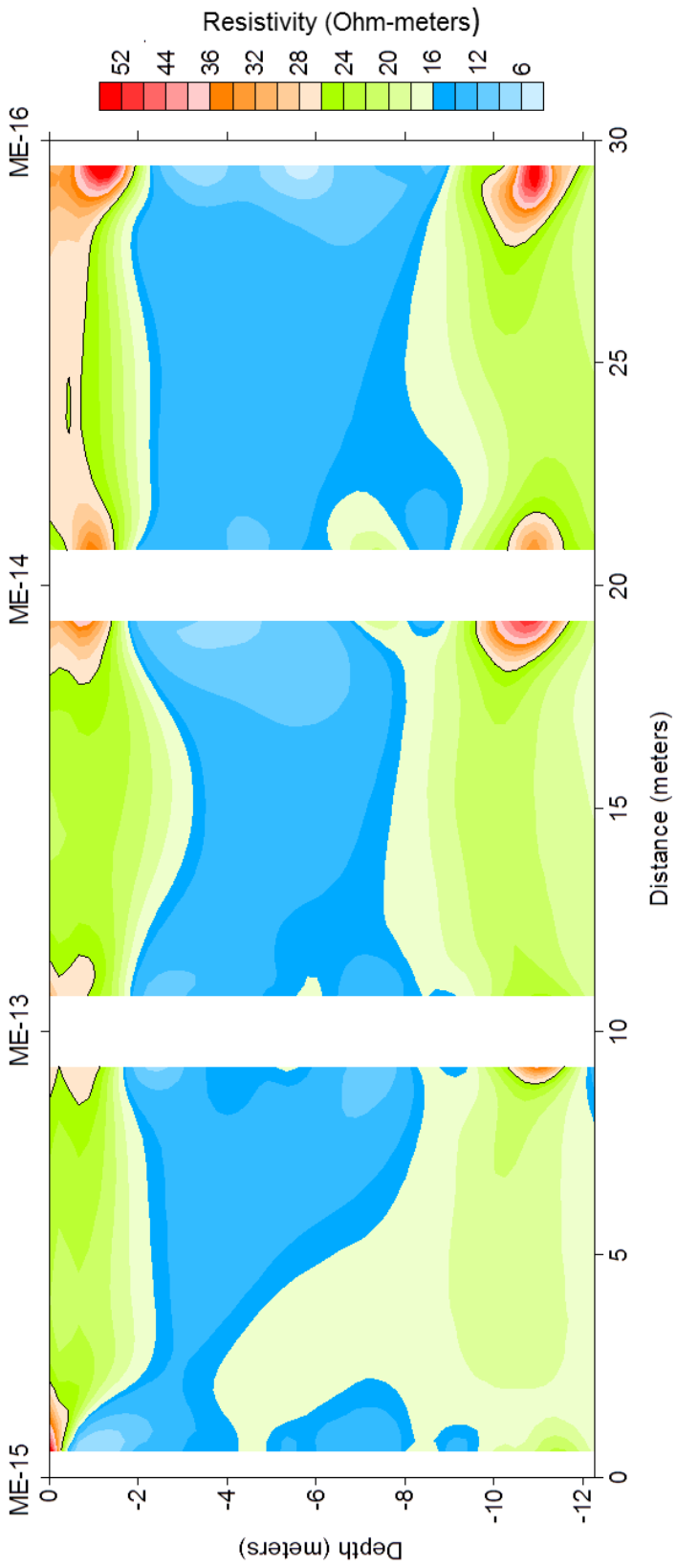

Line 15100406

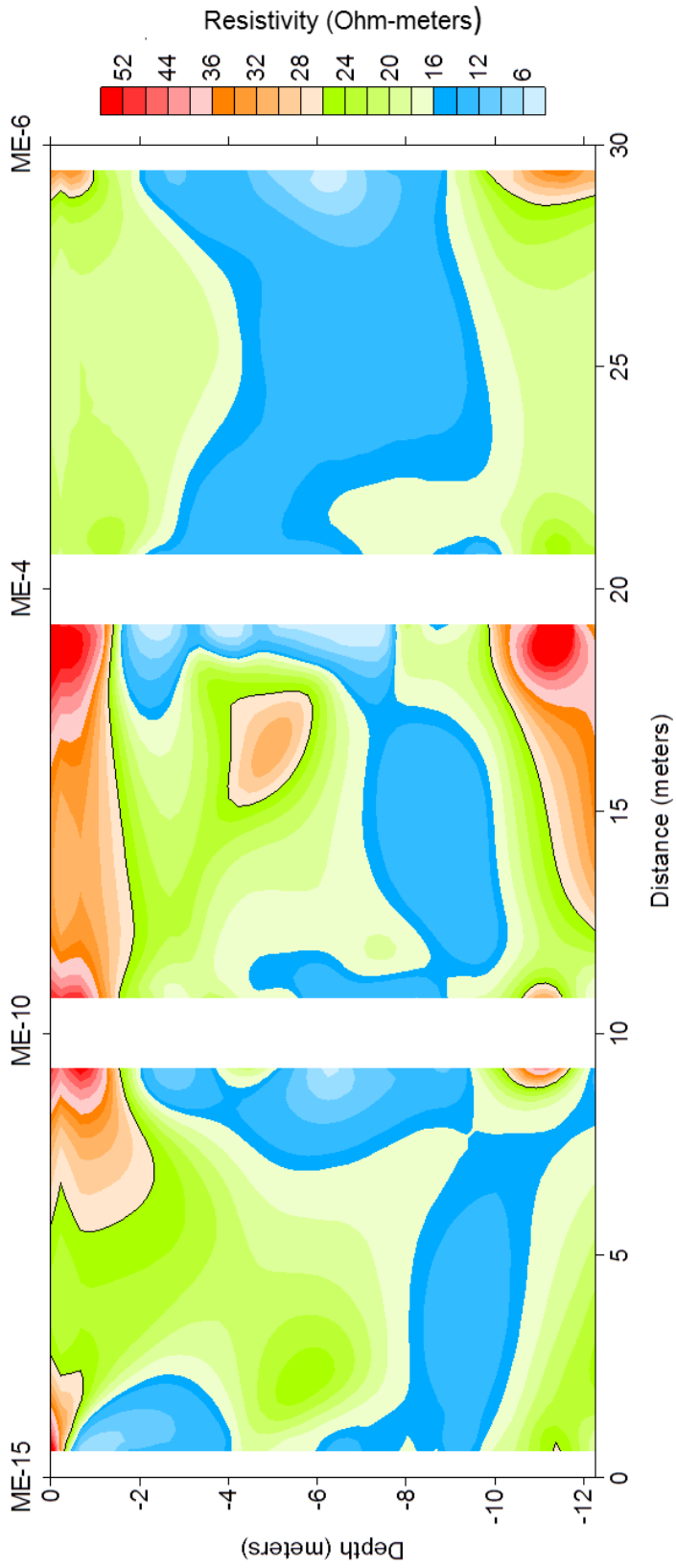

Line 09101112

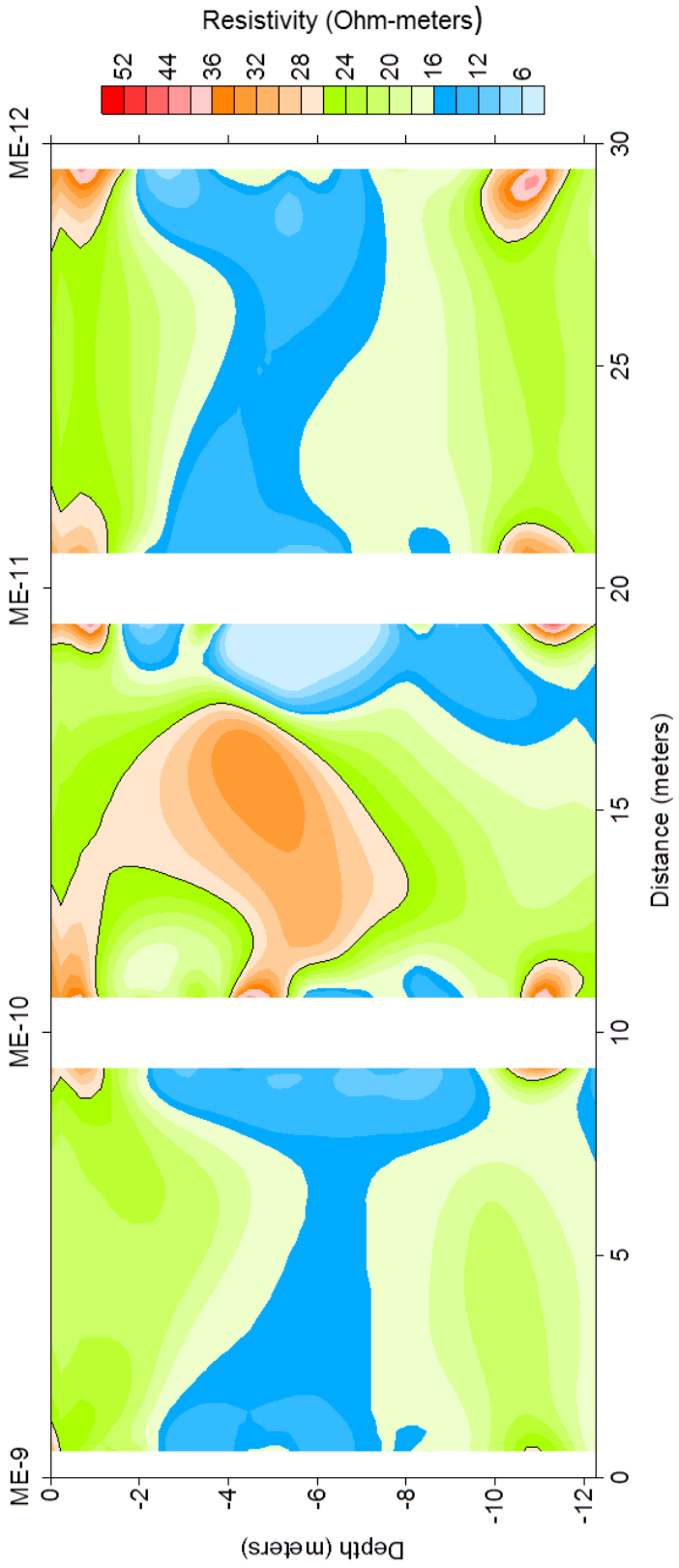

Line 07030408

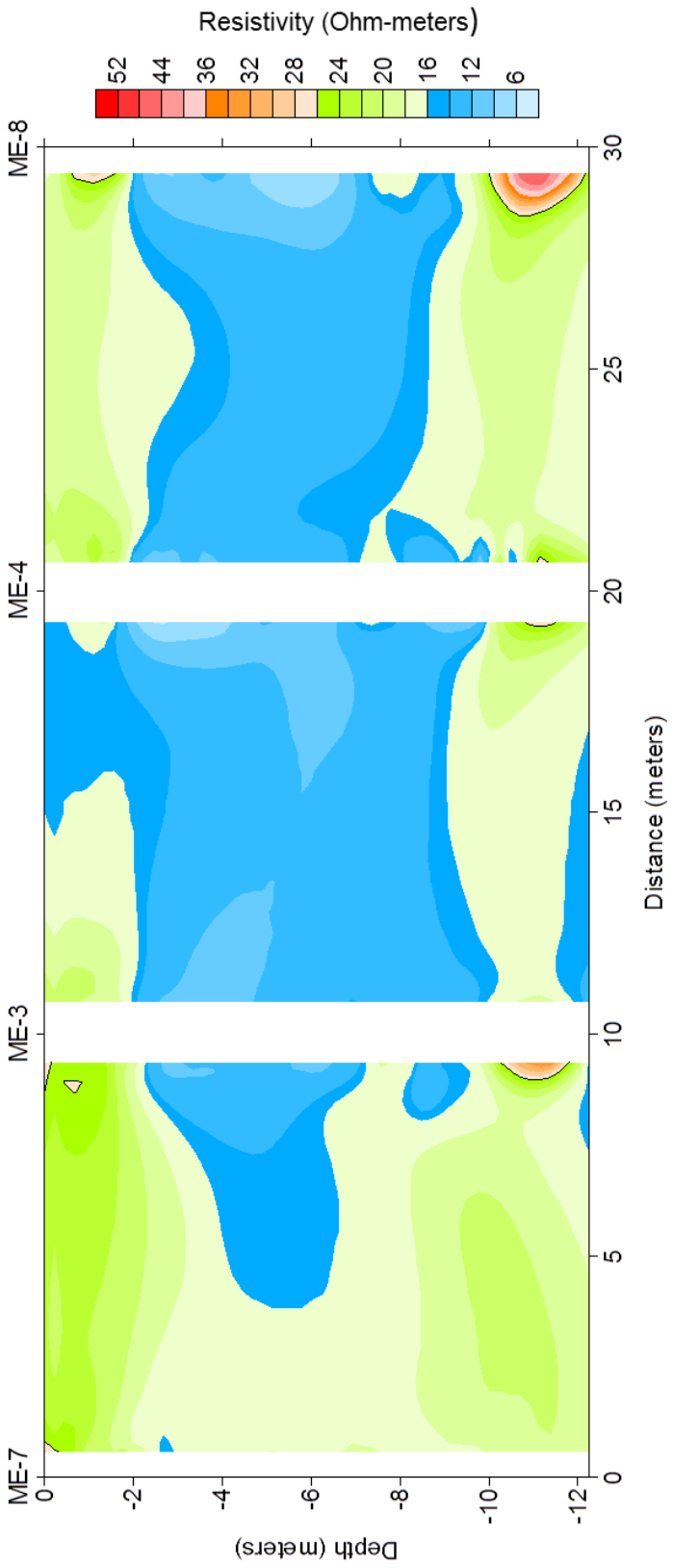

APPENDIX B
MARCH 2011 ERT LINES

This data set contains all the 2-D inverted images from the March 2011 ERT survey. All of the data were collected using the Chicago command file and inverted using EarthImager.

All images run from west to east or south to north. Refer to Figure 1 for locations of lines.

Line 0806

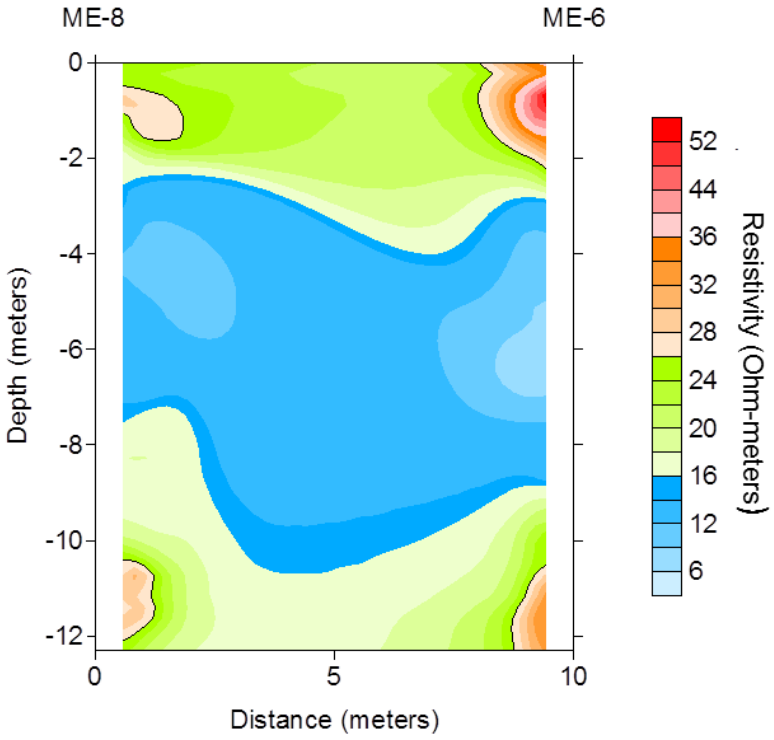

Line 1416

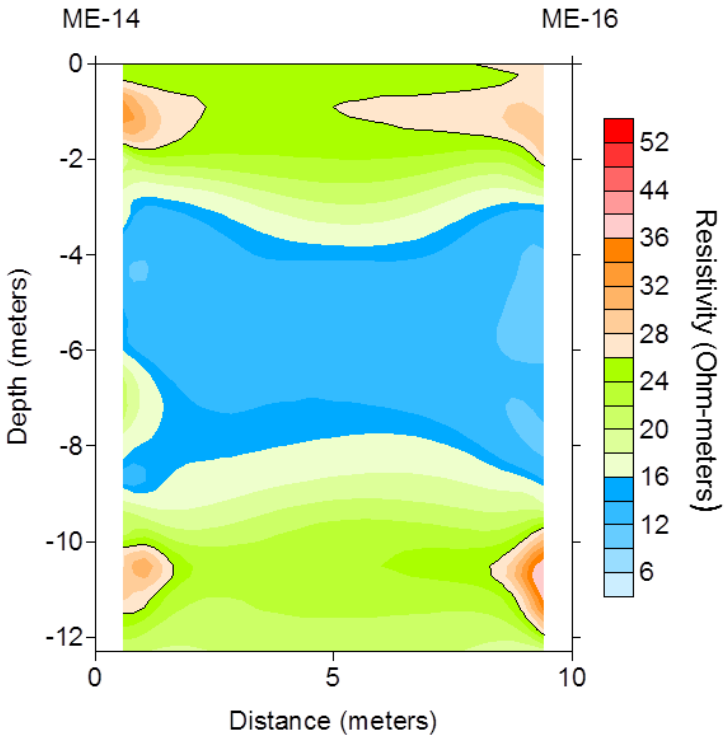

Line 1509

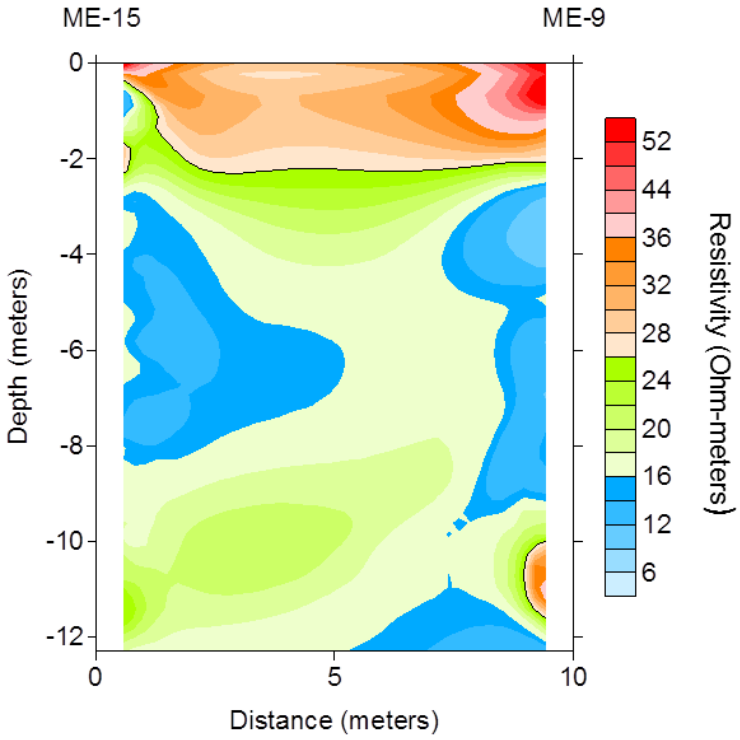

Line 1510

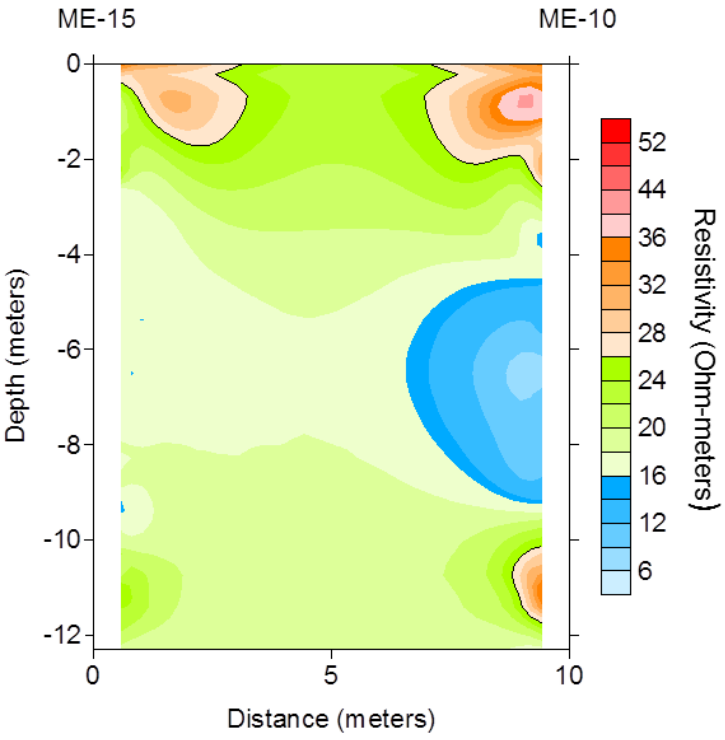

Line 1513

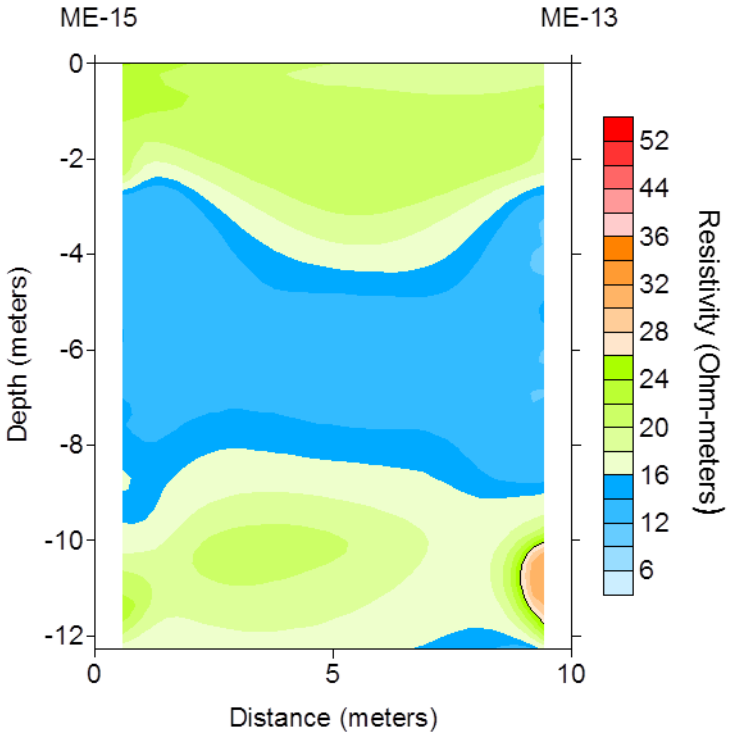
ME-15
ME-13
0
-2
-4
-6
-8
-10
-12
Depth (meters)
0
5
10
Distance (meters)
52
44
36
32
28
24
20
16
12
6
Resistivity (Ohm-meters)

APPENDIX C
DECEMBER 2002–JANUARY 2011 TRANSIENT ERT LINES

This data set contains all the time-lapse or transient 2-D inverted images from the ERT survey. All of the data were collected using the Chicago command file and inverted using EarthImager. In each image the top inverted profile is from December 2002 and the bottom inverted profile is from January 2003.

All images run from west to east or south to north. Refer to Figure 1 for locations of lines.

Line 0412
December 2002-January 2003

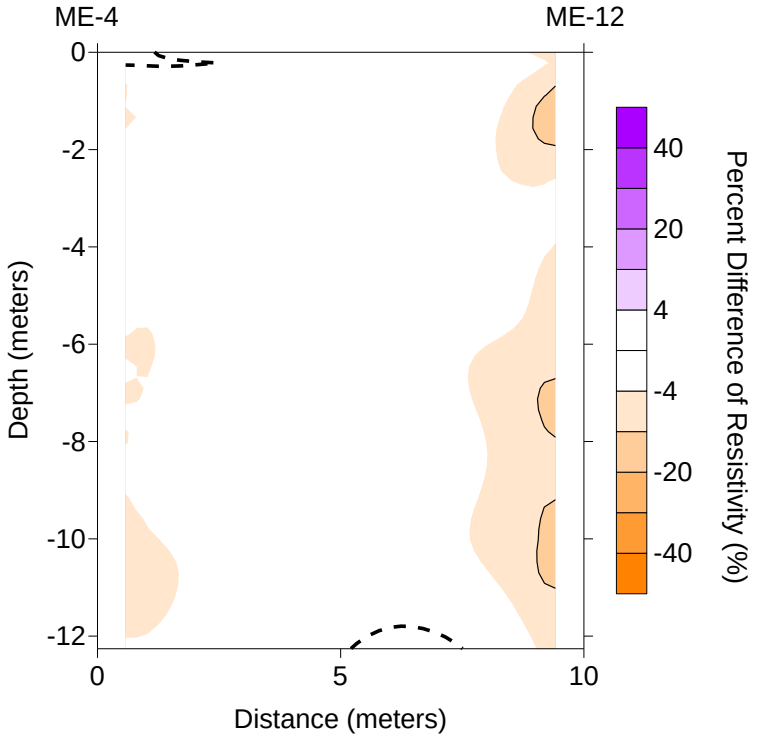

Line 0903
December 2002-January 2003

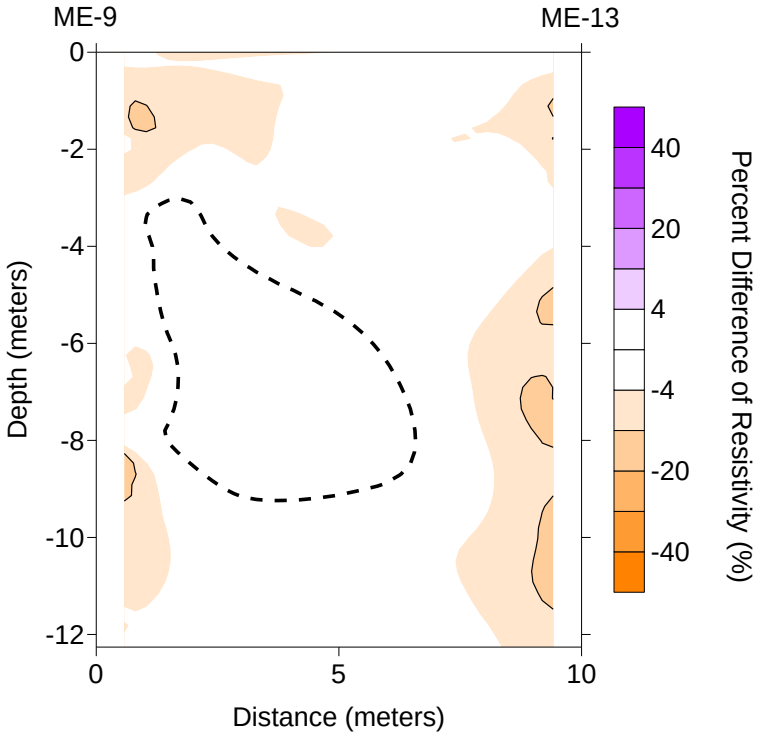

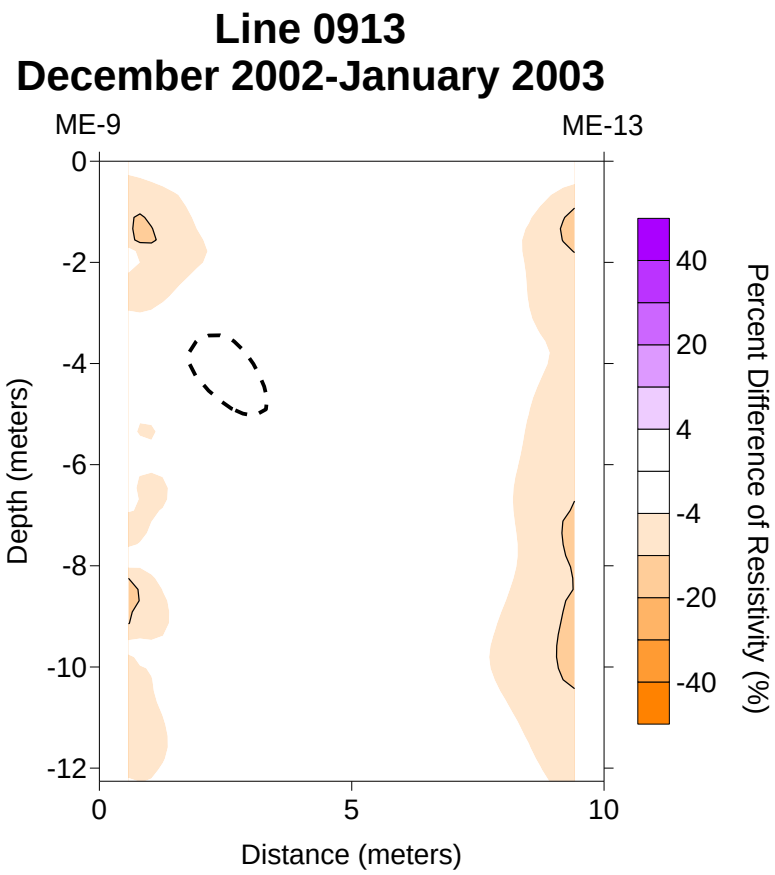
Line 0913
December 2002-January 2003
ME-9
ME-13
0
-2
-4
-6
-8
-10
-12
Depth (meters)
0
5
10
Distance (meters)
40
20
4
-4
-20
-40
Percent Difference of Resistivity (%)

Line 031116
December 2002-January 2003

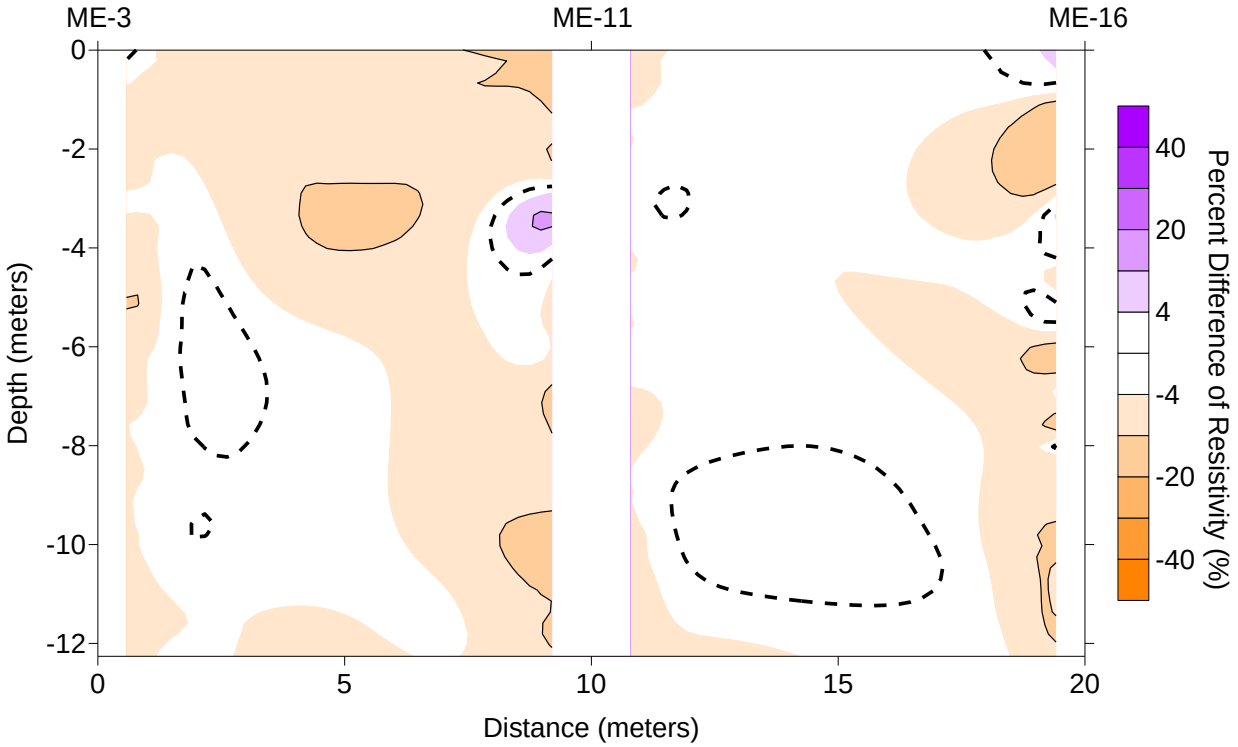

Line 071014
December 2002-January 2003

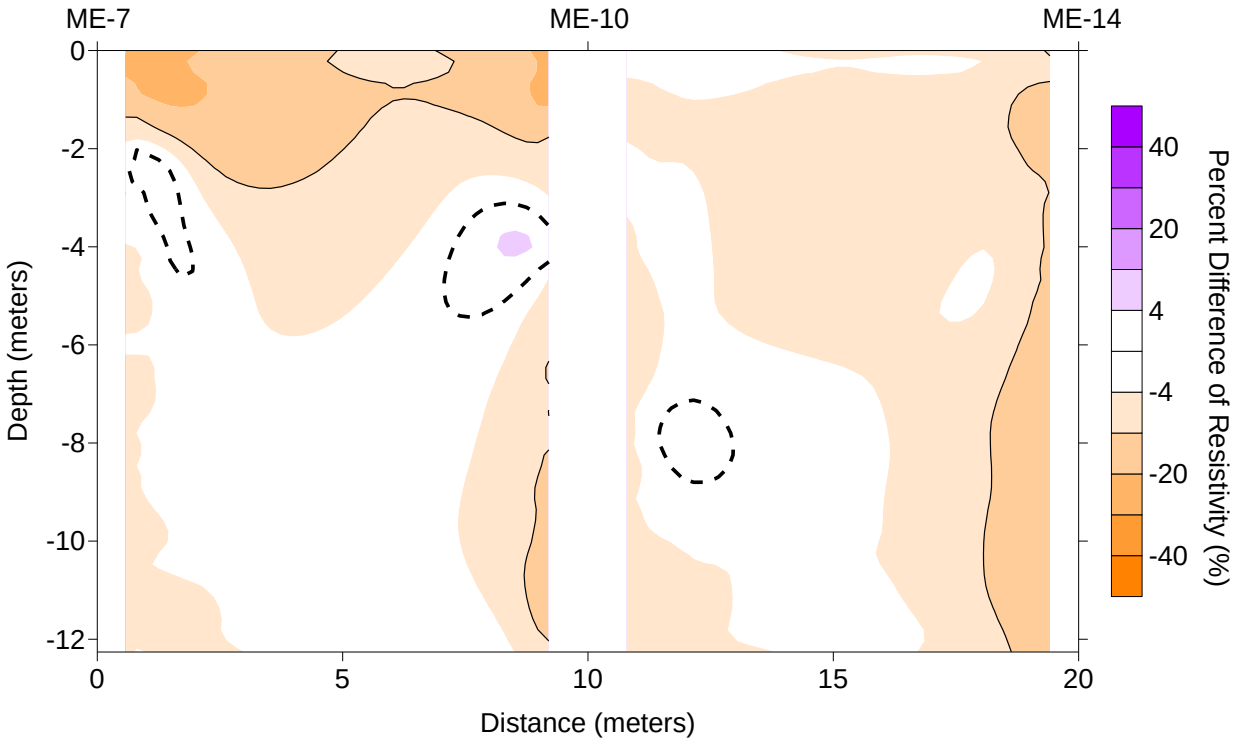

Line 131003
December 2002-January 2003

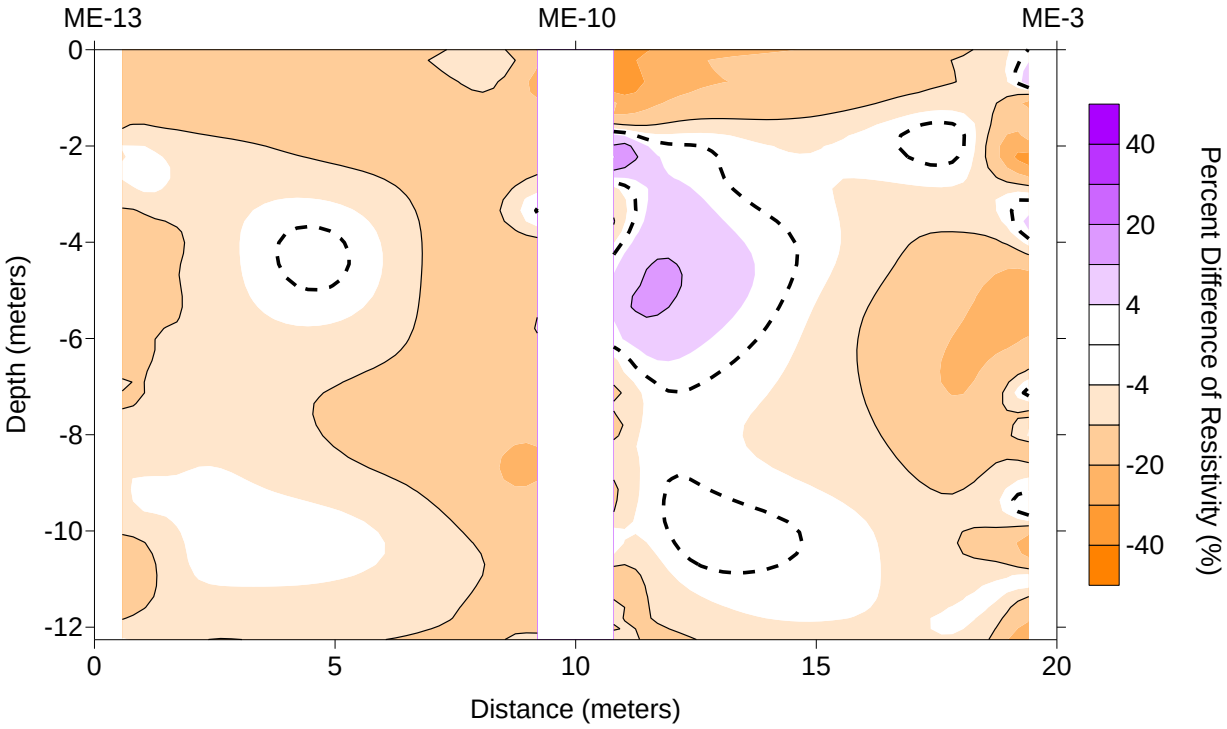

Line 131108
December 2002-January 2003

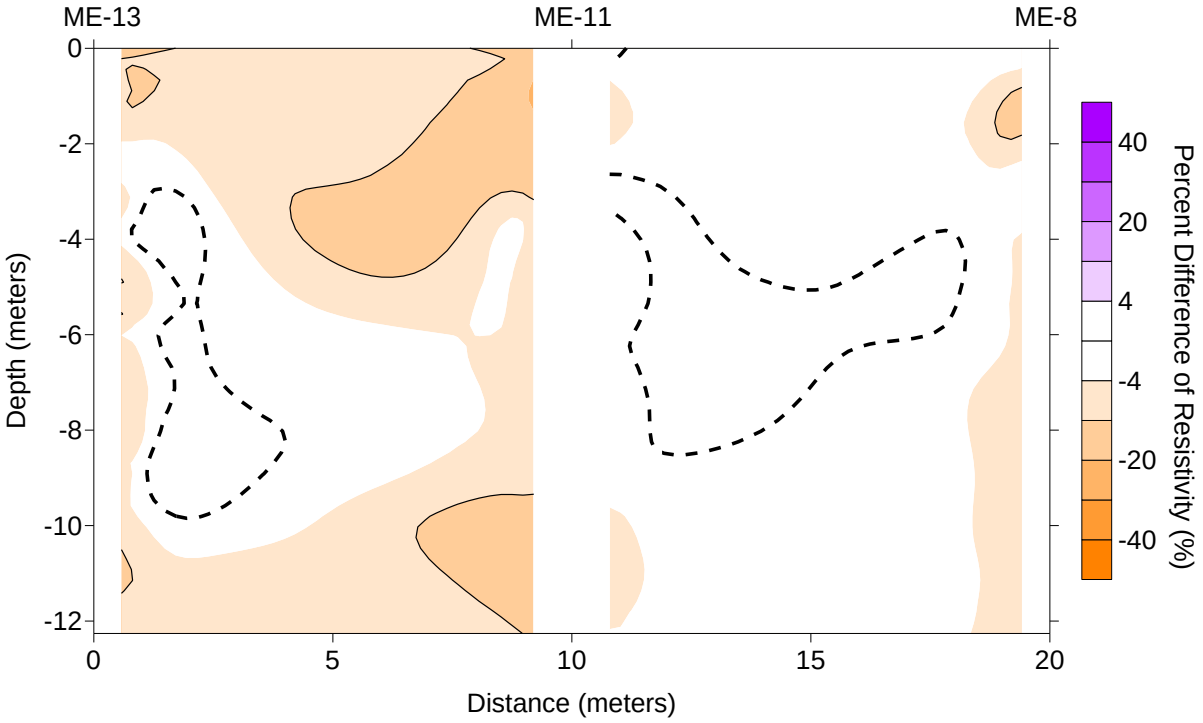

Line 141104
December 2002-January 2003

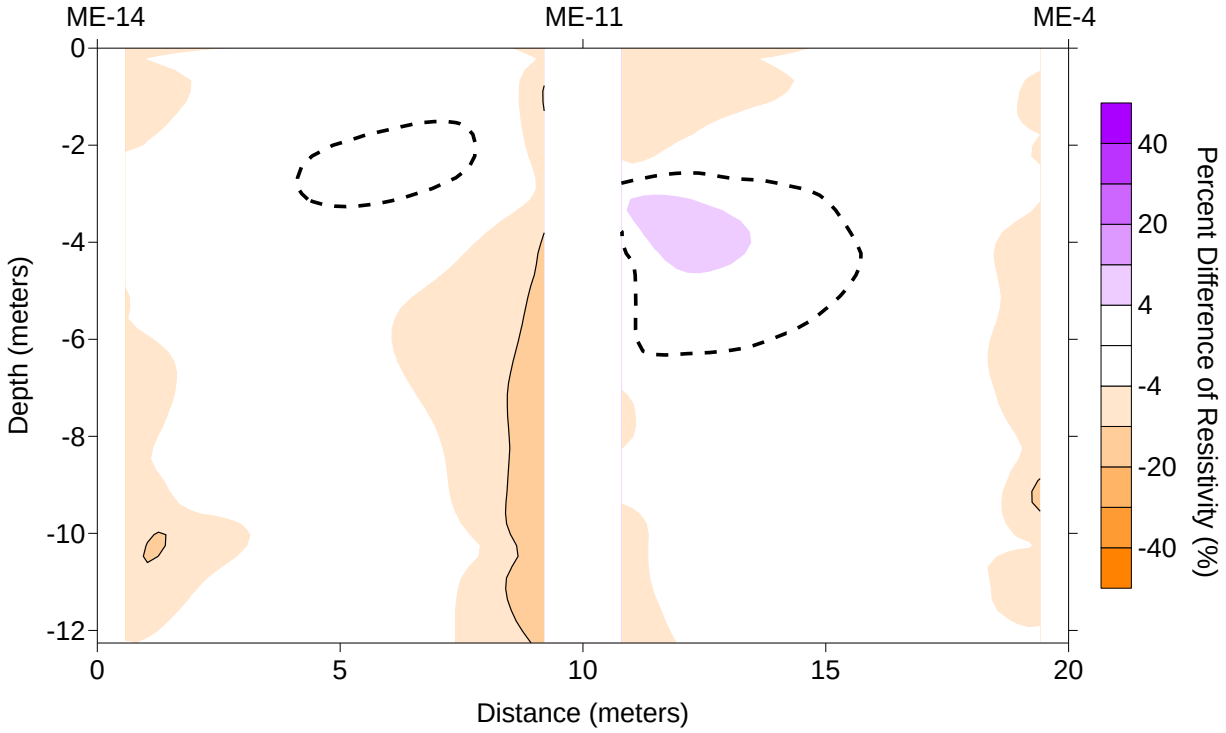

Line 150907
December 2002-January 2003

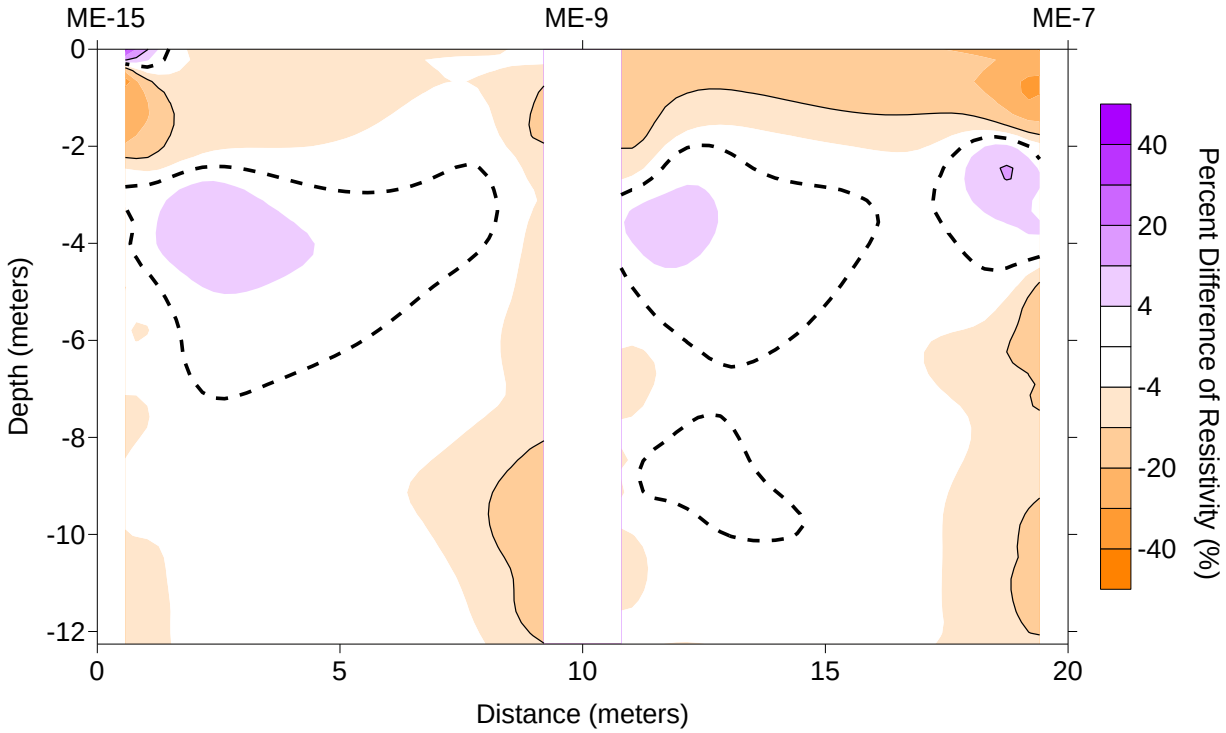

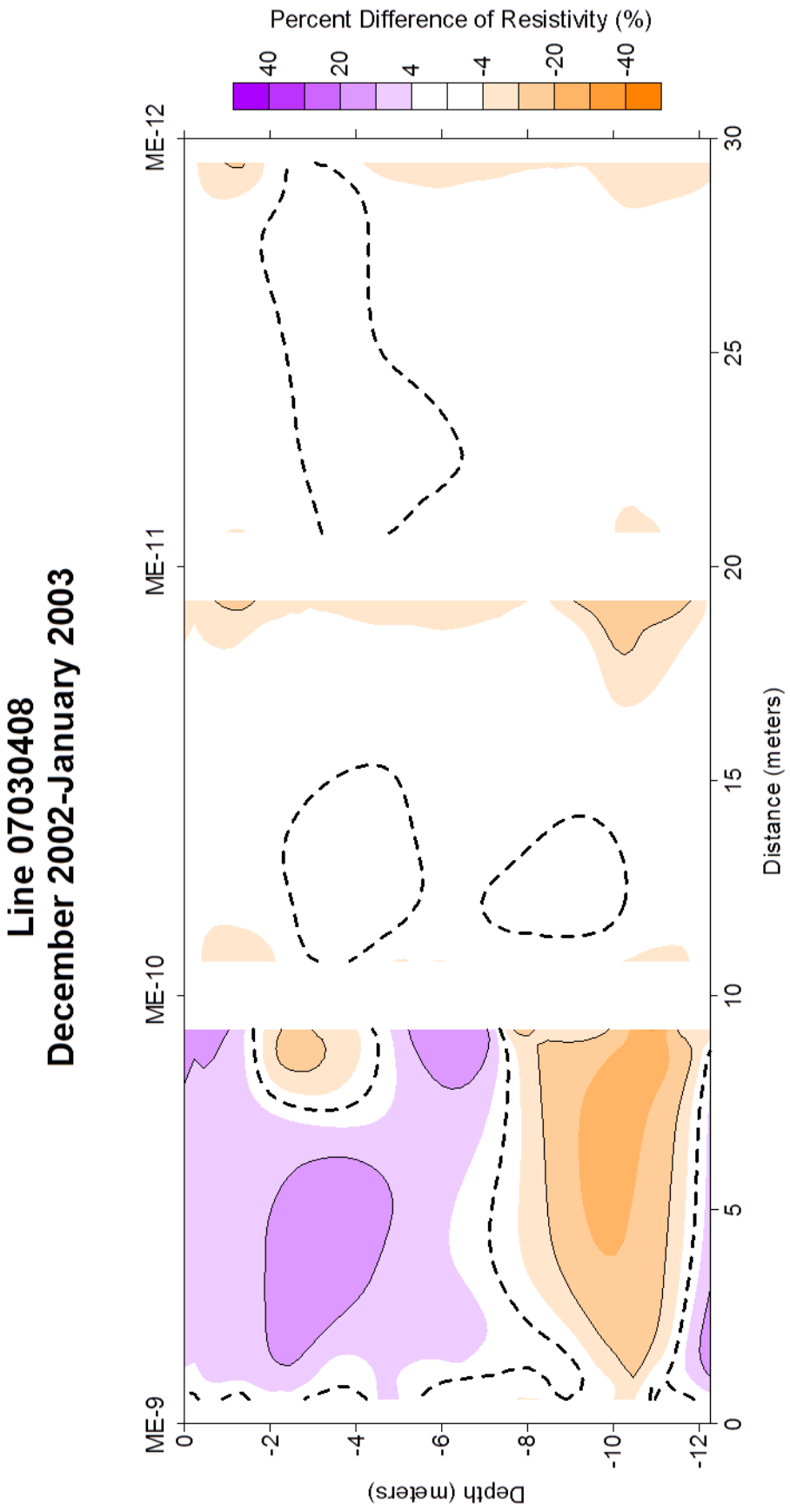
Line 07030408
December 2002-January 2003
Percent Difference of Resistivity (%)
40
20
4
-4
-20
-40
ME-9
ME-10
ME-11
ME-12
0
-2
-4
-6
-8
-10
-12
Depth (meters)
0
5
10
15
20
25
30
Distance (meters)

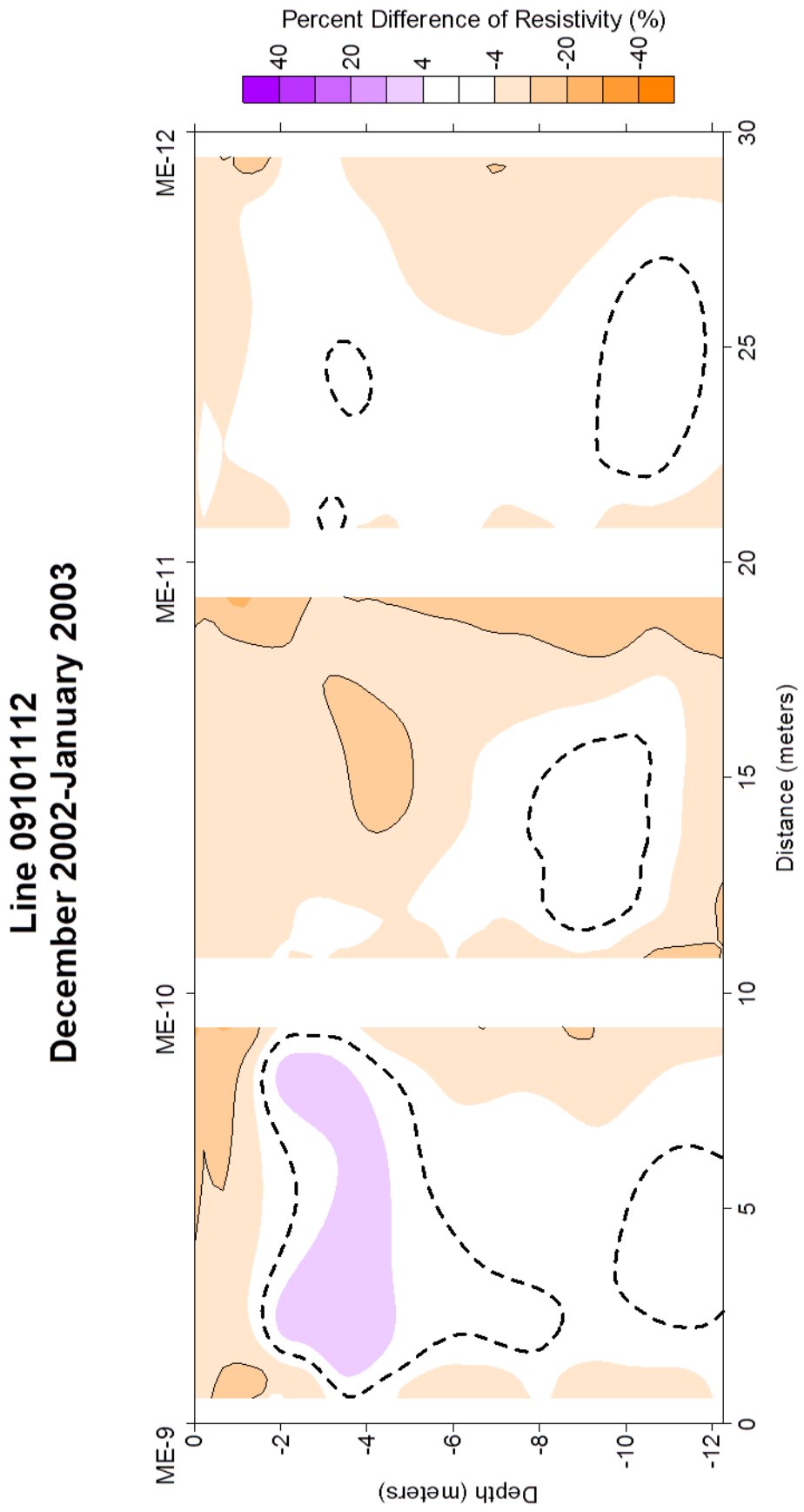
Line 09101112
December 2002-January 2003
Percent Difference of Resistivity (%)
40
20
4
-4
-20
-40
ME-9
ME-10
ME-11
ME-12
0
-2
-4
-6
-8
-10
-12
Depth (meters)
0
5
10
15
20
25
30
Distance (meters)

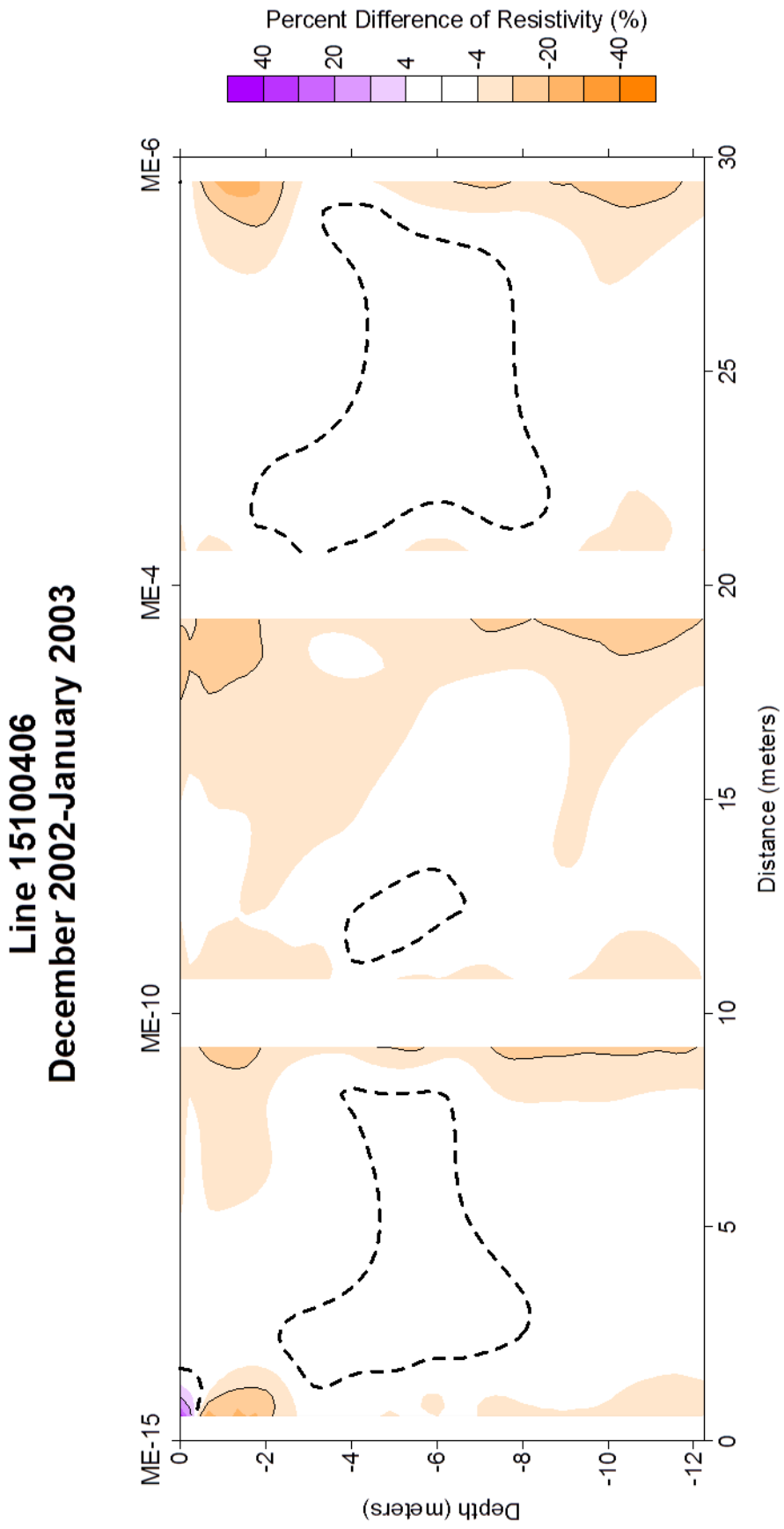
Line 15100406
December 2002-January 2003
Percent Difference of Resistivity (%)
40
20
4
-4
-20
-40
ME-6
ME-4
ME-10
ME-15
0
-2
-4
-6
-8
-10
-12
Depth (meters)
0
5
10
15
20
25
30
Distance (meters)

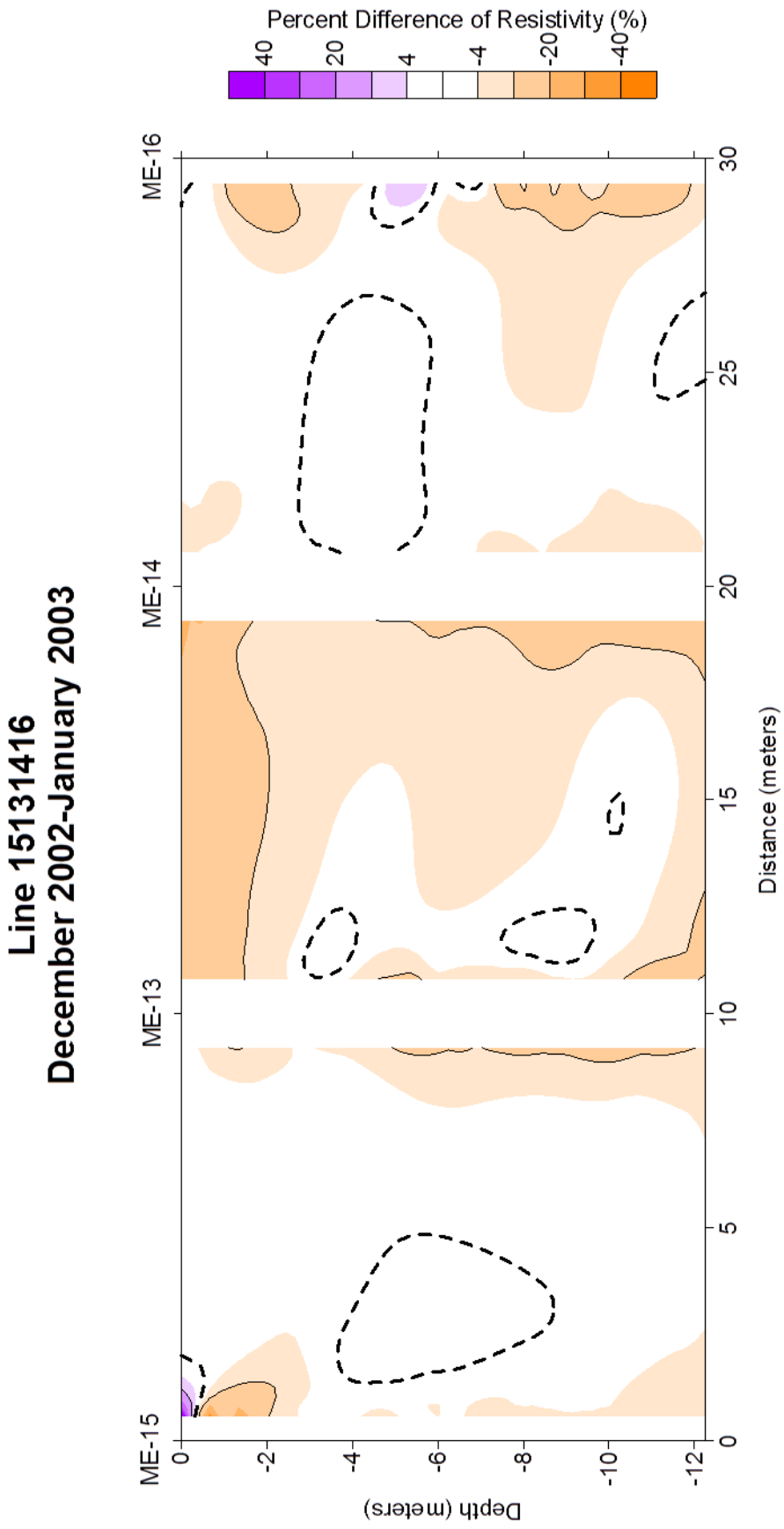
Line 15131416
December 2002-January 2003
Percent Difference of Resistivity (%)
40
20
4
-4
-20
-40
ME-15
ME-13
ME-14
ME-16
0
-2
-4
-6
-8
-10
-12
Depth (meters)
0
5
10
15
20
25
30
Distance (meters)

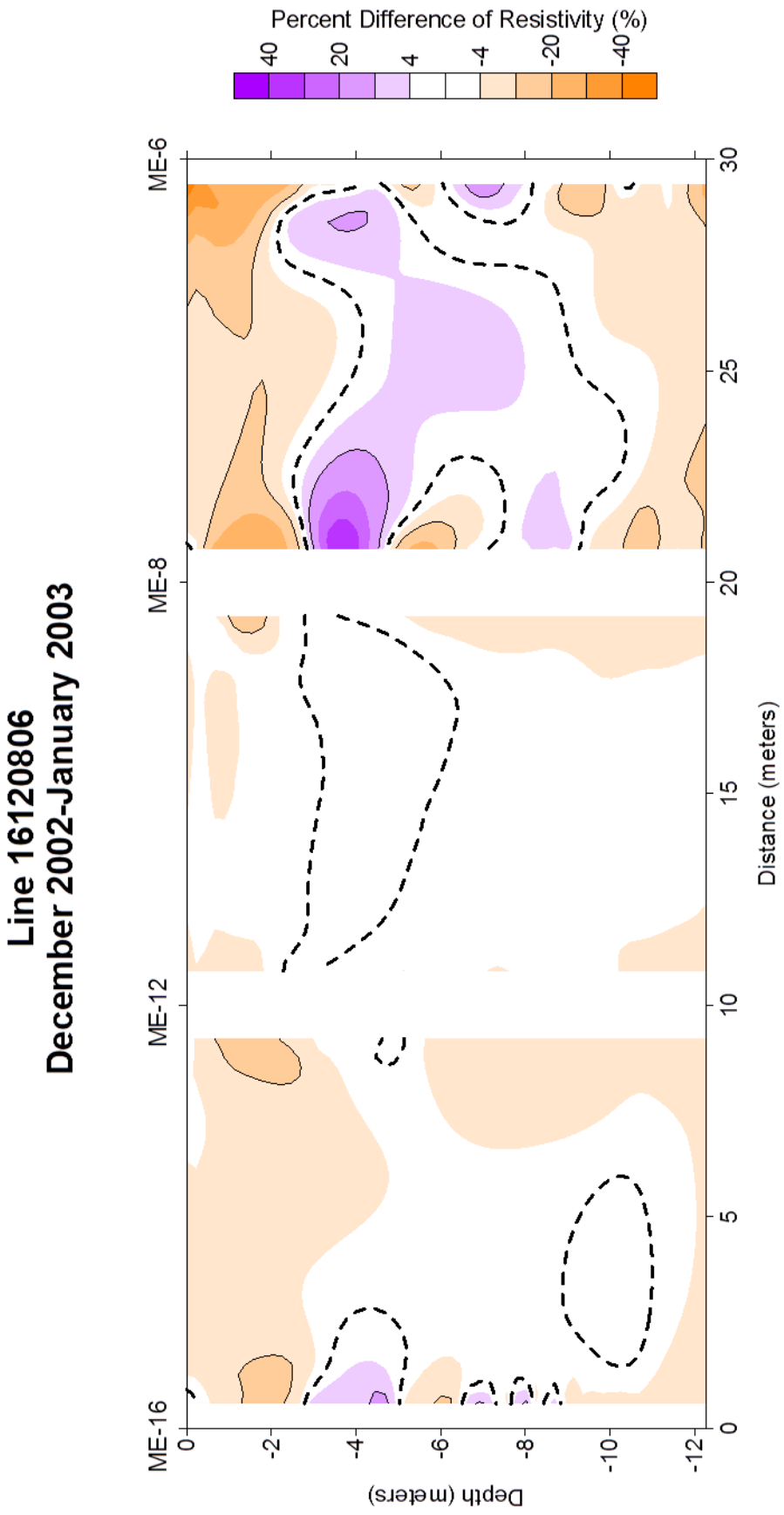
Line 16120806
December 2002-January 2003
Percent Difference of Resistivity (%)
40
20
4
-4
-20
-40
ME-16
ME-12
ME-8
ME-6
0
-2
-4
-6
-8
-10
-12
Depth (meters)
0
5
10
15
20
25
30
Distance (meters)

APPENDIX D
DECEMBER 2002–MAY 2011 TRANSIENT ERT LINES

This data set contains all the time-lapse or transient 2-D inverted images from the ERT survey. All of the data were collected using the Chicago command file and inverted using EarthImager. In each image the top inverted profile is from December 2002 and the bottom inverted profile is from May 2011. Areas that are hatched out are areas of poor data quality or lack of data points.

All images run from west to east or south to north. Refer to Figure 1 for locations of lines.

Line 0412
December 2002-May 2010

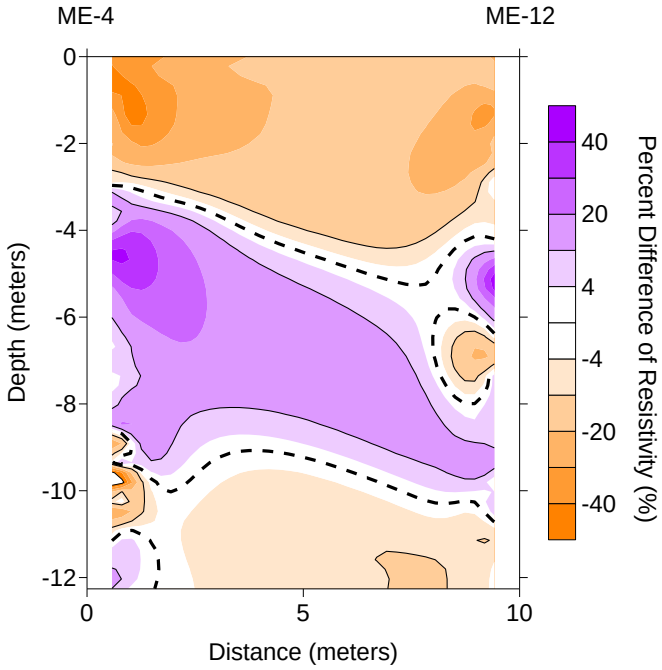

Line 0903
December 2002-May 2010

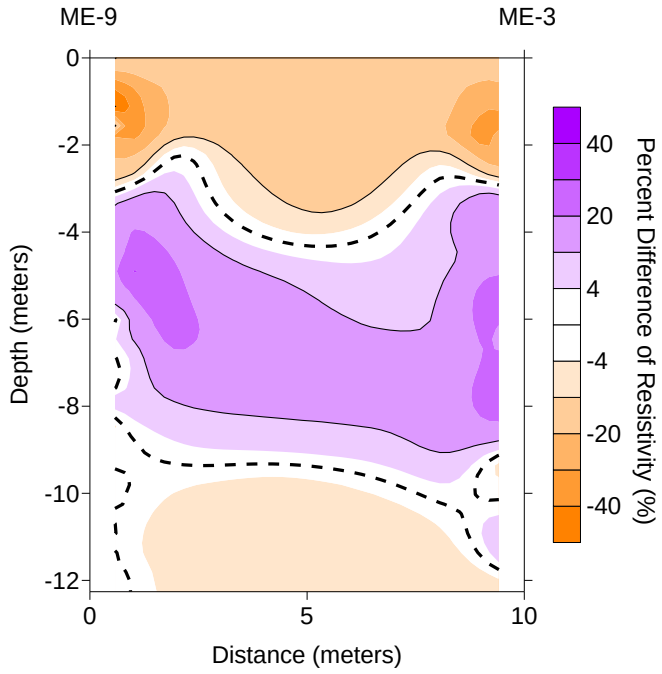

Line 1412
December 2002-May 2010

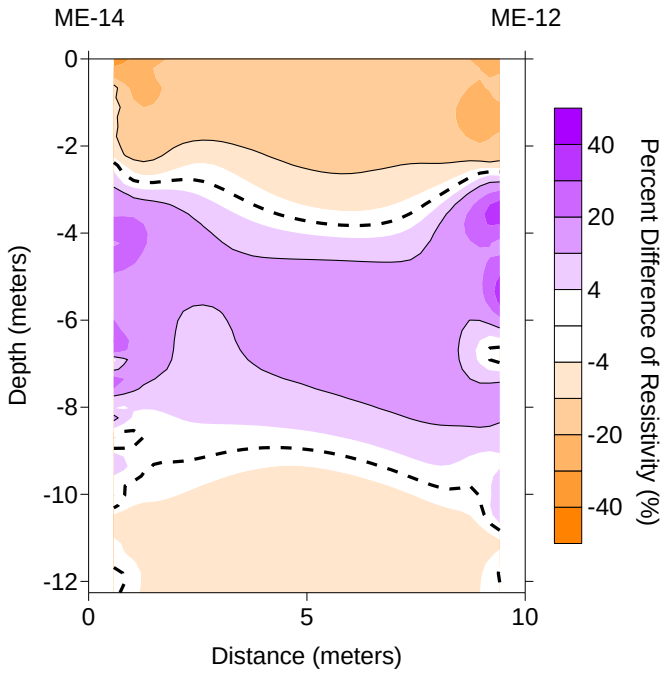

Line 031116
December 2002-May 2010

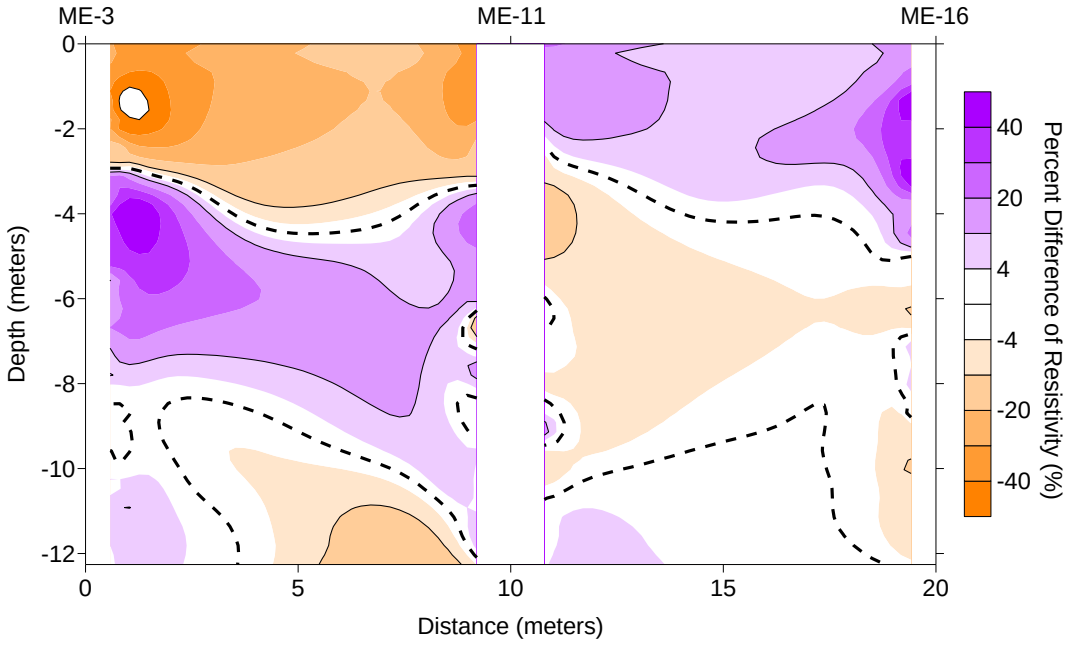

Line 071014
December 2002-May 2010

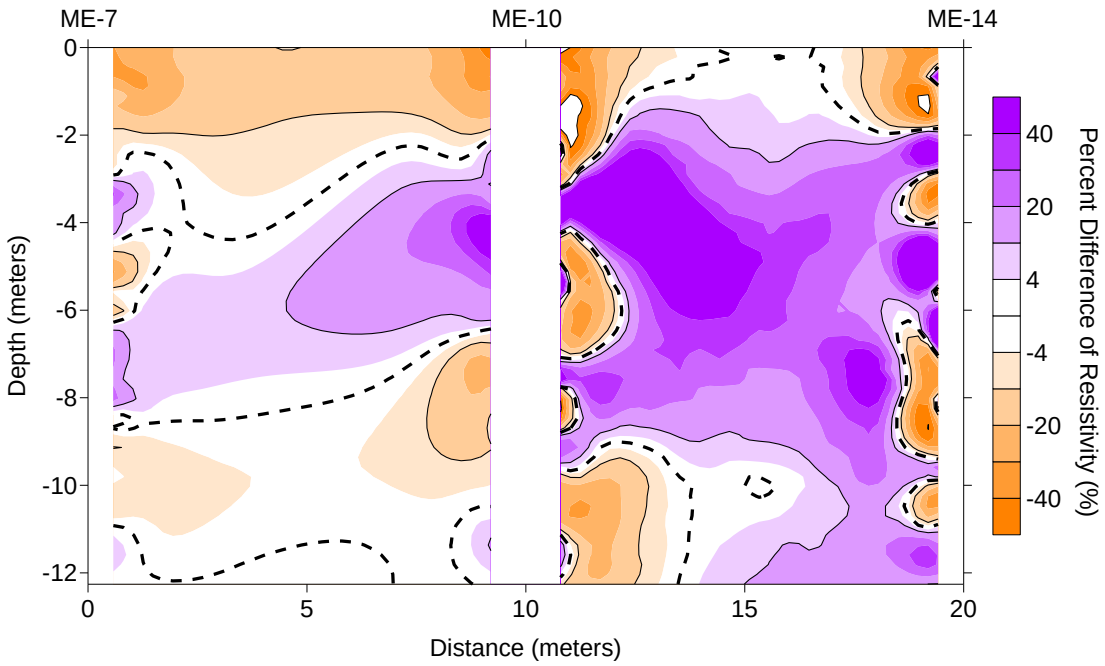

Line 131003
December 2002-May 2010

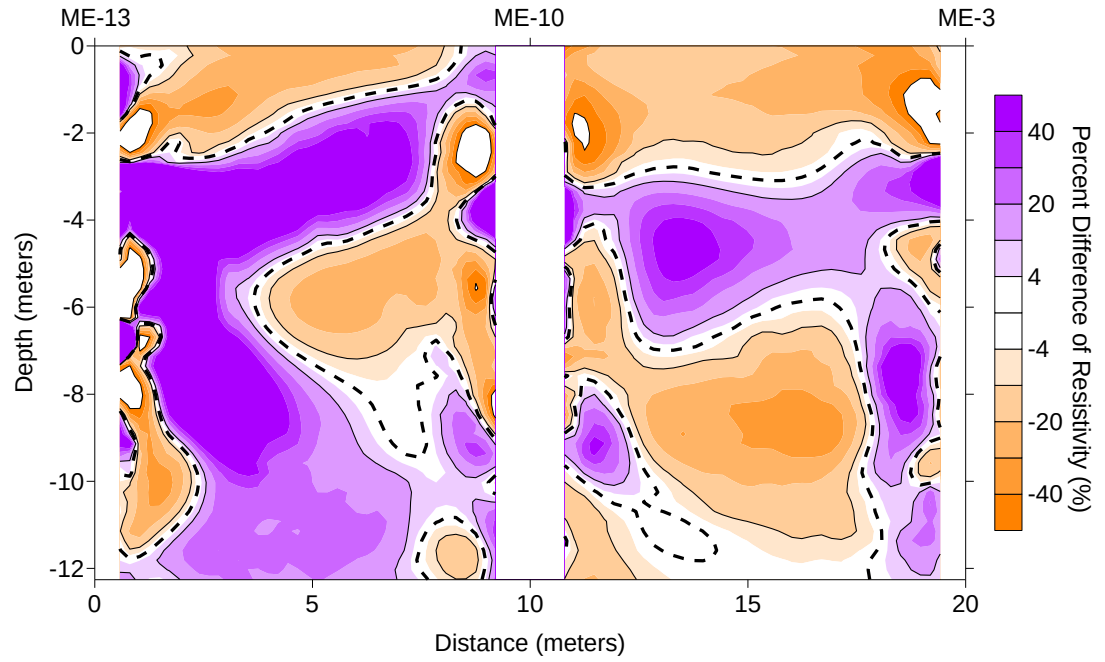

Line 131108
December 2002-May 2010

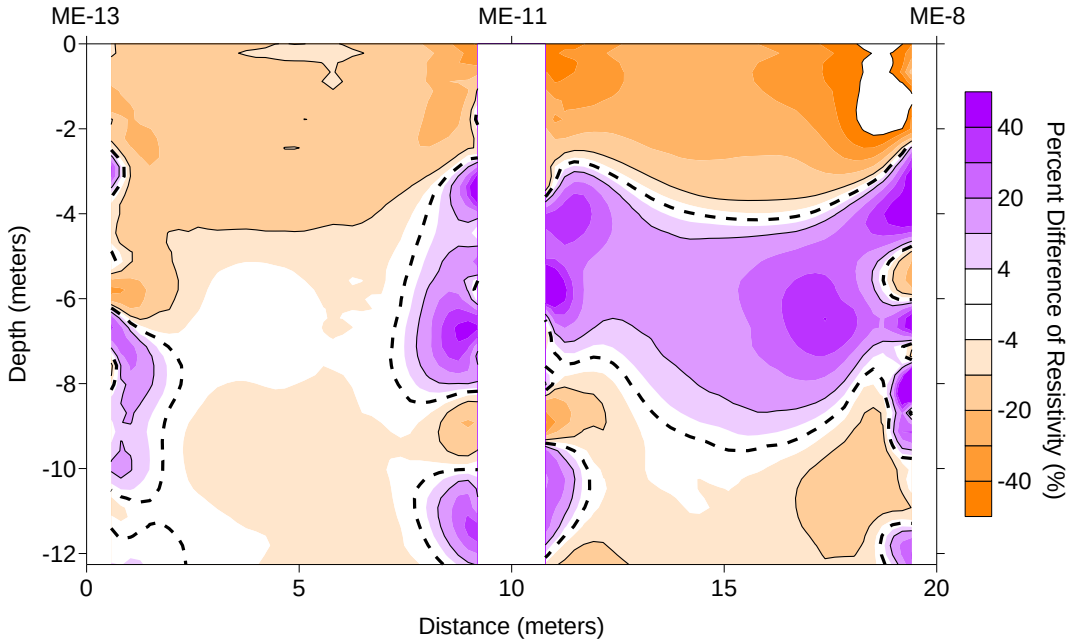

Line 141104
December 2002-May 2010

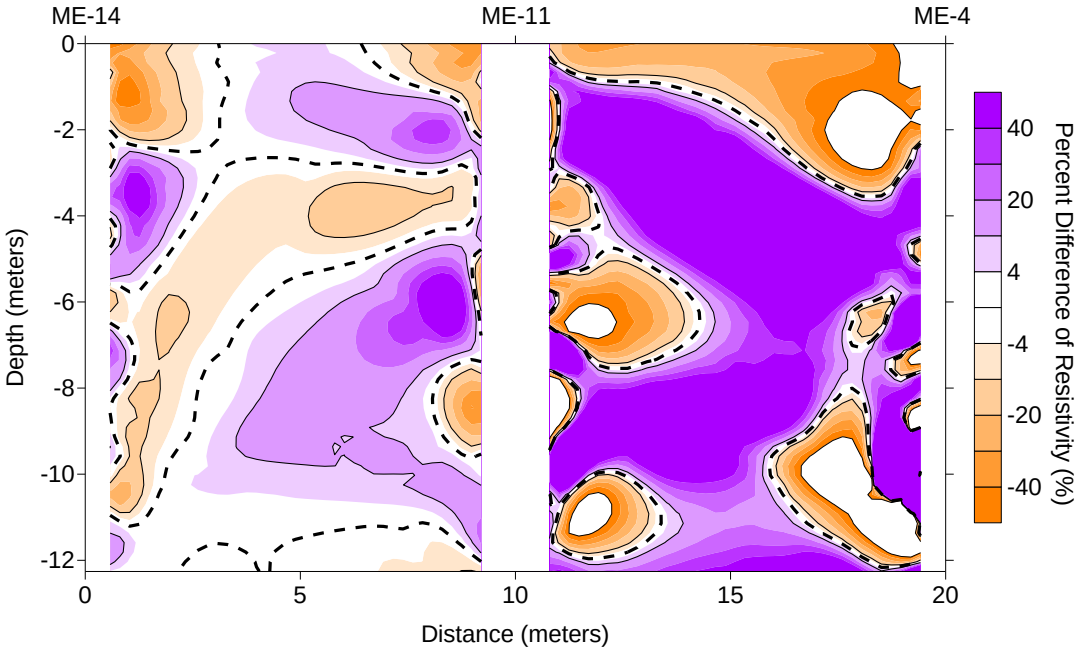

Line 150907
December 2002-May 2010

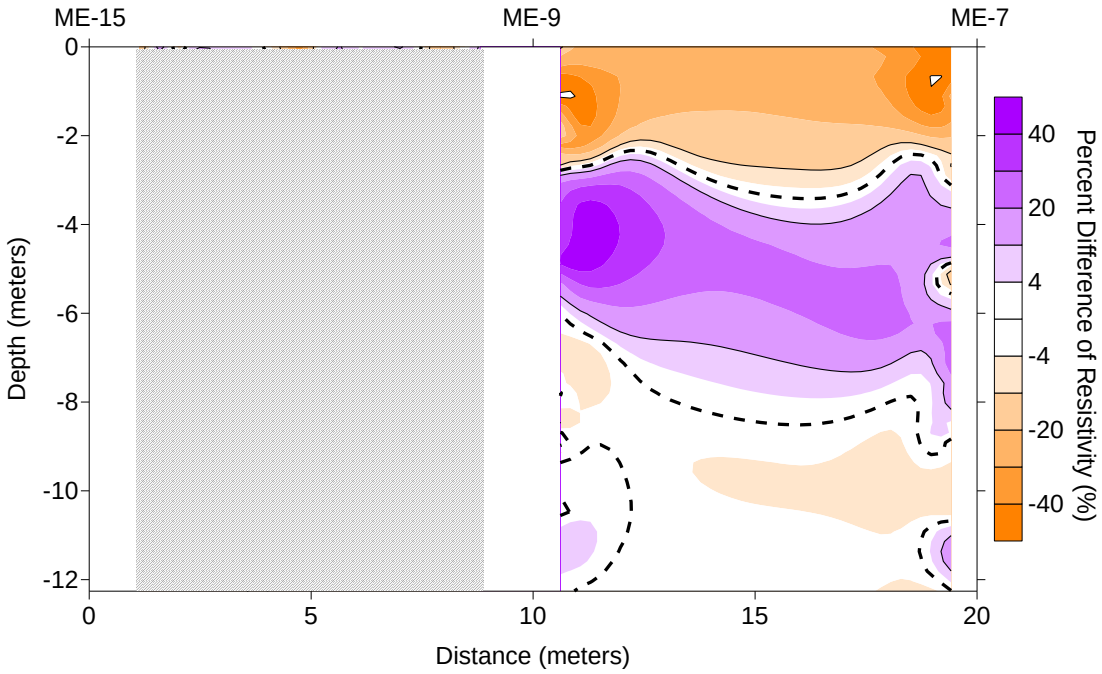

Line 151314
December 2002-May 2010

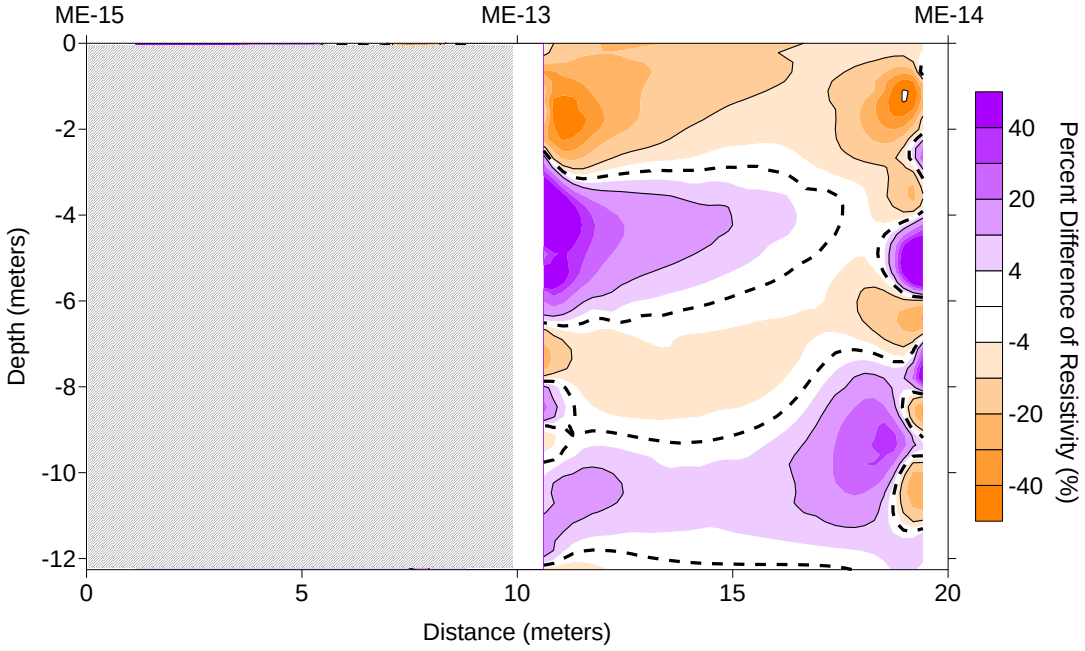

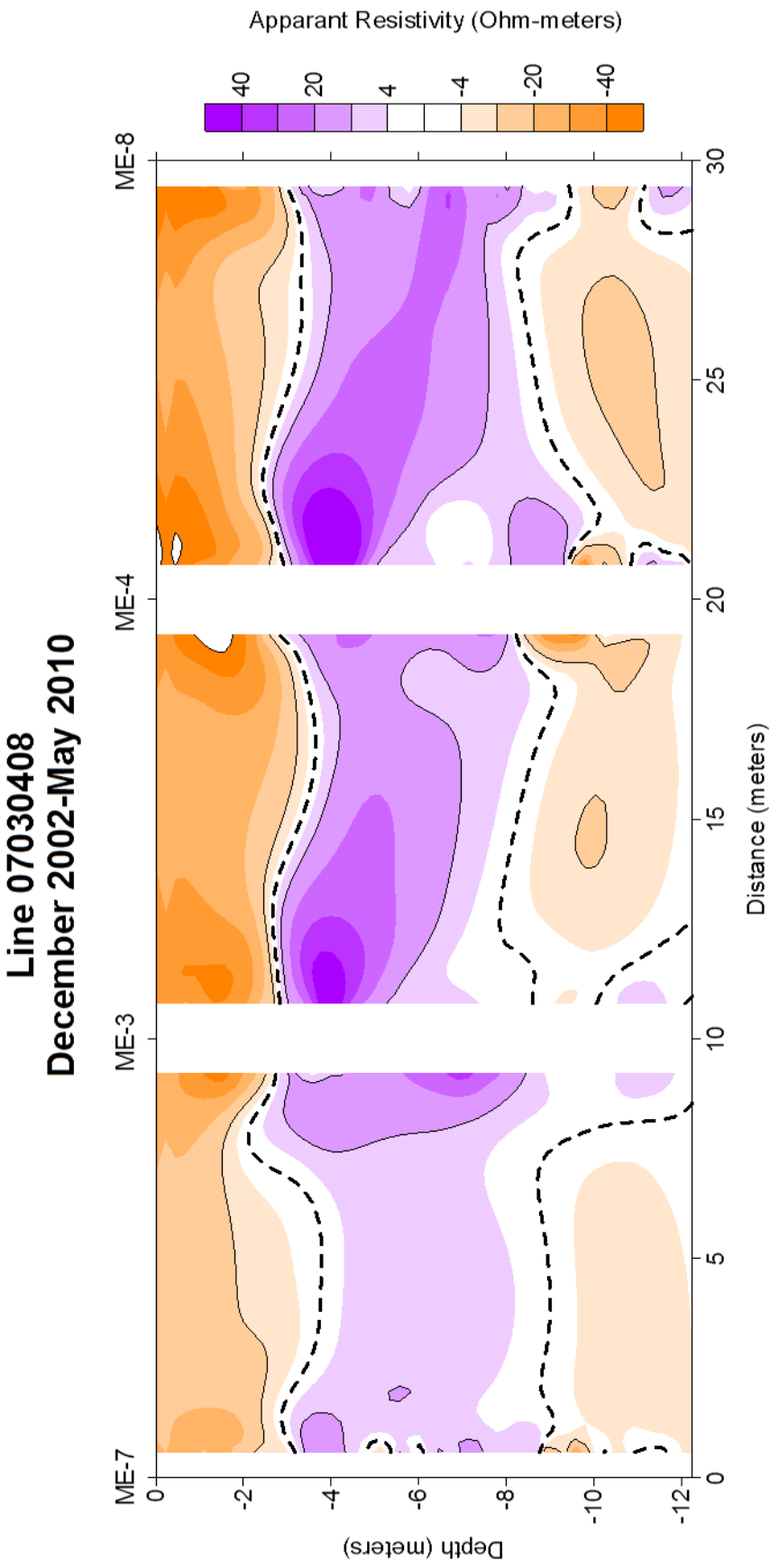
Line 07030408
December 2002-May 2010
Apparant Resistivity (Ohm-meters)
40
20
4
-4
-20
-40
ME-8
ME-4
ME-3
ME-7
0
-2
-4
-6
-8
-10
-12
Depth (meters)
0
5
10
15
20
25
30
Distance (meters)

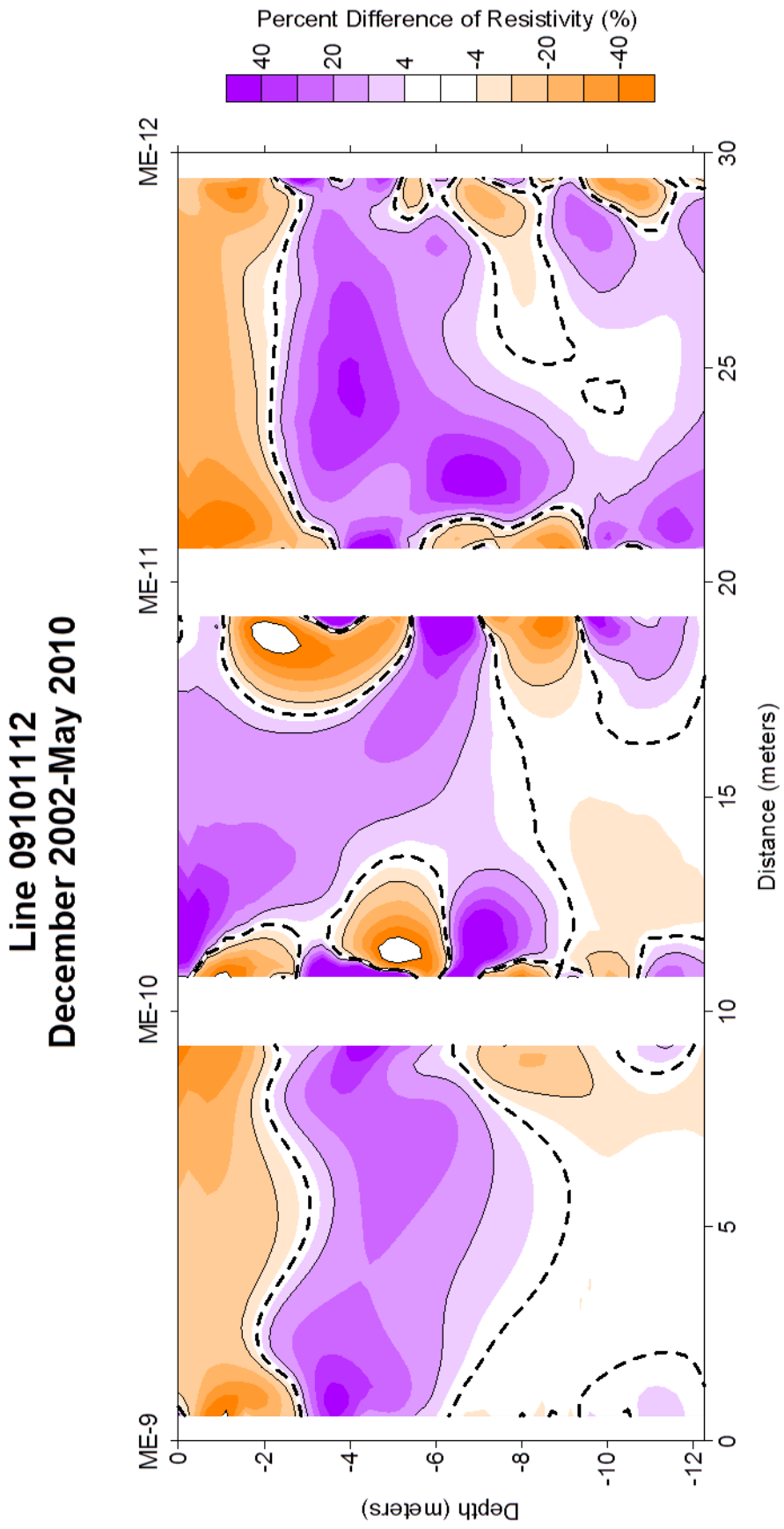
Line 09101112
December 2002-May 2010
Percent Difference of Resistivity (%)
40
20
4
-4
-20
-40
ME-9
ME-10
ME-11
ME-12
0
-2
-4
-6
-8
-10
-12
Depth (meters)
0
5
10
15
20
25
30
Distance (meters)

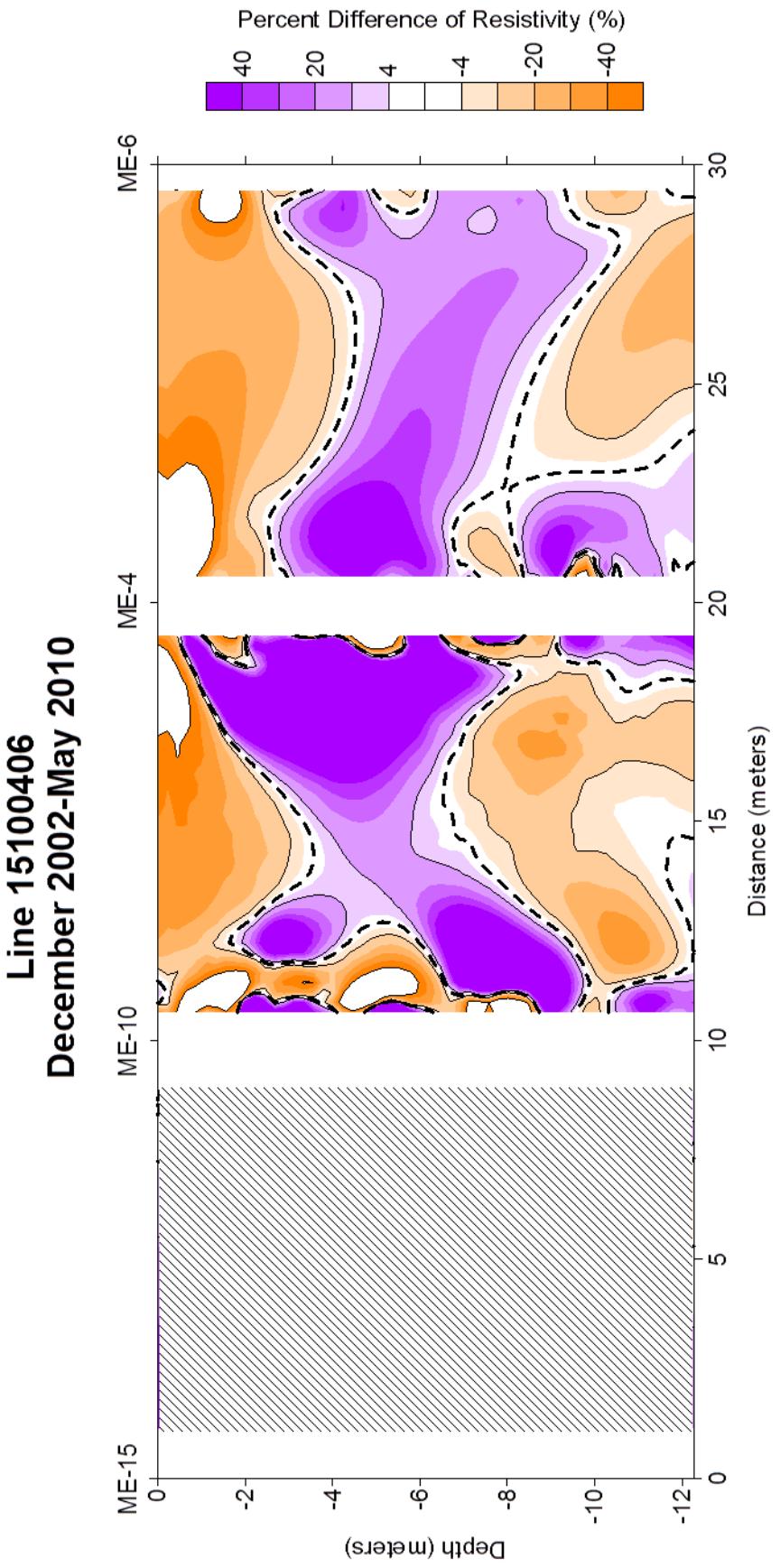
Line 15100406
December 2002-May 2010
Percent Difference of Resistivity (%)
40
20
4
-4
-20
-40
ME-6
ME-4
ME-10
ME-15
0
-2
-4
-6
-8
-10
-12
Depth (meters)
0
5
10
15
20
25
30
Distance (meters)

APPENDIX E
BTX TERNARY DIAGRAMS

This data set contains all of the ternary diagrams generated using the benzene, toluene, and xylene method by Lipson, 2000.

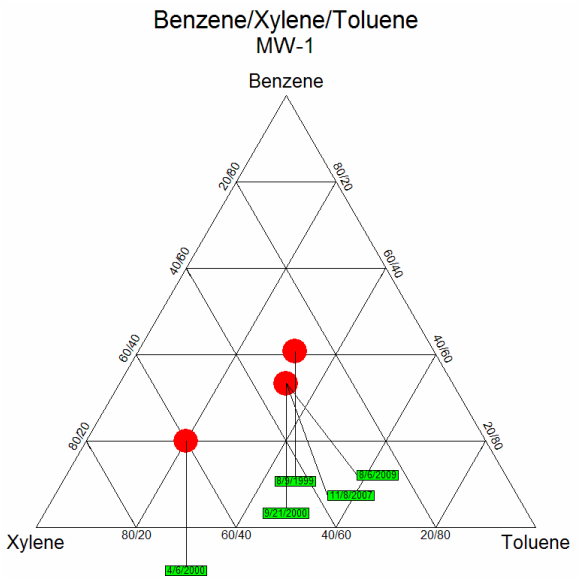
Benzene/Xylene/Toluene
MW-1
Benzene
Xylene
Toluene
20/80
80/20
40/60
60/40
60/40
40/60
80/20
20/80
80/20
60/40
40/60
20/80
8/9/1999
6/6/2009
11/8/2007
5/21/2000
4/6/2000

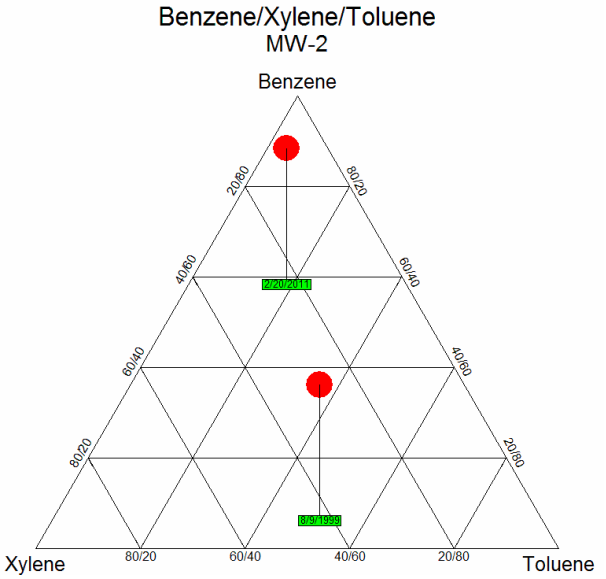
Benzene/Xylene/Toluene
MW-2
Benzene
Xylene
Toluene
20/80
80/20
40/60
60/40
60/40
40/60
80/20
20/80
80/20
60/40
40/60
20/80
2/20/2014
8/9/1999

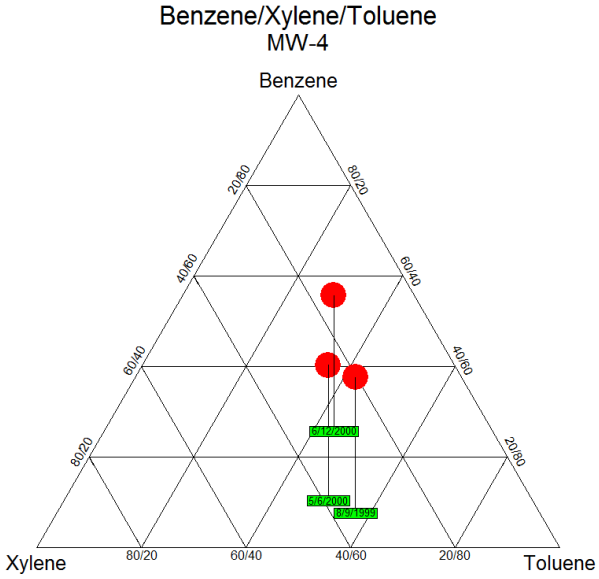
Benzene/Xylene/Toluene
MW-4
Benzene
Xylene
Toluene
20/80
80/20
40/60
60/40
60/40
40/60
80/20
20/80
80/20
60/40
40/60
20/80
6/12/2000
5/6/2000
8/9/1999

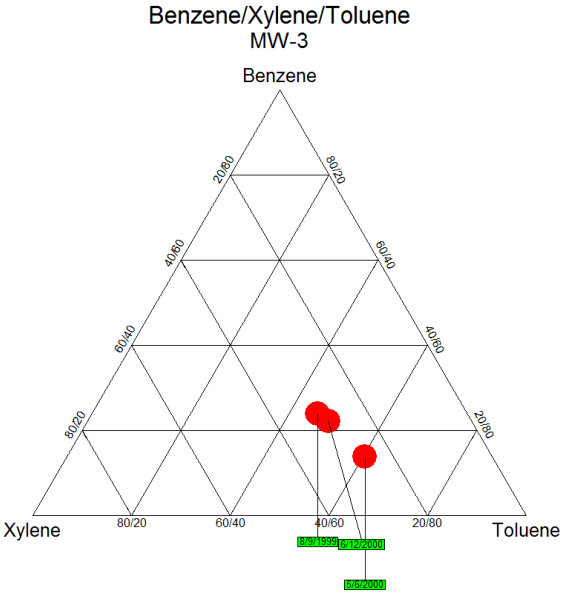
Benzene/Xylene/Toluene
MW-3
Benzene
Xylene
Toluene
20/80
80/20
40/60
60/40
60/40
40/60
80/20
20/80
80/20
60/40
40/60
20/80
8/9/1999
6/12/2000
5/6/2000

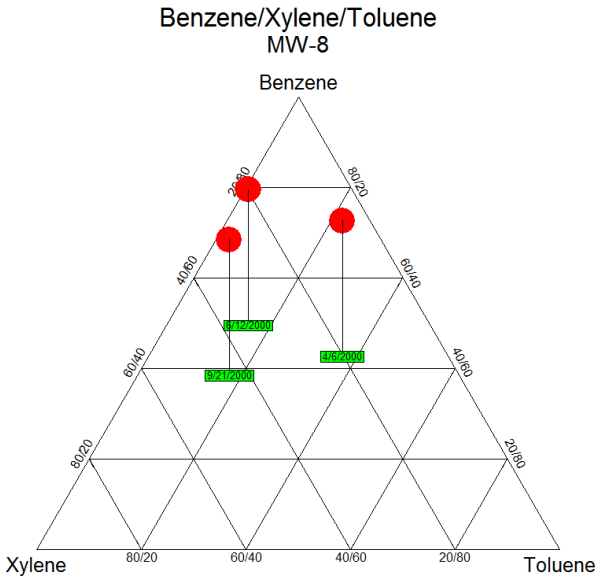
Benzene/Xylene/Toluene
MW-8
Benzene
Xylene
Toluene
80/20
60/40
40/60
20/80
5/12/2000
4/5/2000
9/21/2000

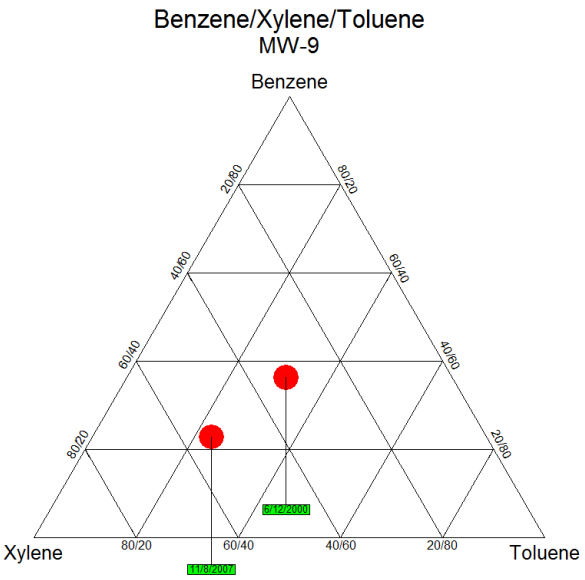
Benzene/Xylene/Toluene
MW-9
Benzene
Xylene
Toluene
80/20
60/40
40/60
20/80
5/12/2000
11/8/2007

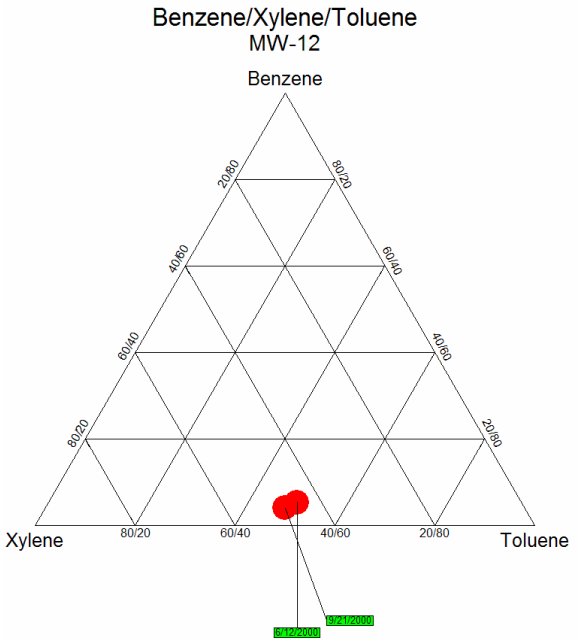
Benzene/Xylene/Toluene
MW-12
Benzene
Xylene
Toluene
80/20
60/40
40/60
20/80
5/12/2000
9/21/2000

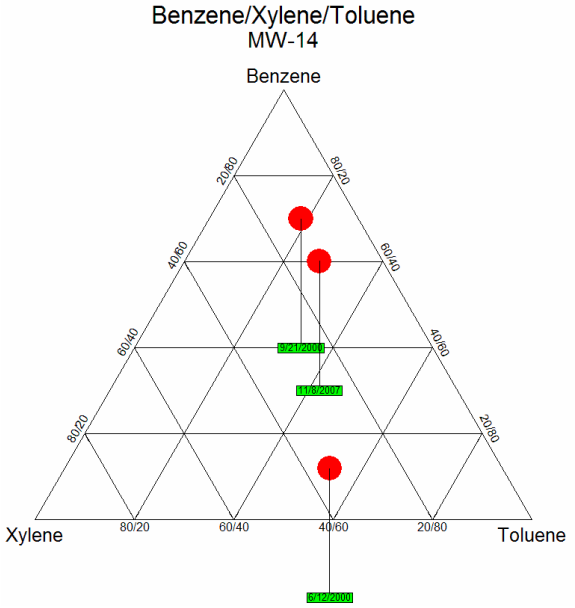
Benzene/Xylene/Toluene
MW-14
Benzene
Xylene
Toluene
80/20
60/40
40/60
20/80
9/21/2000
11/8/2007
5/12/2000

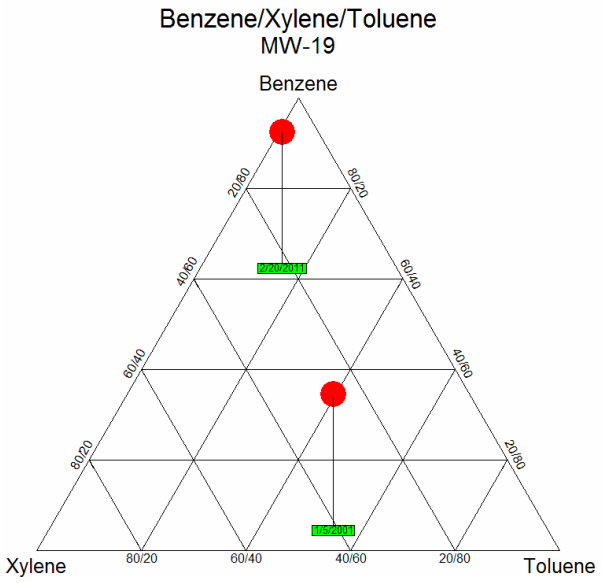
Benzene/Xylene/Toluene
MW-19
Benzene
Xylene
Toluene
20/80
80/20
40/60
60/40
60/40
40/60
80/20
20/80
2/20/2011
1/5/2001

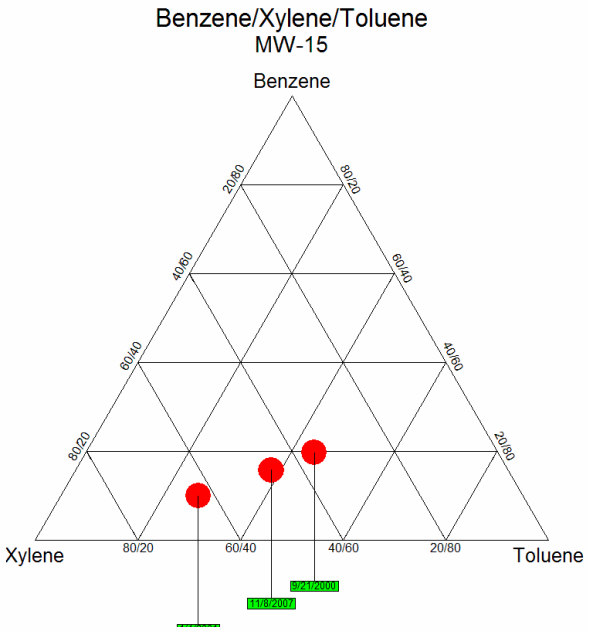
Benzene/Xylene/Toluene
MW-15
Benzene
Xylene
Toluene
20/80
80/20
40/60
60/40
60/40
40/60
80/20
20/80
9/21/2000
11/8/2007

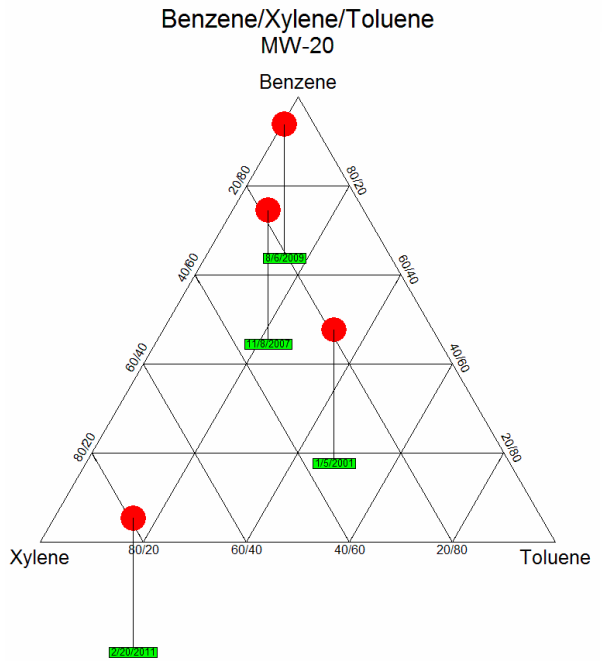
Benzene/Xylene/Toluene
MW-20
Benzene
Xylene
Toluene
20/80
80/20
40/60
60/40
60/40
40/60
80/20
20/80
9/6/2005
11/8/2007
1/5/2001
2/20/2011

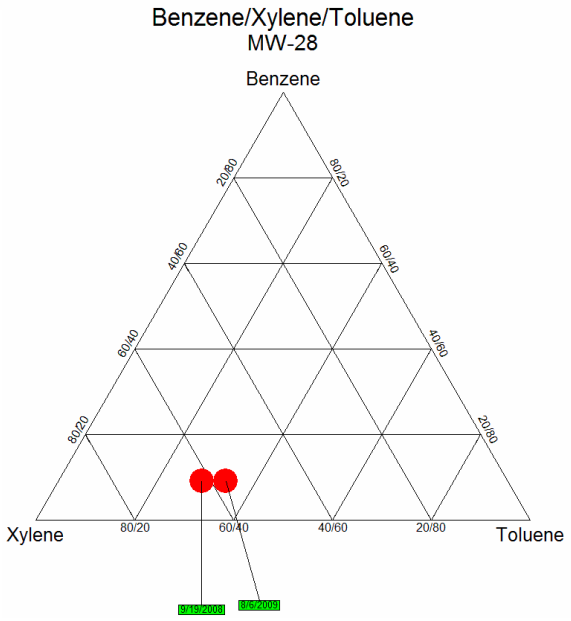
Benzene/Xylene/Toluene
MW-28
Benzene
Xylene
Toluene
20/80
80/20
40/60
60/40
60/40
40/60
80/20
20/80
9/15/2008
9/6/2009

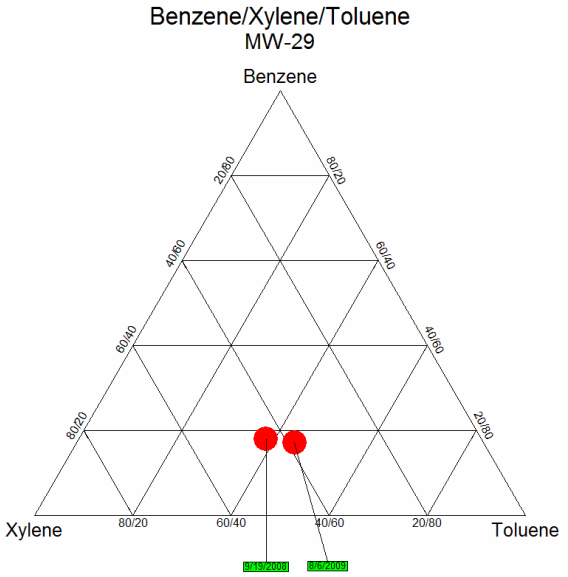
Benzene/Xylene/Toluene
MW-29
Benzene
20/80
80/20
40/60
60/40
60/40
40/60
80/20
20/80
Xylene
80/20
60/40
40/60
20/80
Toluene
9/15/2008
9/6/2009

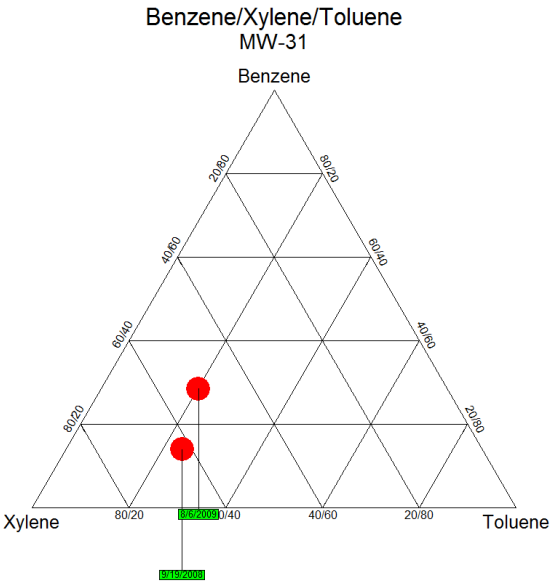
Benzene/Xylene/Toluene
MW-31
Benzene
20/80
80/20
40/60
60/40
60/40
40/60
80/20
20/80
Xylene
80/20
9/6/2009
40/60
20/80
Toluene
9/15/2008

VITA

Shannon Nicole Jeffries

Candidate for the Degree of

Master of Science

Thesis: TRANSIENT HYDROGEOPHYSICAL INVESTIGATION OF A GASOLINE IMPACTED SITE, ENID, OKLAHOMA

Major Field: Geology

Biographical:

Education: Received a Bachelor of Science degree in geology from Missouri State University in Springfield, Missouri in 2008. Completed the requirements for the Master of Science or Arts in geology at Oklahoma State University, Stillwater, Oklahoma, in May 2012.

Experience: Employed as an intern for the Missouri Department of Natural Resources in Springfield, Missouri, from February 2007 to June 2008. Employed at Oklahoma State University School of Geology as a teaching assistant from August 2008 to May 2010. Employed by Greystone Environmental, Inc. in Oklahoma City, Oklahoma, as an intern from September 2008 to May 2009. Employed as an geology intern at El Paso Corporation in Houston, Texas, from May 2009 to August 2009. Employed as a geophysics intern at SM Energy in Tulsa, Oklahoma, from May 2010 to August 2010 and as a Geophysicist from January 2011 to present.

Professional Memberships: Geological Society of America, American Association of Petroleum Geologists, Tulsa Geological Society, Geophysical Society of Tulsa, and Society of Exploration Geophysics.

Name: Shannon Nicole Jeffries Date of Degree: May 2012

Institution: Oklahoma State University Location: Stillwater, Oklahoma

Title of Study: TRANSIENT HYDROGEOPHYSICAL INVESTIGATION OF A GASOLINE IMPACTED SITE, ENID, OKLAHOMA.

Pages in Study: 143 Candidate for the Degree of Master of Science

Major Field: Geology

Scope and Method of Study: The purpose of this study was to examine a gasoline impacted site during remediation. This was done using Multi-channel Analysis of Surface Waves (MASW), Electrical Resistivity Tomography (ERT), and geochemistry of groundwater and soil samples. A second purpose of this study was to determine the effectiveness of ERT cables and electrodes that were left in the boreholes before remediation began. The ERT data collected were then compared to ERT data that were collected pre-remediation to determine the percent change in resistivity of the subsurface, transient ERT. The final methods used were the collection of core and groundwater samples to compare with the results of the transient ERT data. The cores were examined using photoionization detection and samples were sent to a geochemical lab along with the groundwater samples.

Findings and Conclusions: Using MASW the stratigraphy of the subsurface was determined in some locations but raised more questions in other locations. The areas where the data raised more questions were often the location of cores from previous studies conducted at this site. The ERT data collected showed the location of the LNAPL anomalies (higher resistivity). When the data were time lapse processed with data collected pre-remediation there were both positive and negative changes in resistivity that are associated with the LNAPL moving in the subsurface. The core and groundwater sample geochemistry were consistent with the transient ERT; they showed that the site is still contaminated. Specifically, the groundwater geochemistry data showed that the LNAPL is biodegrading as well as volatilizing in different areas of the field site.

ADVISER'S APPROVAL: Todd Halihan